

AD-A207 520

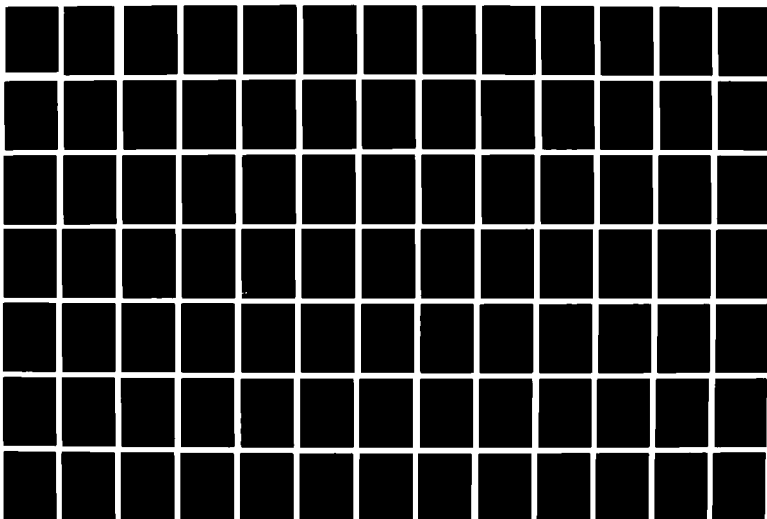
CONTROL OF FLEXIBLE STRUCTURES(U) OPTIMIZATION INC
BLACKSBURG VA J A BURNS ET AL. APR 89 K511-3
AL-TR-89-001 F04611-86-C-0008

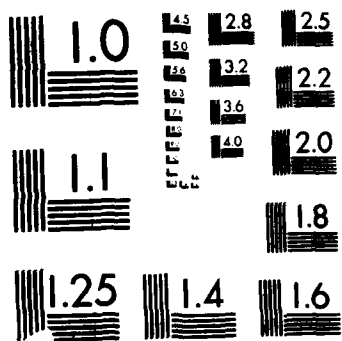
1/2

UNCLASSIFIED

F/G 13/13

NL





AL-TR-89-001

AD:

AD-A207 520



Final Report
for the Period
1 March 1986 to
30 September 1988

Control of Flexible Structures

April 1989

Authors:
J. A. Burns
E. M. Cliff
H. J. Kelley
F. H. Lutze
R. E. Miller

Optimization Incorporated
29 High Meadow Drive
Blacksburg VA 24060

K511-3
F04611-86-C-0008

DTIC
ELECTE
MAY 08 1989
S H D
cb

Approved for Public Release

Distribution is unlimited. The AL Technical Services Office has reviewed this report, and it is releasable to the National Technical Information Service, where it will be available to the general public, including foreign nationals.

Prepared for the :

Astronautics Laboratory (AFSC)

Air Force Space Technology Center
Space Division, Air Force Systems Command
Edwards Air Force Base,
California 93523-5000

NOTICE

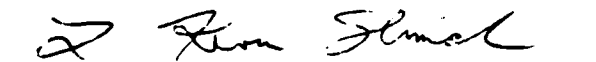
When U.S. Government drawings, specifications, or other data are used for any purpose other than a definitely related Government procurement operation, the fact that the Government may have formulated, furnished, or in any way supplied the said drawings, specifications, or other data, is not to be regarded by implication or otherwise, or in any way licensing the holder or any other person or corporation, or conveying any rights or permission to manufacture, use, or sell any patented invention that may be related thereto.

FOREWORD

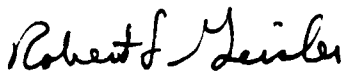
This final report was submitted by by Optimzation Incorporated on completion of contract F04611-86-C-0008 with the Astronautics Laboratory (AFSC), Edwards AFB CA. AFAL Project Manager is Lt Doug De Hart.

This report has been reviewed and is approved for release and distribution in accordance with the distribution statement on the cover and on the DD Form 1473.


DOUGLAS W. DEHART, 1Lt, USAF
Project Manager


L. KEVIN SLIMAK
Chief, Interdisciplinary Space
Technology Branch

FOR THE DIRECTOR


ROBERT L. GIESLER
Director, Aerospace
Vehicle Systems Division

REPORT DOCUMENTATION PAGE

Form Approved
OMB No. 0704-0188

1a. REPORT SECURITY CLASSIFICATION UNCLASSIFIED			1b. RESTRICTIVE MARKINGS		
2a. SECURITY CLASSIFICATION AUTHORITY			3. DISTRIBUTION/AVAILABILITY OF REPORT Approved for Public Release; Distribution is Unlimited		
2b. DECLASSIFICATION/DOWNGRADING SCHEDULE					
4. PERFORMING ORGANIZATION REPORT NUMBER(S) K511-3			5. MONITORING ORGANIZATION REPORT NUMBER(S) AL-TR-89-001		
6a. NAME OF PERFORMING ORGANIZATION Optimization Incorporated		6b. OFFICE SYMBOL (if applicable)	7a. NAME OF MONITORING ORGANIZATION Astronautics Laboratory (AFSC)		
6c. ADDRESS (City, State, and ZIP Code) 29 High Meadow Drive Blacksburg VA 24060			7b. ADDRESS (City, State, and ZIP Code) AL/VSSC Edwards AFB CA 93523-5000		
8a. NAME OF FUNDING/SPONSORING ORGANIZATION		8b. OFFICE SYMBOL (if applicable)	9. PROCUREMENT INSTRUMENT IDENTIFICATION NUMBER F04611-86-C-0008		
8c. ADDRESS (City, State, and ZIP Code)			10. SOURCE OF FUNDING NUMBERS		
PROGRAM ELEMENT NO. 62302F		PROJECT NO. 2864	TASK NO. 00	WORK UNIT ACCESSION NO. EZ	
11. TITLE (Include Security Classification) CONTROL OF FLEXIBLE STRUCTURES (U)					
12. PERSONAL AUTHOR(S) Burns, J.A.; Cliff, E.M.; Kelley, H.J.; Lutze, F.H. and Miller, R.E.					
13a. TYPE OF REPORT Final		13b. TIME COVERED FROM 86/3/1 TO 88/9/30		14. DATE OF REPORT (Year, Month, Day) 89/04	
15. PAGE COUNT 154					
16. SUPPLEMENTARY NOTATION					
17. COSATI CODES			18. SUBJECT TERMS (Continue on reverse if necessary and identify by block number)		
FIELD 13	GROUP 13	SUB-GROUP	Flexible structures, active control, distributed-parameter systems - (J25)		
19. ABSTRACT (Continue on reverse if necessary and identify by block number) This report summarizes the work done under contract F04611-86-C-0008. The principal goals were to develop state-space models and computational algorithms for control of beam and plate type structures, and, more generally, to increase the understanding of the basic problems associated with this development. The state-space approach is based on a distributed parameter model of the structure that includes the fundamental equations without modal truncation. The approach is to use basic physical principles to write down the governing partial differential equations, construct a state-space model from these governing equations, formulate the optimal control problem in terms of the state-space model, develop a convergent approximation scheme and conduct numerical experiments to test the method. The basic view is that it is best to avoid the approximation step until it is required to compute. This process is carried out for various models, with and without actuator dynamics, and for a simple rectangular clamped plate. The basic beam systems are examined and then the effect of delays are studied.					
20. DISTRIBUTION/AVAILABILITY OF ABSTRACT <input checked="" type="checkbox"/> UNCLASSIFIED/UNLIMITED <input type="checkbox"/> SAME AS RPT. <input type="checkbox"/> DTIC USERS			21. ABSTRACT SECURITY CLASSIFICATION UNCLASSIFIED		
22a. NAME OF RESPONSIBLE INDIVIDUAL DOUGLAS W. DEHART, 1LT, USAF			22b. TELEPHONE (Include Area Code) (805) 275-5253		22c. OFFICE SYMBOL AL/VSSC

Block 19. Continued

In addition to the basic program we conducted a survey of joint dynamic model and attempted to evaluate the feasibility of constructing a comprehensive computer code that would be general enough to handle more complex structures composed of basic beam and plate elements.

Accession For	
NTIS GRA&I	<input checked="" type="checkbox"/>
DTIC TAB	<input type="checkbox"/>
Unannounced	<input type="checkbox"/>
Justification	
By	
Distribution/	
Availability Codes	
Dist	Avail and/or Special
A-1	



TABLE OF CONTENTS

	<u>Page</u>
INTRODUCTION	1
DESCRIPTION OF BEAM AND PLATE PROBLEMS	3
EQUATIONS OF MOTION	5
STATE SPACE MODELS	15
Euler-Bernoulli Beam	15
Timoshenko Beam	18
Euler-Bernoulli Beam with Actuator Dynamics	21
Timoshenko Beam with Actuator Dynamics	24
Isotropic Rectangular Plate	26
General Framework	28
THE CONTROL PROBLEM	31
Construction of the Output Operator	36
Form of the Gain Operator K	40
NUMERICAL PROCEDURES	43
Euler-Bernoulli Beam Approximation Scheme	48
Timoshenko Beam Approximation Scheme	53
Euler-Bernoulli with Actuator Dynamics: No Delay	55
Euler-Bernoulli with Delayed Actuator States	55
Timoshenko Beam with Actuator Dynamics	59
Isotropic Rectangular Plate	60
JOINT MODELING	65

	<u>Page</u>
NUMERICAL RESULTS	77
Beam Problems	77
MODEL 1: Euler-Bernoulli Beam; No Actuator	83
MODEL 2: Timoshenko Beam; No Actuator	85
MODEL 3: Euler-Bernoulli Beam; Actuator, No Delay	94
MODEL 4: Euler-Bernoulli Beam; Actuator Dynamics with Delay	99
MODEL 5: Timoshenko Beam; Actuator Dynamics with No Delay	105
MODEL 6: Timoshenko Beam; Actuator Dynamics with Delay . . .	111
MODEL 7: Isotropic Plate	119
SOFTWARE ISSUES	133
CLOSING REMARKS	141
REFERENCES	143

LIST OF FIGURES

<u>Figure</u>	<u>Caption</u>	<u>Page</u>
1.	Beam with Tip Mass	6
2.	Rectangular Plate to be Controlled	12
3.	Fundamental Spline	49
4.	Functional Gain K_5 ; Model 1	86
5.	Functional Gain K_6 ; Model 1	87
6.	Functional Gain K_5 ; Model 2	90
7.	Functional Gain K_6 ; Model 2	91
8.	Functional Gain K_7 ; Model 2	92
9.	Functional Gain K_8 ; Model 2	93
10.	Functional Gain K_5 ; Model 3	97
11.	Functional Gain K_6 ; Model 3	98
12.	Functional Gain K_5 ; Model 4	102
13.	Functional Gain K_6 ; Model 4	103
14.	History Functional Gain; Model 4	104
15.	Functional Gain K_5 ; Model 5	107
16.	Functional Gain K_6 ; Model 5	108
17.	Functional Gain K_7 ; Model 5	109
18.	Functional Gain K_8 ; Model 5	110
19.	Functional Gain K_5 ; Model 6	114
20.	Functional Gain K_6 ; Model 6	115
21.	Functional Gain K_7 ; Model 6	116
22.	Functional Gain K_8 ; Model 6	117

LIST OF FIGURES (continued)

<u>Figure</u>	<u>Caption</u>	<u>Page</u>
23.	History Functional Gain; Model 6	118
24.	Functional Gain K_1 ; $N = 4$; Model 7	123
25.	Functional Gain K_1 , $N = 8$; Model 7	124
26.	Functional Gain K_1 , $N = 12$; Model 7	125
27.	Functional Gain K_1 , Cross Section $y = x$; Model 7 . .	126
28.	Functional Gain K_2 , $N = 4$; Model 7	127
29.	Functional Gain K_2 , $N = 8$; Model 7	128
30.	Functional Gain K_2 , $N = 12$; Model 7	129
31.	Functional Gain K_2 , Cross Section $y = x$; Model 7 . .	130

LIST OF TABLES

<u>Table</u>	<u>Title</u>	<u>Page</u>
1.	Euler-Bernoulli Frequencies, $L = 30$ ft.	81
2.	Timoshenko Frequencies, $L = 30$ ft.	81
3.	Euler-Bernoulli Frequencies, $L = 1$ ft.	82
4.	Timoshenko Frequencies, $L = 1$ ft.	82
5.	Sub-optimal Gains; MODEL 1	84
6.	Closed-Loop Eigenvalues; MODEL 1	85
7.	Sub-optimal Gains; MODEL 2	89
8.	Closed-Loop Eigenvalues; MODEL 2	94
9.	Sub-optimal Gains; MODEL 3	95
10.	Closed-Loop Eigenvalues; MODEL 3	99
11.	Sub-optimal Gains; MODEL 4	101
12.	Sub-optimal Gains; MODEL 5	106
13.	Closed-Loop Eigenvalues; MODEL 5	111
14.	Sub-optimal Gains; MODEL 6	113
15.	Closed-Loop Eigenvalues; MODEL 6	119
16.	Open-Loop Frequencies; MODEL 7	121
17.	Closed-Loop Eigenvalues; MODEL 7	131/132

INTRODUCTION

This report summarizes work done under Contract F04611-86-C-0008 during the period 1 March 1986 through 30 September 1988. The principal goals were to develop state-space models and computational algorithms for control of beam and plate type structures, and, more generally, to increase the understanding of the basic problems associated with this development. The state-space approach is based on a distributed parameter model of the structure that includes the fundamental partial differential equations without modal truncation.

The approach is to use basic physical principles to write down the governing partial differential equations, construct a state-space model from the governing equations, formulate the optimal control problem in terms of the state-space model, develop a convergent approximation scheme and conduct numerical experiments to test the method. The basic view is that it is best to avoid the approximation step until it is required to compute. This process is carried out for various beam models, with and without actuator dynamics, and for a simple rectangular clamped plate. The basic beam systems are examined and then the effect of delays are studied.

In addition to the basic program we conducted a survey of joint dynamic models and attempted to evaluate the feasibility of constructing a comprehensive computer code that would be general enough to handle more complex structures composed of basic beam and plate elements.

This report is divided into nine parts. In the next section we present a general discussion of the types of control problems and structures we considered. In the section EQUATIONS OF MOTION we summarize the basic governing differential equations for the various structures, using Euler-Bernoulli and Timoshenko beam theories and simple plate theory, and include actuator dynamic equations. In the STATE SPACE MODEL section we construct the appropriate state-space models by presenting the state space, the dynamic state operator and the input operator for each problem. We conclude this section by noting the general framework that covers all the problems considered in this study. THE CONTROL PROBLEM section contains a review of the basic distributed parameter Linear-Quadratic Regulator (LQR) problem. The output operators are detailed for each of the structural control problems. The specific form of the optimal gain operator is presented for each beam and plate problem. The NUMERICAL PROCEDURES section begins with a review of the basic approximation theory needed to solve the LQR problems. Also included in this section is a brief description of the particular schemes used in each problem and a comparison of open-loop systems for Euler-Bernoulli and Timoshenko theories. A survey of joint modeling is given in the JOINT MODELING section. Numerical results for the control problems are presented in the NUMERICAL RESULTS section and the results of our feasibility study are summarized in SOFTWARE ISSUES. The last section is devoted to closing remarks and suggestions of problem areas that need further study.

DESCRIPTION OF BEAM AND PLATE PROBLEMS

We consider a variety of mathematical problems in which the fundamental objective is to quickly damp vibrations in various structures. We concentrated our effort on two basic structures; a beam with a tip-body at one end and a clamped rectangular plate.

The beam structure consists of a beam with a tip-body at one end. The other end of the beam is attached to a hub which is free to rotate about a fixed axis. We study only motions in the plane normal to the hub's rotation axis. Four versions of the problem are studied in all. Firstly, we employ two distinct theories to model beam motions. The simplest and most common is the Euler-Bernoulli theory which does not account for strain energy due to shear. In this model the elastic energy is solely due to normal stretching and compression of the beam "fibers" as the beam assumes a deformed shape. A more complete theory, the Timoshenko model, includes strain energy due to shearing and kinetic energy due to rotation of the beam face elements.

The other important feature we study is the model for the torque actuator. In the simplest case one imagines an ideal actuator that can instantly generate the amount of torque required by the control law. An alternative model includes a second-order actuator modelled with a delay differential equation. If the delay terms are set to zero one has a usual second-order actuator model; however, the effect of delays (due to computational requirements, for example) are shown to be important.

The two beam models (Euler-Bernoulli and Timoshenko) are combined with the two actuator models (ideal and second-order delayed) to produce four distinct beam models to be studied. In each case the objective is to derive a control law in state-feedback form. The purpose of the control law is to enhance the decay-rate for the unwanted structural vibrations.

The plate problem considered concerns transverse motions of a rectangular plate which is clamped along its edges. The "control" is produced by modulating the amplitude of a distributed force with fixed spatial variation. That is, the force is given by

$$f(t,x,y) = u(t) \phi(x,y)$$

where $\phi(x,y)$ is given and $u(t)$ is the control. As before, the objective is to formulate a state-feedback control law that will substantially improve the rate at which vibrations decay.

EQUATIONS OF MOTION

In this section we present the equations of motion for the five problems considered in this report. In particular, we summarize the equations for the beam with tip-body and the clamped plate for the following cases:

- An Euler-Bernoulli beam
- A Timoshenko beam
- An Euler-Bernoulli beam with actuator dynamics
- A Timoshenko beam with actuator dynamics
- An isotropic rectangular plate

A detailed derivation of the Euler-Bernoulli model is given in Ref. 2. Inclusion of actuator dynamics are discussed in Ref. 2 and the extension to the Timoshenko beam model follows directly from Ref. 1, Ref. 2 and Ref. 3. The reader is referred to Ref. 4 and Ref. 5 for detailed discussions of plate modeling.

BEAM EQUATIONS

We present the various mathematical models of the beam structure shown in Figure 1. It is assumed that the structure is pivoting about a fixed pivot at point 0, and that the motion is in a plane. The development is achieved by direct application of Newton's Laws to individual members of the structure with the resulting equations summed to determine the overall motion.

The structure consists of three parts, the main frame, or mass A, the beam, or mass B, and the end mass, or mass C. The main frame is

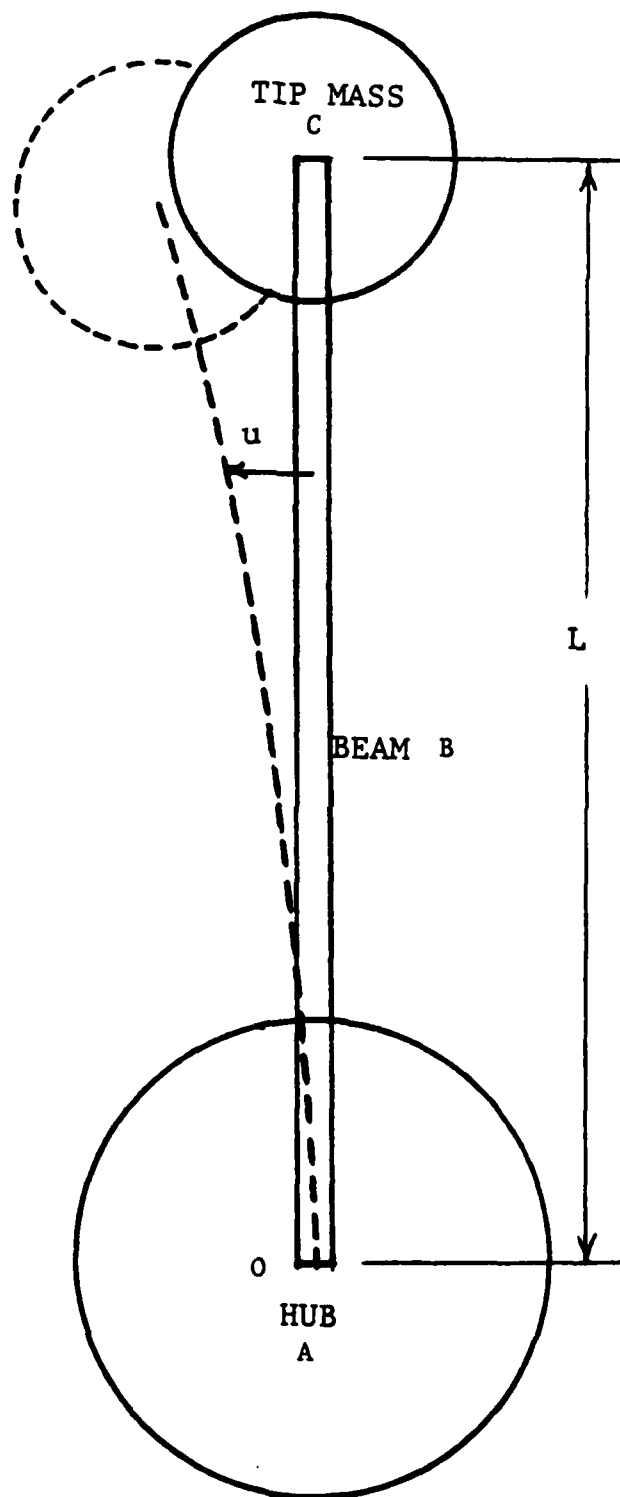


Figure 1. Beam with Tip Mass

assumed to be a rigid body pivoting about point 0. The beam is assumed to be flexible and rigidly attached to the main frame as a cantilevered beam. The end mass is rigidly attached to the end of the beam so that it moves and rotates with the end of the beam. Finally, the attached point is assumed to be at the center of mass of the end mass.

The coordinate system to be used is fixed in the main frame and rotates with it. The origin is at point 0 with the x axis pointing along the undeflected beam, the z axis, the axis of rotation, and the y axis completing the right hand set. The governing equations depend of course on the assumptions about the beam. We summarize these equations for the four cases listed above.

Euler-Bernoulli Beam Theory

It follows from Ref. 2 that the motion of the structure is governed by the system of equations

$$\dot{\theta}(t) = \omega(t) \quad (1)$$

$$I_A \dot{\omega}(t) = EI u_{xx}(t,0) + M_A(t) \quad (2)$$

$$m_c [L\dot{\omega}(t) + \dot{\eta}(t)] = EI u_{xxx}(t,L) , \quad (3)$$

$$I_c [\dot{\omega}(t) + \dot{\xi}(t)] = -EI u_{xx}(t,L) \quad (4)$$

$$u_{tt}(t,x) + x\dot{\omega}(t) = -\frac{EI}{\rho} u_{xxxx}(t,x) \quad (5)$$

where $u(t,x)$ denotes the deflection of the beam, $\theta(t)$ is the angle of hub rotation, $\eta(t)$ is the relative lineal velocity of the tip mass, $\xi(t)$ is the relative angular velocity of the tip mass due to deflection and $M_A(t)$ is the applied moment at the hub.

Since the beam remains joined to the hub, one has the cantilevered boundary conditions

$$\left. \begin{aligned} u(t,0) = u_t(t,0) &= 0 \\ u_x(t,0) = u_{xt}(t,0) &= 0 \end{aligned} \right\} \quad (6)$$

and the integrity of the upper joint requires the boundary conditions

$$\left. \begin{aligned} u_t(t,L) &= \eta(t) \\ u_{xt}(t,L) &= \xi(t) \end{aligned} \right\} \quad (7)$$

It is important to note that both (6) and (7) are geometric (i.e. essential) boundary conditions.

Timoshenko Beam Theory

The Timoshenko beam model includes the rotary inertia and shearing deformations. If $u(t,x)$ denotes the deflection of the beam, then the total slope $u_x(t,x)$ is given by

$$u_x(t,x) = \psi(t,x) + \beta(t,x) \quad (8)$$

where $\psi(t,x)$ is the slope of the deflection curve when shearing is neglected and $\beta(t,x)$ is the angle of shear at the neutral axis. The bending moment $M(t,x)$ and shear force $V(t,x)$ are given by

$$M(t,x) = EI \psi_x(t,x) \quad (9)$$

and

$$V(t,x) = -K'AG \beta(t,x) = -K'AG [u_x(t,x) - \psi(t,x)] , \quad (10)$$

respectively. Here A is the cross-section area, K' is a constant depending on the shape of cross-section and G is the modulus of elasticity in shear (Ref. 3).

The equations for the Timoshenko beam become

$$\dot{\theta}(t) = \omega(t) \quad (11)$$

$$I_A \dot{\omega}(t) = EI \psi_x(t, 0) + M_A(t) \quad (12)$$

$$m_c [L \dot{\omega}(t) + \dot{\eta}(t)] = -K'AG [u_x(t, L) - \psi(t, L)] \quad (13)$$

$$I_c [\dot{\omega}(t) + \dot{\xi}(t)] = -EI \psi_x(t, L) \quad (14)$$

$$[u_{tt}(t, x) + x \dot{\omega}(t)] = K'G [u_{xx}(t, x) - \psi_x(t, x)] \quad (15)$$

$$\rho I [\psi_{tt}(t, x) + \dot{\omega}(t)] = EI \psi_{xx}(t, x) + K'AG [u_x(t, x) - \psi(t, x)] \quad (16)$$

Again, one has the cantilevered boundary conditions at the hub, $x = 0$,

$$\left. \begin{aligned} u(t, 0) &= u_t(t, 0) = 0 \\ \psi(t, 0) &= \psi_t(t, 0) = 0 \end{aligned} \right\} \quad (17)$$

Also, the upper joint requires the boundary conditions

$$\left. \begin{aligned} u_t(t, L) &= \eta(t) \\ \psi_t(t, L) &= \xi(t) \end{aligned} \right\} \quad (18)$$

Euler-Bernoulli Beam with Actuator Dynamics

Returning to the Euler-Bernoulli model (1) - (5) we add a system of equations that incorporates actuator dynamics with a delay. Thus, the total system for the Euler-Bernoulli beam with tip-body and delayed actuator dynamics becomes

$$\dot{\theta}(t) = \omega(t) \quad (19)$$

$$\dot{\omega}(t) = \left(\frac{EI}{I_A} \right) u_{xx}(t, 0) + \left(\frac{1}{I_A} \right) [c_1 x_1(t) + c_2 x_2(t)] \quad (20)$$

$$[L\dot{\omega}(t) + \dot{\eta}(t)] = \left(\frac{EI}{m_c}\right) u_{xxx}(t, L) \quad (21)$$

$$[\dot{\omega}(t) + \dot{\xi}(t)] = \left(-\frac{EI}{I_c}\right) u_{xx}(t, L) \quad (22)$$

$$\frac{\partial}{\partial t} [u_{xx}(t, x)] = \frac{\partial^2}{\partial x^2} [u_t(t, x) + x\omega(t)] \quad (23)$$

$$\frac{\partial}{\partial t} [u_t(t, x) + x\omega(t)] = \left(-\frac{EI}{\rho}\right) \frac{\partial^2}{\partial x^2} [u_{xx}(t, x)] \quad (24)$$

with general second-order actuator model

$$\dot{x}_1(t) = x_2(t) \quad (25)$$

$$\begin{aligned} \dot{x}_2(t) = & a_{11}x_1(t) + a_{12}x_2(t) + a_{21}x_1(t-r) + a_{22}x_2(t-r) \\ & + b_1u_c(t), \end{aligned} \quad (26)$$

where $u_c(t)$ is the commanded input to the actuator and $M_A(t) = c_1x_1(t) + c_2x_2(t)$ is the output. The time delay $r > 0$ was included to illustrate the problems one can encounter if numerical schemes for control designs are improperly constructed. Note that if $a_{21} = a_{22} = 0$, then (25) - (26) is a second order linear actuator.

Timoshenko Beam with Actuator Dynamics

If one rewrites (11) - (16) and adds (25) - (26) to these equations, we obtain the following equations

$$\dot{\theta}(t) = \omega(t) \quad (27)$$

$$\dot{\omega}(t) = \left(\frac{EI}{I_A}\right) \psi_x(t, 0) + \left(\frac{1}{I_A}\right) [c_1x_1(t) + c_2x_2(t)] \quad (28)$$

$$[L\dot{\omega}(t) + \dot{\eta}(t)] = \left(\frac{-K'AG}{m_c}\right) [u_x(t, L) - \psi(t, L)] \quad (29)$$

$$[\dot{\omega}(t) + \dot{\eta}(t)] = \left(\frac{-EI}{I_c} \right) \psi_x(t, L) \quad (30)$$

$$[u_{tt}(t, x) + x \dot{\omega}(t)] = \left(\frac{K'G}{\rho} \right) [u_{xx}(t, x) - \psi_x(t, x)] \quad (31)$$

$$[\psi_{tt}(t, x) + \dot{\omega}(t)] = \left(\frac{E}{\rho} \right) \psi_{xx}(t, x) + \left(\frac{K'AG}{\rho I} \right) [u_x(t, x) - \psi(t, x)] \quad (32)$$

$$\dot{x}_1(t) = x_2(t) \quad (33)$$

$$\begin{aligned} \dot{x}_2(t) = & a_{11}x_1(t) + a_{12}x_2(t) + a_{21}x_1(t-r) + a_{22}x_2(t-r) \\ & + b_1 u_c(t), \end{aligned} \quad (34)$$

where again $M_A(t) = c_1x_1(t) + c_2x_2(t)$ is the output to the actuator (33) - (34).

Isotropic Rectangular Plate

Figure 2 shows a plate with uniform thickness h that is assumed small in comparison with its other dimension. The x - y plane is taken to be the (undeflected) middle plane of the plate. Deflections in the z direction are assumed small in comparison to the thickness and the normals to the x - y plane are assumed to remain normal to the deflected middle surface during vibrations. The governing equation for the loaded undamped plate becomes

$$\bar{m} u_{tt}(t, x, y) + D \Delta^2 u(t, x, y) = f(t, x, y) \quad (35)$$

where \bar{m} is the mass per unit area, $D = \left(\frac{Eh}{12(1-\nu)} \right)$, ν is Poisson's ratio and $f(t, x, y)$ is an applied load. Here Δ is the Laplacian operator

$$\Delta = \frac{\partial^2}{\partial x^2} + \frac{\partial^2}{\partial y^2} \quad (36)$$

so that

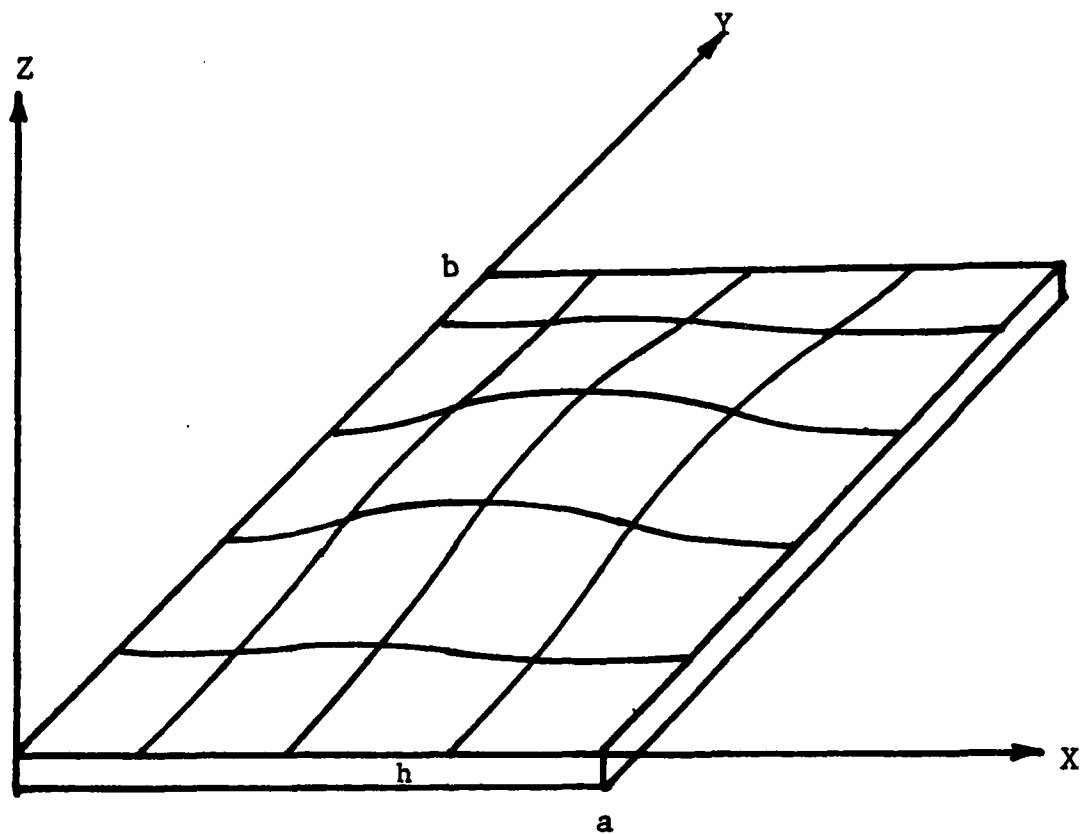


Figure 2. Rectangular Plate to be Controlled

$$\Delta^2 u(t,x,y) = \frac{\partial^4}{\partial x^4} u(t,x,y) + \frac{2 \partial^4}{\partial x^2 \partial y^2} u(t,x,y) + \frac{\partial^4}{\partial y^4} u(t,x,y) \quad (37)$$

Let $\Omega = (0,a) \times (0,b)$ denote the surface of the plate and $\partial\Omega$ denote the boundary (i.e. edges) of the plate. Then, (35) must hold for all $t > 0$ and $(x,y) \in \Omega$ and the clamped boundary conditions are given by

$$u(t,x,y) = \Delta u(t,x,y) = 0, \quad (x,y) \in \partial\Omega \quad (38)$$

We shall consider a control problem for the plate equation (35) with boundary conditions (38).

STATE SPACE MODELS

In this section we construct the state-space models for each of the problems discussed above. These models are used later to formulate control problems, provide explicit representations of optimal control laws and as a basis for constructing computational algorithms.

EULER-BERNOULLI BEAM

In order to construct a state-space model, equation (5) is first written in the form

$$\left. \begin{aligned} \frac{\partial}{\partial t} [u_{xx}(t,x)] &= \frac{\partial^2}{\partial x^2} [u_t(t,x) + x\omega(t)] \\ \frac{\partial}{\partial t} [u_t(t,x) + x\omega(t)] &= \frac{-EI}{\rho} \frac{\partial^2}{\partial x^2} [u_{xx}(t,x)] \end{aligned} \right\} \quad (39)$$

As noted in Ref. 5, this system suggests that the functions $x \rightarrow u_{xx}(t,x)$ and $x \rightarrow [u_t(t,x) + x\omega(t)]$ are natural state components. Thus, the "state vector" $y(t)$ is defined to be

$$y(t) = \begin{bmatrix} \theta(t) \\ \omega(t) \\ \eta(t) + L\omega(t) \\ \xi(t) + \omega(t) \\ u_{xx}(t,x) \\ u_t(t,x) + x\omega(t) \end{bmatrix} \quad (40)$$

The appropriate state space is the Hilbert space

$$\mathcal{H} = R \times R \times R \times R \times L_2(0,L) \times L_2(0,L) \quad (41)$$

with inner product

$$\begin{aligned} \langle y, \hat{y} \rangle_Y = & y_1 \hat{y}_1 + I_A y_2 \hat{y}_2 + m_c y_3 \hat{y}_3 + I_c y_4 \hat{y}_4 \\ & + \int_0^L EI y_5(x) \hat{y}_5(x) dx + \int_0^L EI y_6(x) \hat{y}_6(x) dx . \end{aligned} \quad (42)$$

The space \mathcal{Y} with inner product (42) is a Hilbert space and $\|y\| = \sqrt{\langle y, y \rangle_Y}$ defines a norm on \mathcal{Y} . The product $\langle y, y \rangle_Y$ is essentially the mechanical energy in the physical system at state y .

Let δ_p denote the operator that acts on functions and produces the value of that function at point p , i.e. $\delta_p \phi(\cdot) = \phi(p)$. Moreover, D_x denotes the partial differential operator $\frac{\partial}{\partial x}$. Define the operator A_E on $D(A_E) \subseteq \mathcal{Y}$ by

$$A_E = \begin{bmatrix} 0 & 1 & 0 & 0 & 0 & 0 \\ 0 & 0 & 0 & 0 & \frac{EI}{I_A} \delta_0 & 0 \\ 0 & 0 & 0 & 0 & \frac{EI}{m_c} \delta_L \circ D_x & 0 \\ 0 & 0 & 0 & 0 & -\frac{EI}{I_c} \delta_L & 0 \\ 0 & 0 & 0 & 0 & 0 & D_x^2 \\ 0 & 0 & 0 & 0 & -\frac{EI}{\rho} D_x^2 & 0 \end{bmatrix} \quad (43)$$

where the domain of A_E is given by

$$D(A_E) = \left\{ (y_1, y_2, y_3, y_4, y_5(\cdot), y_6(\cdot))^T \in \mathcal{Y} / \begin{array}{l} y_5, y_6 \in H^2(0, L), \\ y_6(0) = 0, y_6'(0) = y_2, y_6(L) = y_3, y_6'(L) = y_4 \end{array} \right\}. \quad (44)$$

Let B_E be the input operator $B_E: \mathbb{R} \rightarrow \mathcal{Y}$ defined by

$$B_E = \begin{bmatrix} 0 \\ \frac{1}{I_A} \\ 0 \\ 0 \\ 0 \\ 0 \end{bmatrix} \quad (45)$$

and consider the system in \mathcal{Y} given by

$$\dot{y}(t) = A_E y(t) + B_E M_A(t) \quad (46)$$

It was shown in Ref. 1 that A_E generates a C_0 -semigroup $e^{A_E t}$ on \mathcal{Y} and that the variation of parameters formula

$$y(t) = e^{A_E t} y(0) + \int_0^t e^{A_E(t-s)} B_E M_A(s) ds \quad (47)$$

provides weak solutions of the partial differential equations (1) - (6) with initial data in \mathcal{Y} . In particular one has the following result.

THEOREM 1. If $y(0) = y \in D(A_E)$ and $M_A(t)$ belongs to $L_1(0, T)$, then $y(t)$ defined by (47) is a solution to the system (1) - (5) with initial data y_0 .

Theorem 1 provides the basic theoretical result that allows one to construct convergent numerical schemes for control design (see Refs. 1, 2 and 6-15). Later we augment the state space model (46) by adding the actuator dynamics with delays.

It is important to understand that the statement that $y_0 \in D(A_0)$ is initial data for (1) - (5) means that

$$y_0 = \text{col} (\theta_0, \omega_0, \alpha_0, \gamma_0, u_0(x), v_0(x))$$

satisfies (44) and the solution of (1) - (6) satisfies the initial condition $\theta(0) = \theta_0$, $\omega(0) = \omega_0$, $[L\omega(0) + \eta(0)] = \alpha_0$, $[\omega(0) + \xi(0)] = \gamma_0$, $u_{xx}(0, x) = u_0(x)$ and $[u_t(0, x) + x\omega(0)] = v_0(x)$.

TIMOSHENKO BEAM

We first rewrite the second order equations (15) and (16) as the first order system

$$\frac{\partial}{\partial t} [u_t(t, x) + x\omega(t)] = \left(\frac{K'G}{\rho} \right) \frac{\partial}{\partial x} [u_x(t, x) - \psi(t, x)] \quad (48)$$

$$\begin{aligned} \frac{\partial}{\partial t} [\psi_t(t, x) + \omega(t)] &= \left(\frac{E}{\rho} \right) \frac{\partial}{\partial x} \psi_x(t, x) + \left(\frac{K'AG}{\rho I} \right) [u_x(t, x) \\ &\quad - \psi(t, x)] \end{aligned} \quad (49)$$

$$\frac{\partial}{\partial t} \psi_x(t, x) = \frac{\partial}{\partial x} [\psi_t(t, x) + \omega(t)] \quad (50)$$

$$\frac{\partial}{\partial t} [u_x(t, x) - \psi(t, x)] = \frac{\partial}{\partial x} [u_t(t, x) + x\omega(t)] - [\psi_t(t, x) + \omega(t)]. \quad (51)$$

Let $w(t)$ denote the "state-vector"

$$w(t) = \begin{bmatrix} u(t) \\ \omega(t) \\ L\omega(t) + \eta(t) \\ \omega(t) + \xi(t) \\ u_t(t,x) + x\omega(t) \\ \psi_t(t,x) + \omega(t) \\ \psi_x(t,x) \\ u_x(t,x) - \psi(t,x) \end{bmatrix}. \quad (52)$$

The appropriate state space for Timoshenko beam is the Hilbert space

$$\mathbb{W} = R \times R \times R \times R \times L_2 \times L_2 \times L_2 \times L_2, \quad (53)$$

where $L_2 = L_2(0,L)$, and the inner product is given by

$$\begin{aligned} \langle w, \hat{w} \rangle_{\mathbb{W}} &= w_1 \hat{w}_1 + I_A w_2 \hat{w}_2 + m_c w_3 \hat{w}_3 + I_c w_4 \hat{w}_4 \\ &+ \int_0^L \{ A \rho w_5(x) \hat{w}_5(x) + I \rho w_6(x) \hat{w}_6(x) \} dx \\ &+ \int_0^L \{ EI w_7(x) \hat{w}_7(x) + (K'AG) w_8(x) \hat{w}_8(x) \} dx \end{aligned} \quad (54)$$

Here again (54) defines an inner product on (53) and $\langle w, w \rangle_{\mathbb{W}} = \|w\|^2$ is essentially the mechanical energy in the physical system at state w .

Define the differential operator A_T with domain $D(A_T) \subseteq \mathbb{W}$ by

$$A_T = \begin{bmatrix} 0 & 1 & 0 & 0 & 0 & 0 & 0 & 0 \\ 0 & 1 & 0 & 0 & 0 & 0 & \left(\frac{EI}{I_A}\right) & 0 \\ 0 & 0 & 0 & 0 & 0 & 0 & 0 & \left(\frac{-K'AG}{m_c}\right) \delta_L \\ 0 & 0 & 0 & 0 & 0 & 0 & \left(\frac{-EI}{I_c}\right) \delta_L & 0 \\ 0 & 0 & 0 & 0 & 0 & 0 & 0 & \left(\frac{K'G}{\rho}\right) D_x \\ 0 & 0 & 0 & 0 & 0 & 0 & \left(\frac{E}{\rho}\right) D_x & \left(\frac{K'AG}{\rho I}\right) \\ 0 & 0 & 0 & 0 & 0 & D_x & 0 & 0 \\ 0 & 0 & 0 & 0 & D_x & -1 & 0 & 0 \end{bmatrix} \quad (55)$$

where the domain of A_T is given by

$$D(A_T) = \left\{ w = (w_1, w_2, w_3, w_4, w_5(\cdot), w_6(\cdot), w_7(\cdot), w_8(\cdot))^T \in \mathbb{W} / \right. \\ \left. w_5(\cdot), w_6(\cdot), w_7(\cdot), w_8(\cdot) \in H^1(0, L) \text{ and} \right. \\ \left. w_5(0) = 0, w_5(L) = w_3, w_6(0) = w_2, w_6(L) = w_4 \right\} \quad (56)$$

Let B_T be the input operator $B_T : \mathbb{R} \rightarrow \mathbb{W}$ defined by

$$B_T = \begin{bmatrix} 0 \\ \frac{1}{I_A} \\ 0 \\ 0 \\ 0 \\ 0 \\ 0 \\ 0 \end{bmatrix} \quad (57)$$

and consider the system in \mathbb{W} given by

$$\dot{w}(t) = A_T w(t) + B_T M_A(t) . \quad (58)$$

The following result may be established using the methods in Ref. 1.

THEOREM 2. The operator B_T is bounded and A_T generates a C_0 -semigroup $e^{A_T t}$ on the Hilbert space \mathbb{W} .

It also follows that if $w_0 \in D(A_T)$ then

$$w(t) = e^{A_T t} w_0 + \int_0^t e^{A_T(t-s)} B_T M_A(s) ds \quad (59)$$

provides weak solutions to the Timoshenko beam equations (11) - (16)

with initial data w_0 .

We turn now to the addition of the actuator dynamics. The general second-order model (25) - (26) will be written as a system and added to the state-space models for the Euler-Bernoulli beam (46) and the Timoshenko beam (58), respectively.

EULER-BERNOULLI BEAM WITH ACTUATOR DYNAMICS

Let $x = [x_1, x_2]^T$, $C_1 = [c_1, c_2]^T$, $B_1 = [0, b_1]^T$ and

$$A_1 = \begin{bmatrix} 0 & 1 \\ a_{11} & a_{12} \end{bmatrix} , \quad A_2 = \begin{bmatrix} 0 & 0 \\ a_{21} & a_{22} \end{bmatrix} .$$

The system (25) - (26) can be written in matrix form as

$$\dot{x}(t) = A_1 x(t) + A_2 x(t-r) + B_1 u_c(t) \quad (60)$$

and the applied torque $M_A(t)$ is given by

$$M_A(t) = C_1 x(t) \quad (61)$$

The addition of actuator dynamics to the state-space model for the Euler-Bernoulli beam is accomplished by combining (46), (60) and (61) into "state-space form"

$$\left. \begin{aligned} \dot{y}(t) &= A_E y(t) + B_E C_1 x(t) \\ \dot{x}(t) &= A_1 x(t) + A_2 x(t-r) + B_1 u_c(t) \end{aligned} \right\} \quad (62)$$

In order to show that the augmented system (62) is well-posed we must introduce an augmented state-space. We consider two distinct cases, $A_2 = 0$ and $A_2 \neq 0$.

Case 1: No Delay

Let Z_E^0 denote the Hilbert space

$$Z_E^0 = Y \times R \times R = Y \times R^2 \quad (63)$$

with inner product

$$\langle z^0, \hat{z}^0 \rangle_{0E} = \langle y, \hat{y} \rangle_Y + x_1 \hat{x}_1 + x_2 \hat{x}_2 \quad (64)$$

where $z^0 = (y, x_1, x_2)^T$ and $\hat{z}^0 = (\hat{y}, \hat{x}_1, \hat{x}_2)$.

Define A_0 on $D(A_0) \subseteq Z_E^0$ by

$$D(A_0) = \left\{ \begin{bmatrix} y \\ x \end{bmatrix} \middle/ y \in D(A_E) \right\} \quad (65)$$

and

$$A_0 = \begin{bmatrix} A_E & B_E C_1 \\ 0 & A_1 \end{bmatrix} \quad (66)$$

Let $B_0 : R \rightarrow Z_E^0$ be defined by

$$B_0 = \begin{bmatrix} 0 \\ B_1 \end{bmatrix} \quad (67)$$

The augmented system (62) becomes

$$\dot{z}^0(t) = A_0 z(t) + B_0 u_c(t) \quad (68)$$

Moreover, one can easily establish the following result.

THEOREM 3. The operator B_0 is bounded and A_0 generates a C_0 -semigroup $e^{A_0 t}$ on the Hilbert space \tilde{z}_E^0 .

The case with delays is more complex.

Case 2: Delayed Actuator

Let \tilde{z}_E denote the Hilbert space

$$\tilde{z}_E = \tilde{z}_E^0 \times L_2(-r, 0; \mathbb{R}^2) \quad (69)$$

with inner product

$$\langle z, \hat{z} \rangle_E = \langle z^0, \hat{z}^0 \rangle_{\tilde{z}_E^0} + \int_{-r}^0 \langle \phi(s), \hat{\phi}(s) \rangle ds \quad (70)$$

where $z = (z^0, \phi)^T \in \tilde{z}_E$ and $\hat{z} = (\hat{z}^0, \hat{\phi})^T \in \tilde{z}_E$, respectively. Define A on $D(A) \subseteq \tilde{z}_E$ by

$$D(A) = \left\{ \begin{bmatrix} y \\ x \\ \phi \end{bmatrix} \in \tilde{z}_E \middle/ \begin{array}{l} y \in D(A_E) \\ \phi \in H^1(-r, 0) \\ \phi(0) = x \end{array} \right\} \quad (71)$$

and

$$A \begin{bmatrix} y \\ x \\ \phi \end{bmatrix} = \begin{bmatrix} A_E y + B_E C_1 x \\ A_1 x + A_2 \phi(-r) \\ \phi'(\cdot) \end{bmatrix}. \quad (72)$$

The operator $B : \mathbb{R} \rightarrow \tilde{z}_E$ is defined by

$$B = \begin{bmatrix} 0 \\ B_1 \\ 0 \end{bmatrix}. \quad (73)$$

The following result is non-trivial. However, the proof can be given based on the results in Ref. 1 and Refs. 6-10.

THEOREM 4. The operator B is bounded and A generates a C_0 -semigroup e^{At} on the Hilbert space Z_E .

It follows that a state-space model for the Euler-Bernoulli beam with delayed actuator dynamics is given by

$$\dot{z}(t) = Az(t) + Bu_c(t) \quad (74)$$

where A and B are defined by (71) - (73). Moreover, for initial data $z_0 = (y_0, x_0, \phi_0) \in D(A)$ and $u_c(\cdot) \in L_2(0, T)$, (74) has a unique mild solution

$$z(t) = e^{At} z_0 + \int_0^t e^{A(t-s)} B u_c(s) ds \quad (75)$$

that provides a weak solution to the partial-functional differential equations (19) - (26).

TIMOSHENKO BEAM WITH ACTUATOR DYNAMICS

We proceed as in the case for the Euler-Bernoulli beam. If $A_2 = 0$, then set

$$Z_T^0 = W \times R \times R = W \times R^2 \quad (76)$$

with inner product

$$\langle z_0, \hat{z}^0 \rangle_{0T} = \langle w, \hat{w} \rangle_{\mathbb{W}} + x_1 \hat{x}_1 + x_2 \hat{x}_2. \quad (77)$$

Let $\mathcal{D}(A_0)$ be defined by

$$\mathcal{D}(A_0) = \left\{ \begin{bmatrix} w \\ x \end{bmatrix} \in \mathbb{Z}_T^0 \mid w \in \mathcal{D}(A_T) \right\} \quad (78)$$

and

$$A_0 = \begin{bmatrix} A_T & B_T & C_1 \\ 0 & A_1 \end{bmatrix}. \quad (79)$$

Likewise, let $B_0 : \mathbb{R} \rightarrow \mathbb{Z}_T^0$ be defined by

$$B_0 = \begin{bmatrix} 0 \\ B_1 \end{bmatrix}. \quad (80)$$

If $A_2 \neq 0$, then define \mathbb{Z}_T as

$$\mathbb{Z}_T = \mathbb{Z}_T^0 \times L_2(-r, 0; \mathbb{R}^2) = \mathbb{W} \times \mathbb{R}^2 \times L_2(-r, 0; \mathbb{R}^2) \quad (81)$$

with inner product

$$\langle z, \hat{z} \rangle_T = \langle z^0, \hat{z}^0 \rangle_{0T} + \int_{-r}^0 \langle \phi(s), \hat{\phi}(s) \rangle ds \quad (82)$$

where $z = (w, x, \phi)^T$ and $\hat{z} = (\hat{w}, \hat{x}, \hat{\phi})^T \in \mathbb{Z}_T$, respectively.

As for the Euler-Bernoulli beam we define A on $\mathcal{D}(A) \subseteq \mathbb{Z}_T$ by

$$\mathcal{D}(A) = \left\{ \begin{bmatrix} w \\ x \\ \phi \end{bmatrix} \in \mathbb{Z}_T \mid \begin{array}{l} y \in \mathcal{D}(A_T) \\ \phi \in H^1(-r, 0) \\ \phi(0) = x \end{array} \right\} \quad (83)$$

and

$$A \begin{bmatrix} w \\ x \\ \phi \end{bmatrix} = \begin{bmatrix} A_T w + B_T C_1 x \\ A_1 x + A_2 \phi(-r) \\ \phi'(\cdot) \end{bmatrix} \quad (84)$$

The input operator $B : R \rightarrow Z_T$ is defined by

$$B = \begin{bmatrix} 0 \\ B_1 \\ 0 \end{bmatrix}. \quad (85)$$

The following result follows from Theorem 2 and standard estimates from the theory of delay systems.

THEOREM 5. The operator B is bounded and A generates a C_0 -semigroup e^{At} on the Hilbert space Z_T .

Again it follows that a state space model for the Timoshenko beam with delayed actuator dynamics is of the form

$$\dot{z}(t) = Az(t) + Bu_c(t) \quad (86)$$

where A is defined by (83) - (84) and B is defined by (85).

ISOTROPIC RECTANGULAR PLATE

We assume that the control is applied such that in equation (35) $f(t, x, y) = \phi(x, y) u_c(t)$ where $\phi(x, y)$ is a given distribution belonging to $H^1(\Omega)$ and $u_c(t)$ modulates the applied force.

Let \mathcal{V} denote the "energy space"

$$\mathcal{V} = H^2(\Omega) \cap H_0^1(\Omega) \quad (87)$$

where $H^2(\Omega)$ and $H_0^1(\Omega)$ are the standard Sobolev spaces (see Ref. 16).

Let $X = L_2(\Omega)$ and define the differential operator K with domain

$\mathcal{D}(K) \subseteq \mathcal{X}$ by

$$\mathcal{D}(K) = \mathcal{V} \quad (88)$$

and

$$K\phi = \sqrt{\frac{D}{m}} \Delta\phi \quad (89)$$

It follows that the plate equation (35) with boundary condition (38) may be written as the second order equation

$$u_{tt} + K^2 u = \phi(x,y) u_c(t) \quad (90)$$

in $L_2(\Omega)$. We rewrite this as a first order system by using the "state"

$$z(t) = \begin{bmatrix} u(t,x) \\ u_t(t,x) \end{bmatrix}. \quad (91)$$

Let

$$\mathcal{Z}_p = \mathcal{V} \times L_2(\Omega) \quad (92)$$

and define the inner product

$$\begin{aligned} \langle z, \hat{z} \rangle &= D \int_{\Omega} [\Delta u(x,y) \Delta \hat{u}(x,y)] dx dy \\ &\quad + m \int_{\Omega} v(x,y) \hat{v}(x,y) dx dy \end{aligned} \quad (93)$$

where $z = (u,v)$ and $\hat{z} = (\hat{u}, \hat{v}) \in \mathcal{Z}_p$, respectively. As for the beams, $\langle z, z \rangle = \|z\|^2$ is the mechanical energy at the state z .

Let $\mathcal{D}(A_p) \subseteq \mathcal{Z}_p$ be defined by

$$\mathcal{D}(A_p) = \mathcal{D}(K^2) \times \mathcal{D}(K) \quad (94)$$

and

$$A_p = \begin{bmatrix} 0 & I \\ -K^2 & 0 \end{bmatrix}. \quad (95)$$

Also, define $B_p : R \rightarrow Z_p$ by

$$B_p = \begin{bmatrix} 0 \\ \phi(x,y) \end{bmatrix}. \quad (96)$$

The following is a direct consequence of standard results found in Refs. 17, 18 and 19.

THEOREM 6. The operator B_p is bounded and A_p generates a C_0 -group e^{At} on the Hilbert space Z_p .

As in the case of the beam structures, we have a state-space model for the plate of the form

$$\dot{z}(t) = A_p z(t) + B_p u(t) \quad (97)$$

where A_p and B_p are now defined by (94) - (96).

GENERAL FRAMEWORK

All of the problems formulated above fall into a specific class of distributed parameter systems of the form

$$\dot{z}(t) = Az(t) + Bu_c(t) \quad (98)$$

where A generates a C_0 -semigroup on an Hilbert space Z and $B : R \rightarrow Z$ is a bounded linear operator. The space Z is called the state-space and given an initial state $z_0 \in D(A)$, we know that

$$z(t) = e^{At} z_0 + \int_0^t e^{A(t-s)} Bu_c(s) ds \quad (99)$$

define (at least) weak solutions of the partial-differential equations that govern the motion of the particular structure. The particular model (Euler-Bernoulli beam, Timoshenko beam, Euler-Bernoulli beam with actuator dynamics and no delays, etc.) determine the space Z and the operators A and B . We summarize these spaces and operators for the cases presented above.

Euler-Bernoulli: No Actuator Dynamics

$$Z = \mathcal{W} \text{ as defined by (41) - (42)}$$

$$A = A_E \text{ as defined by (43) - (44)}$$

$$B = B_E \text{ as defined by (45)}$$

Timoshenko: No Actuator Dynamics

$$Z = \mathcal{W} \text{ as defined by (53) - (54)}$$

$$A = A_T \text{ as defined by (55) - (56)}$$

$$B = B_T \text{ as defined by (57)}$$

Euler-Bernoulli: Actuator Dynamics, No Delay

$$Z = Z_E^0 \text{ as defined by (63) - (64)}$$

$$A = A_0 \text{ as defined by (65) - (66)}$$

$$B = B_0 \text{ as defined by (67)}$$

Euler-Bernoulli: Actuator Dynamics with Delays

$$Z = Z_E \text{ as defined by (69) - (70)}$$

$$A = A \text{ as defined by (71) - (72)}$$

$$B = B \text{ as defined by (73)}$$

Timoshenko: Actuator Dynamics, No Delay

$$\bar{z} = \bar{z}_T^0 \text{ as defined by (76) - (77)}$$

$$A = A_0 \text{ as defined by (78) - (79)}$$

$$B = B_0 \text{ as defined by (80)}$$

Timoshenko: Actuator Dynamics with Delays

$$\bar{z} = \bar{z}_T \text{ as defined by (81) - (82)}$$

$$A = A \text{ as defined by (83) - (84)}$$

$$B = B \text{ as defined by (85)}$$

Isotropic Rectangular Plate

$$\bar{z} = \bar{z}_p \text{ as defined by (92) - (93)}$$

$$A = A_p \text{ as defined by (94) - (95)}$$

$$B = B_p \text{ as defined by (96)}$$

THE CONTROL PROBLEM

The abstract state-space formulation of the various beam and plate systems provides a convenient framework in which to formulate and approximate control problems. Recall that in all cases the number of controls available is finite, indeed for the problems considered here we have a single control.

As noted previously, the purpose of active control is to increase the effective damping; that is, to enhance the decay rate of unwanted vibrations. The decay rate can be understood in terms of the eigenvalues of the closed-loop system. Over the past thirty years a considerable literature has developed on the use of linear-quadratic control theory to design controllers for finite-dimensional system (see, for example, the excellent book by Kwackernaak & Sivan (Ref. 20)). While this theory has deficiencies, such as requiring accurate knowledge of the open-loop dynamics, it is a useful part of a comprehensive control design strategy. Accordingly, we shall formulate a linear-quadratic control problem for our (infinite-dimensional) Hilbert-space setting. The control laws we develop for the beam and plate models are based on this formulation.

All of the state-space formulations developed in the section above required a Hilbert space \mathcal{Z} , a dynamic operator A with $D(A) \subseteq \mathcal{Z}$ and an input operator $B: \mathbb{R} \rightarrow \mathcal{Z}$. We assume that A generates a C_0 -semigroup e^{At} and B is bounded.

In order to formulate an LQR problem, we introduce an output operator

$$C : Z \rightarrow R^k$$

and assume that C is bounded and linear. It may be helpful to think of C as a mapping that "reads out" physical meaningful quantities at certain locations on the structures (e.g. velocity or strain measurements). Mathematically, we require that C has the form

$$C_z = \begin{bmatrix} C_1 z \\ C_2 z \\ \vdots \\ C_n z \end{bmatrix} \quad (100)$$

where each "sensor" C_i , $i = 1, 2, \dots, n$ is a bounded linear functional from Z to R^1 . Examples will be given below.

One can now describe the control system which is governed by the state-equation in Z

$$\dot{z}(t) = Az(t) + Bu_c(t) \quad (101)$$

with initial data

$$z(0) = z_0 \in D(A) \quad (102)$$

and output in R^k

$$y(t) = Cz(t) \quad (103)$$

It should be noted that "output" is used here in the sense that it is a variable to be controlled. The control law we construct will require state feedback and we do not consider the estimation problem.

The optimal control problem on Z is to choose a control $u_c \in L_2(0, +\infty; R)$ to minimize the cost functional

$$J(z, u) = \frac{1}{2} \int_0^{+\infty} \{ \|y(t)\|_S^2 + R \|u_c(t)\|^2 \} dt \quad (104)$$

where $S \geq 0$ is a $k \times k$ semi-definite matrix, $R > 0$ and $\|y\|_S^2 = \langle Sy, y \rangle$ is the standard weighted semi-norm. It should be noted that the cost functional can be generalized to include cross-terms in y and u by formulating a quadratic weight on the composite vector $(y, u)^T$.

Let $Q : Z \rightarrow Z$ denote the self-adjoint bounded operator defined by

$$Q = C^* S C \quad (105)$$

where $C^* : R^k \rightarrow Z$ is the adjoint of C . Note that one can rewrite the cost function (104) in the equivalent form

$$J(z_0, u) = \frac{1}{2} \int_0^{+\infty} \{ \langle Qz(t), z(t) \rangle + \langle Ru_c(t), u_c(t) \rangle \} dt \quad (106)$$

and hence the optimal control problem described by (101) - (104) is the direct generalization of the standard finite dimensional (LQR)-problem. Much of the theory for the finite-dimensional problem carries over to this Hilbert space setting. In particular, we shall make use of the variation of parameters formula

$$z(t) = e^{At} z_0 + \int_0^t e^{A(t-s)} B u_c(s) ds \quad (107)$$

for the mild solution of (101) - (102).

A function $u \in L_2(0, +\infty; R)$ is an admissible control for the initial state z , or simply an admissible control for z , if $J(z, u)$ is finite; i.e., if the state $z(t)$ corresponding to the control $u(t)$ and the

initial condition $z(0) = z_0$ is in $L_2(0, \infty; E)$.

Let the operators A , B , Q , and R be as defined above. A bounded linear operator $\Pi : Z \rightarrow Z$ is a solution of the operator Riccati equation if Π maps the domain of A into the domain of A^* and satisfies the Riccati equation

$$A^* \Pi + \Pi A - \Pi B R^{-1} B^* \Pi + Q = 0. \quad (108)$$

The following result may be found in Ref. 15.

THEOREM 7. There exists a non-negative self-adjoint solution of the operator Riccati equation (108) if and only if, for each $z \in Z$, there is an admissible control for the initial state z . If Π is the minimal non-negative self-adjoint solution of (108), then the unique control $\bar{u}_c(\cdot)$ which minimizes J and the corresponding optimal trajectory $\bar{z}(\cdot)$ are given by

$$\bar{u}_c(t) = -R^{-1} B^* \Pi \bar{z}(t) = -K \bar{z}(t) \quad (109)$$

and

$$\bar{z}(t) = \mathcal{S}(t) z \quad (110)$$

where $\mathcal{S}(t)$ is the C_0 -semigroup generated by

$$[A - B R^{-1} B^* \Pi].$$

The semigroup e^{At} is called the open-loop semigroup and the semigroup $\mathcal{S}(t)$ is called the optimal closed-loop semigroup.

Note that if the open-loop system is exponentially stable, i.e. there exists $M_1, \alpha_1 > 0$ such that

$$\|e^{At}\| \leq M_1 e^{-\alpha_1 t}, \quad (111)$$

then $u_c(t) \equiv 0$ is an admissible control for all $z \in \mathbb{Z}$. In this case Theorem 7 applies.

In the beam and plate problems formulated in the previous sections, (111) does not hold. This is due to two factors; there is no damping in the models and for the beam problems there are rigid body modes. In order to overcome these problems we introduce damping into the models. In particular, if equation (35) is replaced by

$$\bar{m} u_{tt}(t,x,y) + \gamma \Delta u_t(t,x,y) + D \Delta^2 u(t,x,y) = f(t,x,y) \quad (112)$$

where the damping term $\gamma \Delta u_t(t,x,y)$ is added, $\gamma > 0$, then the basic state-space $\mathbb{Z}_p = \mathcal{V} \times L_2(\Omega)$ is unchanged. However, the operator (no damping) A_p given by (95) does change and for this case (112) leads to a new state operator

$$\tilde{A}_p = \begin{bmatrix} 0 & I \\ -K^2 & -\gamma \Delta \end{bmatrix} \quad (113)$$

with the same domain $D(\tilde{A}_p) = D(A_p)$. Moreover, $e^{\tilde{A}_p t}$ will satisfy a decay rate of the form (111). A similar (but slightly more complex) thing occurs if the damping term $\gamma \Delta u_t(t,x,y)$ is replaced by the so-called Kelvin-Voigt damping term $\gamma \Delta^2 u_t(t,x,y)$.

In the beam problems we added a viscous damping term to the beam models. As in the example above, the state-space \mathbb{Z} does not change but the state operator becomes modified much like A_p is changed to \tilde{A}_p . However, one still does not obtain an estimate of the form (111) because of rigid body modes. It happens that even though these modes do not have exponential decay rates, they are stabilizable. Thus, the basic Theorem 7 can be used to show that for each $z \in \mathbb{Z}$ the LQR problem

for all of the structures considered here has a unique optimal solution given by (109) where Π solves (108), provided that we add damping to the structural elements.

Another feature that is apparent from the Riccati equation (108) is that the adjoint operator A^* plays an essential role in the determination of Π . For the structural control problems, the operator A is a differential operator and for the case where there is no damping and no delays in the actuator, then $A = -A^*$. However, as indicated above it is essential to include damping and hence for all the damped systems it follows that $A \neq -A^*$.

The key point is that if one wishes to use approximations of the state operator A to solve the Riccati equation (108), then these approximations must also provide good estimates of A^* . This is particularly important when delays are included in the model (or if other types of damping models are used, see Refs. 2, 13 and 21). This turns out to be a crucial point that is often overlooked in finite element and modal control approaches to these problems.

CONSTRUCTION OF THE OUTPUT OPERATOR

We indicate the form of the output operator for the beam and plate control systems. We provide details for the Euler-Bernoulli beam problems and indicate the necessary changes for the Timoshenko models.

Recall the problem with no actuator dynamics. For the Euler-Bernoulli beam the state is given by (40), i.e.

$$z(t) = \begin{bmatrix} z_1(t) \\ z_2(t) \\ z_3(t) \\ z_4(t) \\ z_5(t) \\ z_6(t) \end{bmatrix} = \begin{bmatrix} \theta(t) \\ \omega(t) \\ \eta(t) + L\omega(t) \\ \xi(t) + \omega(t) \\ u_{xx}(t, x) \\ u_t(t, x) + x\omega(t) \end{bmatrix}. \quad (114)$$

Consider the problem where we measure $\theta(t)$, $\omega(t)$, $\eta(t) + L\omega(t)$, $\xi(t) + \omega(t)$, the average strain in neighborhoods of selected points $0 \leq \bar{x}_1 < \bar{x}_2 < \dots < \bar{x}_p \leq L$ along the beam and the average velocity in neighborhoods of selected points $0 \leq \hat{x}_1 < \hat{x}_2 < \dots < \hat{x}_q \leq L$ along the beam.

We proceed now to give the precise mathematical definitions needed to describe the above output operator. Let $\epsilon > 0$ and $x \in [0, L]$ be a fixed point along the beam. We consider the cases i) $x = 0$, ii) $x = L$, and iii) $0 < x < L$. If $x = 0$, let $m^\epsilon(x) = m^\epsilon(0)$ denote the bounded linear functional defined from $L_2(0, L)$ to \mathbb{R} by

$$[m^\epsilon(x)] \phi(\cdot) = [m^\epsilon(0)] \phi(\cdot) = \frac{1}{\epsilon} \int_0^\epsilon \phi(s) ds \quad (115)$$

If $x = L$, let $m^\epsilon(x) = m^\epsilon(L)$ denote the bounded linear functional defined by

$$[m^\epsilon(x)] \phi(\cdot) = [m^\epsilon(L)] \phi(\cdot) = \frac{1}{\epsilon} \int_{L-\epsilon}^L \phi(s) ds \quad (116)$$

If $0 < x < L$ we pick $\epsilon > 0$ such that $0 < x - \epsilon < x < x + \epsilon < L$ and let $m^\epsilon(x)$ denote the bounded linear functional defined by

$$[m^e(x)] \phi(\cdot) = \frac{1}{2e} \int_{x-e}^{x+e} \phi(s) ds \quad (117)$$

If $m^e(x)$ is defined by (115) - (117) then the mean strain in the e -neighborhood of a point \bar{x}_i with $0 < \bar{x}_i - e < \bar{x}_i < \bar{x}_i + e < L$ is given by

$$[m^e(\bar{x}_i)] u_{xx}(t) = \frac{1}{2e} \int_{\bar{x}_i-e}^{\bar{x}_i+e} u_{xx}(t,s) ds. \quad (118)$$

Let $e > 0$, $0 < \bar{x}_1 < \bar{x}_2 < \dots < \bar{x}_p < L$ and $0 < \hat{x}_1 < \hat{x}_2 < \dots < \hat{x}_q < L$ be such that $0 < \bar{x}_i - e < \bar{x}_i < \bar{x}_i + e < L$, $i = 1, 2, \dots, p$ and $0 < \hat{x}_i - e < \hat{x}_i < \hat{x}_i + e < L$, $i = 1, 2, \dots, q$. Let $c_s : Z \rightarrow R^p$ and $c_v : Z \rightarrow R^q$ be defined by

$$c_s z = \begin{bmatrix} [m^e(\bar{x}_1)] z_5(\cdot) \\ [m^e(\bar{x}_2)] z_5(\cdot) \\ \vdots \\ [m^e(\bar{x}_p)] z_5(\cdot) \end{bmatrix}, \quad (119)$$

and

$$c_v z = \begin{bmatrix} [m^e(x_1)] z_6(\cdot) \\ [m^e(x_2)] z_6(\cdot) \\ \vdots \\ [m^e(x_q)] z_6(\cdot) \end{bmatrix}, \quad (120)$$

respectively. We now define the output operator $c_E : Z \rightarrow R^k$ where $k = 4 + p + q$ by

$$C_E z = \begin{bmatrix} z_1 \\ z_2 \\ z_3 \\ z_4 \\ \text{---} \\ C_S z \\ \text{---} \\ C_V z \end{bmatrix}. \quad (121)$$

In summary then, for the Euler-Bernoulli beam without actuator dynamics, the output

$$y(t) = C_E z(t)$$

has its first four components given by $y_1(t) = \theta(t)$, $y_2(t) = \omega(t)$, $y_3(t) = [u_t(t, L) + L\omega(t)]$ and $y_4(t) = [u_{xt}(t, L) + \omega(t)]$. The next p components are mean strains $y_i(t) = [M^E(\bar{x}_i)] u_{xx}(t, \cdot)$, $i = 1, 2, \dots, p$ and the last of components are the mean velocities $y_i(t) = [M^E(\hat{x}_i)] [u_t(t, \cdot)] + \hat{x}_i \omega(t)$. We can add weights to the output by selecting the $k \times k$ matrix S_E to be a diagonal matrix of the form

$$S_E = \text{dia } (c_1^2, c_2^2, \dots, c_k^2) \quad (122)$$

where c_i , $i = 1, 2, \dots, k$ are real constants.

The introduction of the delayed actuator dynamics for the Euler-Bernoulli beam problem leads to additional states for the actuator $x(t) = \text{col } (x_1(t), x_2(t))$ and (in case $A_2 \neq 0$) the history function $x(\cdot) = \text{col } (x_1(\cdot), x_2(\cdot)) \in L_2(-r, 0; \mathbb{R}^2)$. To account for these features we augment the output operator C_E defined by (121) and the weighting matrix defined by (122) to include the two actuator states

$x_1(t)$ and $x_2(t)$. We did not "sense" the history states (although this is clearly possible).

The Timoshenko beam model is treated in a completely analogous fashion. The output operator for the plate problem is also constructed to read out the mean velocities at selected points $(\hat{x}_i, \hat{y}_i) \in \Omega$, $i = 1, 2, \dots, q$ and mean values for the Laplacian $[u_{xx}(t, x, y) + u_{yy}(t, x, y)]$ at selected points $(\bar{x}_i, \bar{y}_i) \in \Omega$, $i = 1, 2, \dots, p$. The output operator $C_p : Z_p \rightarrow R^{p+q}$ is again a bounded linear map.

FORM OF THE GAIN OPERATOR K

As noted above the optimal control is of the form

$$\bar{u}_c(t) = -R^{-1} B^* \Pi \bar{z}(t) = -K \bar{z}(t)$$

where $K : Z \rightarrow R$ is the optimal gain operator. The particular form of K depends only on the choice of the state-space Z and the corresponding inner product $\langle \cdot, \cdot \rangle$. In each of the applications above, the state-space has a specific Hilbert space structure and the Riesz Representation Theorem (see Ref. 22) can be applied to yield a specific form for the optimal feedback gain operator. We present these representations for the basic problems.

Euler-Bernoulli: No Actuator Dynamics

$$\begin{aligned} K_E z_E(t) = & k_1 \theta(t) + k_2 \omega(t) \\ & + k_3 [u_t(t, L) + L\omega(t)] \\ & + k_4 [u_{xt}(t, L) + \omega(t)] \\ & + \int_0^L k_5(x) [u_{xx}(t, x)] dx \\ & + \int_0^L k_6(x) [u_t(t, x) + x\omega(t)] dx \end{aligned} \quad (123)$$

where $k_5(\cdot) \in L_2(0,L)$ and $k_6(\cdot) \in L_2(0,L)$ are the functional gains for strain and velocity, respectively.

Timoshenko: No Actuator Dynamics

$$\begin{aligned}
 K_T z_T(t) = & k_1 \theta(t) + k_2 \omega(t) \\
 & + k_3 [u_t(t,L) + L\omega(t)] \\
 & + k_4 [\psi_t(t,L) + \omega(t)] \\
 & + \int_0^L k_5(x) [u_t(t,x) + x\omega(t)] dx \\
 & + \int_0^L k_6(x) [\psi_t(t,x) + \omega(t)] dx \\
 & + \int_0^L k_7(x) [\psi_x(t,x)] dx \\
 & + \int_0^L k_8(x) [u_x(t,x) - \psi(t,x)] dx .
 \end{aligned} \tag{124}$$

Euler-Bernoulli: Actuator Dynamics, No Delay

Here $z = z_E^0 = \text{col} (z_E, x_1, x_2)$ where z_E is defined by (40) and

$$K_{EO} z_E^0(t) = K_E z_E(t) + k_7 x_1(t) + k_8 x_2(t) . \tag{125}$$

Euler-Bernoulli: Actuator Dynamics with Delays

Here $z = \text{col} (z_E^0, \phi) = (z_E, x_1, x_2, \phi_1(\cdot), \phi_2(\cdot))^T$ and

$$K_{ED} z(t) = K_{EO} z_E^0(t) + \int_{-\tau}^0 k_9(s) \phi_1(s) ds + \int_{-\tau}^0 k_{10}(s) \phi_2(s) ds . \tag{126}$$

Timoshenko: Actuator Dynamics, No Delay

Here $z = z_T^0 = \text{col} (z_T, x_1, x_2)$ where z_T is defined by (75) and

$$K_{T0} z_T^0(t) = K_T z_T(t) + k_9 x_1(t) + k_{10} x_2(t) \quad (127)$$

Timoshenko: Actuator Dynamics with Delays

Here $z = \text{col} (z_T^0, \phi) = (z_T, x_1, x_2, \phi_1(\cdot), \phi_2(\cdot))^T$ and

$$K_{TD} z(t) = K_{T0} z_T^0(t) + \int_{-r}^0 k_{11}(s) \phi_1(s) ds + \int_{-r}^0 k_{12}(s) \phi_2(s) ds. \quad (128)$$

Isotropic Rectangular Plate

$$\begin{aligned} K_P z_P(t) = & \int_{\Omega} k_1(x,y) \Delta u(t,x,y) dx dy \\ & + \int_{\Omega} k_2(x,y) u_t(t,x,y) dx dy \end{aligned} \quad (129)$$

where $k_1(x,y) = \Delta \tilde{k}(x,y)$ with $\tilde{k}_1(\cdot, \cdot) \in \mathcal{V}$ and $k_2(\cdot, \cdot) \in L_2(\Omega)$.

Equations (123) - (129) indicate the basic computation problem is to find numerical schemes for approximating the various gains and functional gains that appear in the representations (123) - (129). This is the objective of the computational algorithms described in the next section.

NUMERICAL PROCEDURES

In order to develop numerical schemes for solving the LQR problem defined by (101) - (104) one must introduce approximations and analyze the convergence. In this section we review the basic ideas behind the approximation methods and state a general convergence result due to Gibson (Ref. 14).

In order to obtain approximate solutions to the Riccati operator equation (108), it is necessary to approximate the operators A , A^* , B , B^* and Q . Since $Q = C^* S C$, this implies that one must also approximate C and C^* . For the problems considered here, the most difficult aspect of this problem is the development of convergent approximation schemes for A and A^* . More to the point, we need approximations of the semigroups e^{At} and e^{A^*t} .

An approximating sequence for the control problem defined by equations (101) - (104) is a sequence of finite dimensional subspaces $\mathbb{Z}^N \subseteq \mathbb{Z}$, projections $P^N : \mathbb{Z} \rightarrow \mathbb{Z}^N$, and linear operators

$$\left. \begin{aligned} A^N &: \mathbb{Z}^N \rightarrow \mathbb{Z}^N \\ B^N &: R \rightarrow \mathbb{Z}^N \\ C^N &: \mathbb{Z}^N \rightarrow R^k \end{aligned} \right\} \quad (130)$$

satisfying

$$\left. \begin{aligned} \|P^N\| &\leq 1, \quad N = 1, 2, \dots, \\ P^N z &\rightarrow z \quad \text{for all } z \in \mathbb{Z}, \end{aligned} \right\} \quad (131)$$

$$\left. \begin{aligned} B^N u &\rightarrow Bu, \quad \text{for all } u \in R \\ Q^N P^N z &= [C^N]^* S C^N P^N z \rightarrow Qz, \quad \text{for all } z \in Z \end{aligned} \right\} \quad (132)$$

The semigroups $e^{A^N t}$, $e^{[A^N]^* t}$ must have the property

$$\left. \begin{aligned} e^{A^N t} P^N z &\rightarrow e^{At} z \\ e^{[A^N]^* t} P^N z &\rightarrow e^{A^* t} z \end{aligned} \right\} \quad (133)$$

for all $z \in Z$, uniformly for t in compact intervals (see Ref. 14). The construction of approximating sequences for the control problem (101) - (104) is a problem in numerical analysis and approximation theory. The basic idea is to approximate the (differential) operator by a finite-dimensional operator A^N (i.e. using finite elements, finite differences, modal truncation, etc.) and then showing that A^N converging to A implies (133). This is a nontrivial problem in functional analysis. In fact, the basic question (when does $A^N P^N z \rightarrow Az$ imply (133)) is not yet fully understood. A partial answer to the convergence question is provided by the now famous Trotter-Kato Theorem (see Ref. 23). Although there are a number of extensions of this theorem (see Theorem 3.1 in Ref. 6), we state a simple version that is sufficient for the problems considered here.

THEOREM 8 (TROTTER-KATO THEOREM). Let A be the generator of a strongly continuous semigroup e^{At} satisfying $\|e^{At}\| \leq Me^{\beta t}$. Assume that A^N is a sequence of operators generating strongly continuous semigroups $e^{A^N t}$ satisfying

$$1) \quad \|e^{A^N t}\| \leq Me^{\beta t}, \quad N = 1, 2, \dots$$

ii) $A^N z \rightarrow Az$ for $z \in D$, D dense in Z

iii) There exists λ_0 with $\text{Re}(\lambda_0) \geq \beta$ such that $(A - \lambda_0 I)D$ is dense in Z . Then $e^{A^N t} z \rightarrow e^{At} z$ for all $z \in Z$ and the convergence is uniform for $t \in [0, T]$.

In terms of numerical analysis, condition i) is the stability requirement and condition ii) is the consistency requirement. Thus convergence of the approximation scheme is dependent upon having a consistent and stable numerical scheme that also satisfies the technical condition iii). Any numerical scheme that does not satisfy conditions i) - iii) may not produce an approximating sequence for the control problem (101) - (104). Moreover, even if the approximating sequence is such that i) - iii) are satisfied, there is no assurance that the dual semigroups will converge strongly, i.e. that $e^{[A^N]^*} p_z^N \rightarrow e^{At^*}_z$

The following convergence results were first established by Gibson (Refs. 12-14). We assume that we have an approximating sequence $\Sigma^N = (Z^N, P^N, A^N, B^N, C^N)$ that satisfies (130) - (133) and consider the approximating Riccati equation

$$[A^N]^* \Pi^N + \Pi^N A^N - \Pi^N B^N R^{-1} [B^N]^* \Pi^N + Q^N = 0. \quad (134)$$

The basic issue is the convergence of Π^N to Π .

THEOREM 9. Suppose that Σ^N satisfies (130) - (133) and for each N there is a non-negative self-adjoint operator Π^N that solves (134). If there exist constants $M, \hat{M} > 0, \beta > 0$ (independent of N) such that the closed-loop semigroup

$$S^N(t) = \exp ([A^N - B^N R^{-1} [B^N]^* \Pi^N] t) \quad (135)$$

satisfies

$$\|\mathcal{S}^N(t)\| \leq M e^{-\beta t}, \quad t > 0, \quad (136)$$

and

$$\|\Pi^N\| \leq \hat{M}, \quad (137)$$

then the operator Riccati equation (108) has a non-negative self-adjoint solution Π and for each $z \in \mathbb{Z}$

$$\Pi^N P_z^N \rightarrow \Pi z \quad (138)$$

and

$$\mathcal{S}^N(t)z \rightarrow \mathcal{S}(t)z \quad (139)$$

uniformly in $t > 0$.

The approximating gain operators are given by

$$K^N = R^{-1} [B^N]^* \Pi^N. \quad (140)$$

The crucial issue is the convergence of K^N to the optimal gain operators K defined by (109). Since our structural control problems have a finite number of controls (i.e. one input), the following result applies to our problems.

THEOREM 10. Assume all of the conditions in Theorem 9 hold. If the number of inputs is finite, then

$$\|K^N P^N - K\| \rightarrow 0 \quad (141)$$

as $N \rightarrow \infty$.

A proof of this result may be found in Ref. 13 and in the preprint Ref. 14. In order to use this result one must show that the approximation scheme one proposes to use to solve the control satisfies (130) - (133) and (136) - (137). Usually it is not difficult to

establish (131) and (132) and most of the effort in terms of numerical analysis comes from verifying conditions (133), (136) and (137).

The Trotter-Kato Theorem is the basic tool needed to establish (133). The work required to establish (136) and (137) is essentially the same as showing the approximating systems are all uniformly (with respect to N) stabilizable (see Ref. 13, Ref. 14 and Ref. 24). This can be difficult. However, for damped structures and many of the "standard schemes," (136) - (137) can often be shown to hold. We turn now to a brief description of the approximation schemes for the various applications.

While the approximation theory we employ is rooted in the state-space formulation, it is important to employ 'physical' insights when constructing specific approximation schemes. When considering the Euler-Bernoulli beam model, for example, it is helpful to keep in mind that the "infinite" dimensional aspect of the state-space is engendered by the fifth and sixth components of the state-vector and that these are each related to the beam deflection [i.e. $z_5 \sim u_{xx}$, while $z_6 \sim u_t$]. Thus, if one thinks of approximating the deflection by a suitable combination of shape function

$$u(t,x) = \sum \alpha_i(t) h_i(x)$$

then the basis functions used to approximate z_5 would be the h_i'' , while those used to approximate z_6 would be h_i . In addition, the basis functions should satisfy the essential boundary conditions.

EULER-BERNOULLI BEAM APPROXIMATION SCHEME

We consider a uniform grid with N 'panels' on the interval $[0, L]$. To represent deflections of the beam we employ cubic B -splines, which form an $(N + 3)$ -parameter family of C^1 functions (see Refs. 25 and 26). The elements of this family are denoted by $B_i^N(\cdot)$, $i = -1, 0, 1, \dots, N+1$. We shall abuse notations and suppress the dependence on the mesh parameter N . The domain of the $\{B_i\}$ is the interval $[0, L]$. Each of the B_i can be constructed by stretching and shifting the argument of a fundamental cubic-spline, $B : [R] \rightarrow R$. The fundamental spline is supported on the interval $[-2, 2]$ (i.e. it's identically zero outside this interval). A graph of the fundamental spline is shown in Figure 3. To construct an element $B_i(\cdot)$ one employs the rule

$$B_i(x) \equiv B(N \cdot (x/L) - i) . \quad (142)$$

The essential boundary conditions for the deflections of the Euler-Bernoulli beam require that the shape functions and their first derivatives should vanish at the root ($x = 0$). Thus, we are led to use combinations of the B -splines that satisfy these two conditions. This leads to the $(N + 1)$ parameter family of shape functions

$$h_1(x) \equiv B_0(x) - 2 [B_1(x) + B_{-1}(x)] \quad (143)$$

$$h_i(x) \equiv B_i(x) , \quad i = 2, \dots, N+1 \quad (144)$$

The shape functions are used to construct basis vectors in the state-space $Z(= \mathfrak{H})$ as defined by (41) - (42). To represent the "beam-velocity" we use the vectors

$$e_i = [0, 0, h_i(L), h_i(L), 0, h_i(\cdot)]^T \quad (145)$$

($i = 1, 2, \dots, N+1$).

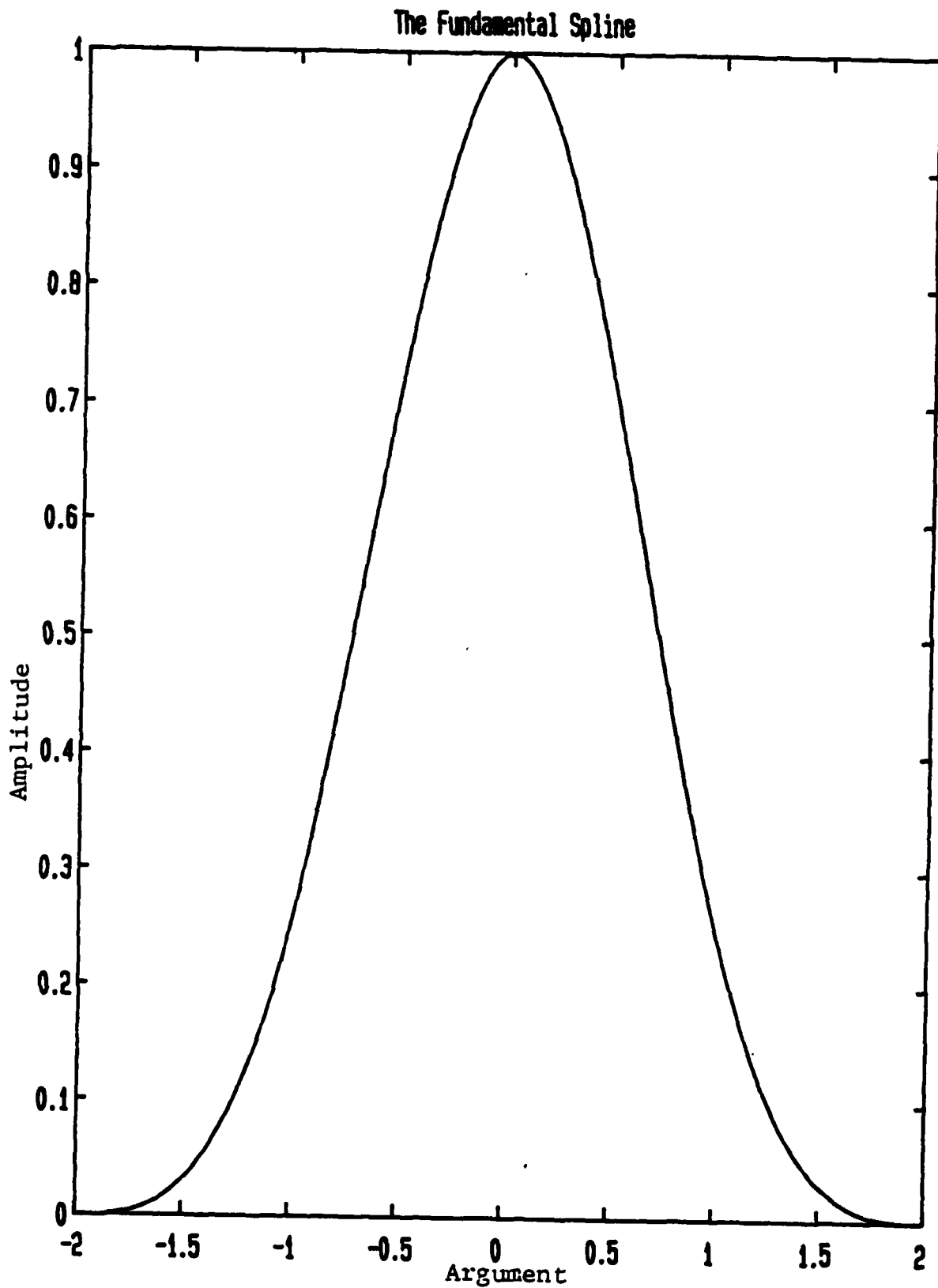


Figure 3. Fundamental Spline

Note that each e_i has been constructed to satisfy the tip end-conditions. The 'beam-stress' will be presented by the vectors

$$e_{N+1+i} = [0, 0, 0, 0, h_i''(\cdot), \theta] \quad (146)$$

($i = 1, 2, \dots, N+1$).

In addition to the beam deflections one must, of course, also include the hub motions in the finite-dimensional model. For the hub velocity $[\omega(t)]$ we employ the element

$$e_0 = [0, 1, L, 1, 0, x]^T \quad (147)$$

while for the hub position the element is

$$e_{-1} = [1, 0, 0, 0, 0, 0]^T. \quad (148)$$

The subspace \mathcal{Z}^N is generated as the span of the set $\{e_i\}$ and has dimensions $(2N + 4)$, i.e.

$$\mathcal{Z}^N = \text{span} \{e_i / i = -1, 0, \dots, 2N+2\} \quad (149)$$

where the e_i are defined by (142) - (148).

Following the general procedure outlined above leads to the Galerkin approximation for the system (101) - (103) restricted to the subspace \mathcal{Z}^N . The form of this model is

$$G_E^N \dot{\alpha}^N(t) = H_E^N \alpha^N(t) + E_E^N u(t) \quad (150)$$

$$y^N(t) = C_E^N \alpha^N(t) \quad (151)$$

The components of α^N (i.e. $\alpha_{-1}, \alpha_0, \dots, \alpha_{2N+2}$) are the co-ordinates for the representation of the state in terms of our basis for \mathcal{Z}^N .

That is,

$$z^N(t) = \sum_{i=-1}^{2N+2} \alpha_i(t) e_i^N. \quad (152)$$

The matrix G_E^N is in the form

$$G_E^N = \left[\begin{array}{ccc|ccc|c} 1 & 0 & 0 & & & 0 & 0 \\ 0 & f_0 & f_1 & \dots & \dots & f_{N+1} & 0 \\ \hline 0 & f_1 & & & & & \\ & \vdots & & & G_1 & & 0 \\ & \vdots & & & & & \\ & f_{N+1} & & & & & \\ \hline 0 & & & & 0 & & I \end{array} \right] \quad (153)$$

where the scalars f_i ($i = 0, 1, \dots, N+1$) are defined by

$$f_0 = 1/3 + [I_A + m_c L^2 + I_c]/\rho L^3$$

$$f_i = [m_c h_i(L) L + I_c h_i'(L)]/\rho L^3$$

and the $(N+1) \times (N+1)$ symmetric matrix G_1 is given by

$$G_1 = [m_c h_i(L) h_j(L) + I_c h_i'(L) h_j'(L)$$

$$+ \rho \int_0^L h_i(x) h_j(x) dx]/\rho L^3.$$

I is the identity matrix of order $(N+1)$ and

$$H_E^N = \begin{bmatrix} 0 & 1 & | & 0 & | & 0 \\ 0 & 0 & | & & | & \\ \hline & 0 & | & 0 & | & -\alpha G_2 \\ \hline 0 & & | & I & | & 0 \end{bmatrix} \quad (154)$$

where $\alpha = (EI/\rho L^4)$ is a frequency parameter and

$$G_2(1,j) = L \int_0^L h_i''(x) h_j''(x) dx .$$

E_E^N is a $(2N+4)$ component column matrix with all zeroes except for $(1/\rho L^3)$ in the second entry.

Referring to equation (121) it is seen that the C^N matrix has $(4 + p + q)$ rows and $(2N+4)$ columns. This is most easily described by considering the individual rows (or blocks of them). The first output is the angular position θ and the corresponding row is given by

$$C_E^N(1, \cdot) = [1, 0, 0, 0] , \quad (155)$$

where the block 0 is an $(N+1)$ vector. The second row (angular velocity ω) is given by

$$C_E^N(2, \cdot) = [0, 1, 0, 0] . \quad (156)$$

The third output is the tip-mass velocity and its row in C_E^N is

$$C_E^N(3, \cdot) = [0, L, h^N(L), \dots, h_{N+1}^N(L), 0] . \quad (157)$$

The fourth output is the angular velocity of the tip-mass and is given by

$$C_E^N(4, \cdot) = [0, 1, h'(L), \dots, h'_{N+1}(L), 0] . \quad (158)$$

The next block of p outputs correspond to measurement of the beam strain at specified points (\bar{x}_i) on the beam. A typical row in this block is

$$C_E^N(4 + i, \cdot) = [0, 0, 0, \mathbb{M}^e(\bar{x}_i)h''(\cdot), \dots, \mathbb{M}^e(\bar{x}_i)h_{N+1}''(\cdot)] \quad (159)$$

where $\mathbb{M}^e(\bar{x}_i)$ is the approximation to the delta function (see equation (117)). The final block of q outputs describe measurement of the total beam velocity at specified points (\hat{x}_i) on the beam. A typical row in this block is

$$C_E^N(4 + p + i, \cdot) = [0, \hat{x}_i, \mathbb{M}^e(\hat{x}_i) h_1(\cdot), \dots, \mathbb{M}^e(\hat{x}_i) h_{N+1}(\cdot), 0] \quad (160)$$

TIMOSHENKO BEAM APPROXIMATION SCHEME

For the Timoshenko beam the state-space $Z (= \mathbb{W}) = R \times R \times R \times R \times L_2 \times L_2 \times L_2 \times L_2$ (see (53), (54)). The fifth co-ordinate is related to the beam's transverse velocity $[u_t]$ while the sixth is related to the angular velocity $[\psi_t]$. The seventh co-ordinate is the curvature $[\psi_x]$ and the eighth is the shear deformation $[u_x - \psi]$. If one thinks of approximating the functions u and ψ then it is 'natural' to combine the $(N+3)$ cubic B -splines to enforce the essential boundary conditions on u and $[u_t(t,0) = \psi_t(t,0) = 0]$. This leads to the $(N+2)$ parameter family of shape functions that vanish at the left end:

$$q_0(x) = B_0(x) - 4 B_{-1}(x) \quad (161)$$

$$q_1(x) = 4 B_1(x) - B_0(x) \quad (162)$$

$$q_i(x) \equiv B_i(x), \quad i = 2, 3, \dots, N+1 \quad (163)$$

The basis vectors for the lineal velocity are

$$e_i \equiv [0, 0, q_i(L), 0, q_i(\cdot), 0, 0, 0]^T \quad (164)$$

$i = 0, 1, \dots, N+1$. Similarly the basis elements for the rotational velocity are

$$e_{n+2+i} = [0, 0, 0, q_i(L), 0, q_i(\cdot), 0, 0]^T. \quad (165)$$

$i = 0, 1, \dots, N+1$. To represent the ψ distribution the basis elements are

$$e_{2N+4+i} = [0, 0, 0, 0, 0, 0, q_i'(\cdot), -q_i(\cdot)] \quad (166)$$

while the basis elements for the u_x distribution is

$$e_{3N+6+i} = [0, 0, 0, 0, 0, 0, 0, q_i'(\cdot)] \quad (167)$$

As in the Euler-Bernoulli case, the hub motions require the elements

$$e_{-1} = [1 \ 0 \ 0 \ 0 \ 0 \ 0 \ 0 \ 0]^T \quad (168)$$

and

$$e_0 = [0 \ 1 \ L \ 1 \times 1 \ 0 \ 0]^T. \quad (169)$$

The subspace generated by the $\{e_i\}$ defined by (161) - (164) is again denoted by

$$Z^N = \text{span} \{e_i / i = -1, 0, \dots, 4N+4\} \quad (170)$$

and is $[4N+6]$ dimensional.

Again one applies the general theory for approximating the system to produce a model of the form

$$G_T^N \dot{x}^N(t) = H_T^N x^N(t) + E_T^N u(t) \quad (171)$$

$$y^N(t) = C_T^N x^N(t) \quad (172)$$

In this case the square matrices G_T^N and H_T^N are of order $(4N+6)$ and E_T^N is a compatible column matrix. The matrix C_T^N has $(4N+6)$ columns and $(4+p+q)$ rows.

EULER-BERNOULLI WITH ACTUATOR DYNAMICS: NO DELAY

In this case the state space $Z (= Z_E^0)$ is the 'Euler-Bernoulli' state-space y augmented with the two additional actuator states [see (63) - (64)]. Because of the cascade structure of the system (62) it is relatively simple to extend the approximations used for the Euler-Bernoulli beam with no actuator (i.e. (143) - (144)) to produce the approximation for Z_E^0 . Specifically, each of the $(2N+4)$ basis vectors defined by (145) - (148) can be injected into Z_E^0 by augmenting two zeroes in the places for the actuator states. The additional basis vectors needed to cover the actuator states are taken as

$$e_{2N+5} = (0, 1, 0) \quad (173)$$

and

$$e_{2N+6} = (0, 0, 1) , \quad (174)$$

where 0 is the zero vector in y (defined by (41) - (42)).

With these basis vectors in hand it is clear that the subspace Z_{0E}^N is $(2N+6)$ dimensional and the standard procedure is used to generate the matrices needed to represent the approximating system. In fact the cascade structure of the system leads to a simple block structure for the matrices. More is said about this feature in the next section.

EULER-BERNOULLI WITH DELAYED ACTUATOR STATES

The inclusion of delays in the dynamical model for the actuator leads to some complication in the approximation procedures. Because

the actuator is linked to the Euler beam in "cascade" fashion the state-space \mathbb{Z}_F has the product structure described above (see (69)).

$$\mathbb{Z}_E = \mathbb{Y} \times \mathbb{R}^2 \times L^2(-r, 0; \mathbb{R}^2) .$$

Moreover, the dynamics of the coupled system has the cascade structure

$$\dot{y}(t) = A_E y(t) + B_E C_1 x(t) \quad (175)$$

$$\dot{x}(t) = A_1 x(t) + A_2 x(t-r) + B_1 u_c(t) \quad (176)$$

We develop the approximation for this system in two stages.

Firstly, using the scheme discussed above, one approximates the operator A_E and hence the Euler-Bernoulli dynamics. This leads to the system (150) which can be put in normal form by (effectively) inverting the Gram matrix G_0^N . Define the matrices A_E^N and F_E^N as

$$A_E^N \equiv [C_E^N]^{-1} H_E^N \quad (177)$$

$$F_E^N \equiv [C_E^N]^{-1} E_E^N C_1 . \quad (178)$$

This approximate Euler-Bernoulli model when coupled with the delayed actuator can be written as the delay differential system

$$\begin{aligned} \dot{z}^N(t) = & \begin{bmatrix} A_E^N & F_E^N \\ 0 & A_1 \end{bmatrix} z^N(t) + \begin{bmatrix} 0 & 0 \\ 0 & A_2 \end{bmatrix} z^N(t-r) \\ & + \begin{bmatrix} 0 \\ B_1 \end{bmatrix} u_c(t) \end{aligned} \quad (179)$$

Here z^N has dimension $(2N+6)$.

The system (179) is still "infinite dimensional" because of the history term $z^N(t-r)$. There are many numerical schemes for constructing approximations for such delay-differential systems [Refs. 6-8, 13].

The averaging scheme [see Ref. 6] uses piecewise constant functions with a uniform grid (say M sub-intervals) on the interval $[-r, 0]$. This leads to an (approximating) system of ordinary differential equations.

$$\dot{v}^{N,M}(t) = A_E^{N,M} v^{N,M}(t) + B_E^{N,M} u_c(t) \quad (180)$$

where $v^{N,M}$ is a vector of dimension $(M+1)(2N+6)$. The matrix $A_E^{N,M}$ is given by

$$A_E^{N,M} = \begin{bmatrix} A_E^N & F_E^N & 0 & . & . & . & 0 & 0 \\ 0 & A_1 & 0 & . & . & . & 0 & A_2 \\ & & \frac{M}{r} I & -\frac{M}{r} I & & & & \\ & & & & & & & \\ & & & & & & & \\ & & & & & & & \\ 0 & 0 & & \frac{M}{r} I & & & -\frac{M}{r} I & \end{bmatrix} \quad (181)$$

where again I is the identity of order $(2N+6)$. The control matrix $(M+1)(2N+6) \times 1$ is

$$B_E^{N,M} = \begin{bmatrix} 0 \\ B_1 \\ 0 \\ \vdots \\ 0 \end{bmatrix}, \quad (182)$$

while the output matrix is

$$C_E^{N,M} = \begin{bmatrix} C_E^N & 0 & 0 \\ 0 & \alpha I & 0 \end{bmatrix}, \quad (183)$$

where I is the (2×2) identity and α is a scalar. Clearly $C_E^{N,M}$ has $(6+p+q)$ rows; the last two rows read out the actuator 'states' $x_1(t)$ and $x_2(t)$.

There are several important observations that can be made about the system (180) with dynamical matrix $A_E^{N,M}$ (181). First, the $A_E^{N,M}$ has a block structure that is independent of the details in the delay differential equation (179). Specifically, the matrix operating on $z^N(t)$ (see (181)) appears in the upper left block of $A_E^{N,M}$ while the matrix operating on the delayed 'state' $z^N(t-r)$ is in the upper right block. The main diagonal below the $(1,1)$ block has $(-M/r) \cdot I$ in each block, while the subdiagonal has blocks with $(M/r) \cdot I$.

The $(1,1)$ block, itself has some structure with the Euler approximation $[A_E^N]$ in the upper left and the (2×2) actuator matrix A_1 in the lower right. The term F_E^N in the upper right depends on C_0^N and H_0^N from the Euler approximation [see (178)] and on the actuator state-to-torque matrix C_1 [see (61)].

The matrix in the upper right block of $A_E^{N,M}$ has the (delayed) actuator matrix A_2 as its only non-zero entry. Similarly the control matrix $B_E^{N,M}$ has the (1×2) actuator control matrix B_1 in its only non-zero block.

The output matrix $C_E^{N,M}$ has zero blocks corresponding to the 'history' 'states'. That is, the output depends on the first $(2N+6)$ element 'block' in the $(M+1)(2N+6)$ vector $v^{N,M}$.

In the task of assembling the matrices $A_E^{N,M}$, $B_E^{N,M}$ and $C_E^{N,M}$ one thinks of the matrices C_E^N , H_E^N , F_E^N and C_E^N as "data" (describing approximate Euler beam dynamics). Similarly, the matrices A_1 , A_2 , B_1 and C_1 , and the scalar r , are "data" for the actuator. This view is also exploited when the Timoshenko beam is coupled to the actuator.

Finally, since only the last two components of the $(2N+6)$ vector $z^N(t-r)$ are really needed, it is clear that considerable saving is possible. In particular one can compress $v^{N,M}$ to length $(2N+6) + 2M$ without affecting the input-output behavior of the approximating system [see Ref. 10]. Indeed, if A_2 has rank " ℓ " ($\ell \in [0,1,2]$), then $v^{N,M}$ can be compressed to length $(2N+6) + \ell M$. Of course, with $\ell = 0$ the A_2 matrix is null and the system is identical to the non-delayed actuator case.

TIMOSHENKO BEAM WITH ACTUATOR DYNAMICS

In view of the discussion of the structure of the delayed actuator model for the Euler-Bernoulli beam, it is possible to describe the case for a Timoshenko beam (with and without delays) very simply.

The matrices for this case are of the same form as $A_E^{N,M}$ except that the blocks A_E^N , F_E^N and C_E^N are replaced by the corresponding blocks from the Timoshenko model. Specifically

$$A_T^N \equiv [G_T^N]^{-1} H_T^N, \quad (185)$$

$$F_T^N \equiv [G_T^N]^{-1} E_T^N C_1, \quad (186)$$

and

$$C_T^{N,M} = \begin{bmatrix} C_T^N & 0 & 0 \\ 0 & \alpha I & 0 \end{bmatrix}. \quad (187)$$

The dimension of the system is $(4N+8) + 2M$ where, as before, l is the rank of A_2 .

ISOTROPIC RECTANGULAR PLATE

The state space model for this system is given by equations (91) - (96). In particular, if $u(t,x,y)$ is the transverse deflection of a point on the plate then our state is identified with

$$z(t) = \begin{bmatrix} u(t,x,y) \\ u_t(t,x,y) \end{bmatrix}. \quad (188)$$

The (clamped) boundary conditions require that u vanishes on the boundary of the rectangular domain and also that the Laplacian $(u_{xx} + u_{yy})$ vanish there.

Again one thinks of expressing the deflection in terms of shape functions, say $\phi(x,y)$. Because the geometry of the boundary is rectangular, it is convenient to express each shape function as a product of one-space variable functions. Specifically, we write

$$u(t,x,y) = \sum_{i,j} \alpha_{ij}(t) q_i(x) q_j(y) . \quad (189)$$

The boundary conditions require that each q_i and its second derivative vanish at the edges. To construct a suitable set of q_j we again use the cubic B-splines which form an $(N+3)$ parameter family, where N is the grid parameter. Since there are four boundary conditions, it is reasonable that we end up with an $(N-1)$ parameter family of q_i .

Specifically, we have

$$q_1(x) = B_1(x) - B_{-1}(x) \quad (190)$$

$$q_i(x) = B_i(x) \quad i = 2, \dots, N-2 \quad (191)$$

$$q_{N-1}(x) = B_{N+1}(x) - B_{N-1}(x) . \quad (192)$$

The spatial variables x and y are, of course, independent. Thus, when constructing the B_i for the x variable the scale length is L_x and the grid parameter is N_x [see equation (142)].

For the purposes of displaying the basis vectors it is preferable to enumerate the approximating functions by a single index (say k) rather than a double index (i and j). Hence we define

$$p_k(x,y) = q_i(x) q_j(y) \quad (193)$$

where $k \equiv (j-1) \cdot (N_x - 1) + i$ and $i \in [1, 2, \dots, N_x - 1]$ and $j \in [1, 2, \dots, N_y - 1]$. There are $M \equiv (N_x - 1)(N_y - 1)$ independent functions p_k , and each satisfies the boundary conditions.

The basis vectors used to generate \mathbf{z}^N are the "displacement" elements

$$e_i \equiv [p_i, 0] \quad (194)$$

$i = 1, 2, \dots, M$

and the "velocity" elements

$$e_{M+i} [0, p_i] \quad (195)$$

$i = 1, 2, \dots, M$. Hence the subspace \mathcal{Z}^N spanned by e_i defined by (190) - (195) has $2(N_x - 1)(N_y - 1)$ elements.

With the basis chosen the matrices needed to represent the dynamics on the subspace \mathcal{Z}^N can be constructed by the standard Galerkin procedure. Specifically, one substitutes the approximate form

$$z^N(t) = \sum_{k=1}^{2M} \alpha_k(t) e_k \quad (196)$$

into the system

$$\dot{z}_p(t) = A_p z_p(t) + B_p u(t) . \quad (197)$$

The coefficients are then found from the normal equations (see Refs. 25, 26) as

$$C_p^M \dot{\alpha}^M(t) = H_p^M \alpha^M(t) + E_p^M u(t) \quad (198)$$

where G_p^M is the $2M$ -square (symmetric) Gram matrix

$$G_p^M(i, j) \equiv \langle e_i, e_j \rangle , \quad (199)$$

and

$$H_p^M(i, j) = \langle A e_i, e_j \rangle \quad (200)$$

and

$$E_p^M(j) = \langle B_p, e_j \rangle . \quad (201)$$

The inner product is given by the equation (93).

The output map C_p^M is found by substituting the approximate form (196) into the output equation (103). C_p^M has $p + q$ rows and $2M$ columns. The k th column is given by

$$C_p^{M[k]} = \epsilon_p e_k . \quad (202)$$

JOINT MODELING

A large space station is generally constructed with various structural members joined together to yield the desired configuration. The points at which these members are joined are called the structural joints and may vary widely in type and configuration. The types of joints of interest here fall into two categories: those whose characteristics are related to friction properties or friction joints, and those whose characteristics are related to the properties of the materials which compose the joint or integral joints. Friction joints are typically formed by two friction surfaces in contact under the action of a constant clamping force such as two beams joined with a bolt or a rivet. Integral joints are formed by some bonding procedure such as welding or by shaping the connecting portions such as inserting a rod in a hole or some similar arrangement. Clearly some joints (probably most) have characteristics associated with both types. The purpose of this section is to examine various models which can be used to describe the properties of the joints with various levels of fidelity.

The purpose of a joint is to maintain the geometric integrity of the structure and at the same time transmit the loads from one member to another. Typically a fastener is used to keep the lineal dimensions of the structure intact while friction is used to keep the rotational relation of the structural members intact. A typical example of this type of joint would be a nut, bolt and washer connecting two slender

beams. If the bolt were loose, the joint would approximate a pure pinned joint, while if tight it would approximate a rigid joint. Unfortunately neither of these two extremes are realizable and we must settle for something in between.

A considerable amount of experimental work has been carried out with the object of determining the properties of these joints, particularly for the case of structures which are vibrating. Of general interest is the damping effect on the motion while on the other hand particular interest is paid to the mathematical model of the joint which will predict the detailed force-displacement-time relationships and also allow one to predict the contribution to damping.

The bulk of investigations pertain to friction type joints. Beards and Woowet [Ref. 27] present experimental results indicating that the amount of structural damping can be improved by proper selection of the clamping force in friction type joints. They observed that a low value of this force (maybe too low for practical application, i.e. the structure loses some of its integrity) leads to the optimum damping. They do not concern themselves with a mathematical model of the joint.

An effort to validate an early model of a friction joint was made by Richardson and Nolle [Ref. 28]. Their work tests the Panovko [Ref. 29] model as refined by Metherell and Diller [Ref. 30]. Here a normal force P acts on the cylindrical friction joint consisting of two cylindrical members with a friction interface. An application of an external moment causes friction shear stresses to be formed at the interface and a microscopic slip displacement takes place between the

two members. This slip may take place over all or part of the interface but gross sliding between the two members is excluded in the model. The assumptions are that the interfacial slip occurs for all values of the load and begins at the outer edge of the contact circle and, as the load is increased, the slipped region extends radially inward as needed to provide the required load. The slipped region is a circular annulus. The loading cycle is considered in three parts: initial loading for a previously unloaded joint where the moment goes from 0 to M_{\max} , unloading of the joint where the moment goes from M_{\max} to M_{\min} , and finally reloading of the joint where the moment increases to M_{\max} again.

For the initial loading the inner bound of the radius of the slipped region is determined from moment equilibrium:

$$M = \int_a^R 2\pi r^2 \mu P dr \quad (203)$$

where a = inner radius

R = radius of friction joint

r = radius to generic point

μ = coefficient of static friction

P = normal force (clamping force)

Hence

$$a^3 = R^3 - 3M/2\pi \mu P \quad (204)$$

When M , the moment becomes large enough, $a \rightarrow 0$ and gross sliding occurs. A relation between the moment and the joint displacement is

given by (see Ref. 28)

$$\phi = \frac{\mu PR}{GS} \left[2 - 3 \frac{a}{R} + \left(\frac{a}{R} \right)^3 \right] . \quad (205)$$

Here a is dependent on the moment as in equation (204) and

$$\frac{1}{GS} = \frac{1}{\ell_1 G_1} + \frac{1}{\ell_2 G_2} ,$$

where ℓ_1, ℓ_2 are the thicknesses of each part of the cylindrical joint between body 1 and body 2, G_1, G_2 are the shear modulus of body 1 and body 2 and are properties of the material adjacent to the friction interface.

During unloading the joint displacement is shown to be

$$\phi_u = \frac{\mu PR}{GS} \left[-2 - 3 \left(\frac{a_{\max}}{R} \right) + \left(\frac{a_{\max}}{R} \right)^3 + 6 \left(\frac{b}{R} \right) - 2 \left(\frac{b}{R} \right)^3 \right] \quad (206)$$

where $a_{\max} = a$ when $M = M_{\max} < M_{\text{gross}}$ slipping and b is determined from

$$M_{\max} - M = \int_b^R (2\mu P) 2\pi r^2 dr = \frac{4\pi \mu P}{3} (R^3 - b^3) \quad (207)$$

where M is the value of the moment during the unloading with the lower bound of M_{\min} .

Subsequent reloading to M_{\max} again provides the following joint displacement

$$\begin{aligned} \phi_{rl} = \frac{\mu PR}{GS} \left[2 - 3 \left(\frac{a_{\max}}{R} \right) + \left(\frac{a_{\max}}{R} \right)^3 + 6 \left(\frac{b_{\max}}{R} \right) - 2 \left(\frac{b_{\max}}{R} \right)^3 \right. \\ \left. - 6 \left(\frac{C}{R} \right) + 2 \left(\frac{C}{R} \right)^3 \right] \quad (208) \end{aligned}$$

where C is determined from

$$M - M_{\min} = \frac{4\pi \mu P}{3} (R^3 - C^3) . \quad (209)$$

The moment-displacement characteristics are given in general by equations (206) and (208) as the moment is cycled between M_{\max} and M_{\min} with equation (205) applying only for the first quarter cycle. Since the equations depend upon the fact that the load is increasing or decreasing, the complete cycle forms a hysteresis loop with the energy dissipation given by

$$\begin{aligned} \Delta E &= \int_{M_{\min}}^{M_{\max}} (\phi_u - \phi_{rl}) dM \\ &= \frac{2\pi \mu^2 P^2 R^4}{3S} \left[1 - 2 \left(\frac{b_m}{R} \right) + 2 \left(\frac{b_m}{R} \right)^3 - \left(\frac{b_m}{R} \right)^4 \right] \end{aligned} \quad (210)$$

where $\frac{b_m}{R}$ is determined from

$$M_{\max} - M_{\min} = \frac{4\pi \mu PR^3}{3} \left[1 - \left(\frac{b_m}{R} \right)^3 \right] . \quad (211)$$

One of the chief objections to the above model is the apparent difficulty in obtaining the value of μ for the static coefficient of the joint. Recall that this is not the value that occurs for gross sliding but that associated with a microscopic slip displacement.

The friction joint discussed in the above problem has a friction interface between two bodies with each body having some thickness and a torsional shear modulus of G . The load is applied to the faces of the joint away from the friction interface. If the thickness of these two bodies approaches zero, then the restriction of no gross sliding becomes more difficult to satisfy. In the limit the only motion

between the two bodies would be sliding. The friction force which opposes this relative motion is what is normally called coulomb friction. The model for this type of motion is

$$F = K \begin{cases} 1 & \text{if } \dot{x} - \dot{y} > 0 \\ -1 & \text{if } \dot{x} - \dot{y} < 0 \end{cases} \quad (212)$$

where \dot{x} and \dot{y} are the velocities of the two adjacent surfaces. If the motion is cyclic, the force-displacement curves form a hysteresis loop and the energy loss per cycle can be determined. Analysis along these lines is presented in Refs. 31 and 32.

The key feature in reference 31 that pertains to this work was the observation that under the assumption of coulomb friction several types of motion within the joint can occur depending upon the properties of the joint, e.g. the value of K which is related to the clamping force, and the inertial properties of the driven member. If K is low and the inertia high, then it is likely that there is always relative motion between the two surfaces and equation (212) always holds. On the other hand if K is large and the inertia low, there will never be slip and the joint can be treated as rigid. Of course, it is the interesting case which falls between these two where there can be slip followed by a non-slip condition or vice-versa which is most likely to occur. Reference 31 examines all three possibilities for the case where the input displacement is sinusoidal. Results are presented in the form of phase plane diagrams for a joint with angular motion. Expressions for energy loss per cycle are given noting that the first case of pure slip gives the maximum value of loss and that the value

of K which is best in terms of energy loss is given by

$$K = \sqrt{2} A\omega^2/\pi \quad (213)$$

where A = the amplitude of the motion (angular), ω = the frequency.

The maximum energy loss per cycle using the K in equation (213) was found to be

$$E = \frac{4IA^2\omega^2}{\pi} \quad (214)$$

where I is the moment of inertia of the damper or unit driven by the friction.

All the previous investigations examined coulomb type friction of some interface between two joint members. In addition the more sophisticated analyses included consideration of the material properties on each side of the interface. In all cases all motion and structural deflections are assumed to be in the same plane. In References 33 and 34 the interaction of out-of-plane deflection and the in-plane motion are considered. In particular slipping at the interface occurs in the zones where the pressure (related to the flexural vibrations) is the lowest. Using these ideas these authors were able to arrive at an equivalent viscous damping ratio for the out-of-plane vibrational modes. A similar result was obtained in a different manner in Ref. 35. Here a simpler model was used for the normal force variation. It was assumed the normal force was proportional to a normal displacement with a constant K_1 . This normal displacement is modeled as proportional to the in-plane displacement x , e.g. $y = cx$. The joint friction force in the in-plane direction is then assumed to have the following form:

$$F = - \mu \bar{k}_1 c |x| \text{sign} (\dot{x}) \quad (215)$$

Earlier references which support these ideas are given in references 36 through 40.

All the previous works emphasize the slipping of the interface between the two joint members. If such slipping does not occur, as in the case where the normal force is extremely large and the inertial loads are small, or if the joints are fitted or welded together, then the joint properties become similar to that of the material and can be modeled in several different ways.

The simplest model is a pure elastic joint which can be modelled as a spring and has no losses. Hence the force (or moment) transmitted through the joint is proportional to the deflection, $F = kx$. An equally simple model is the viscous joint where the force is proportional to the deflection rate, and not related to the deflection. In some cases slipping joints can be approximated by this assumption. The force transmitted through the joint is given by $F = c\dot{x}$.

Two additional joint models build on these two by considering the elements to be in parallel (Voigt model) or in series (Maxwell model). The force transmitted would be $F = kx + c\dot{x}$ for the Voigt model. The force transmitted for the Maxwell model is given by $F = c\dot{x}_1$ where

$$\dot{x}_1 = \frac{k}{c} [x - x_1] \quad (216)$$

Hence additional dynamic properties have been added due to the joint model.

Additional models can be generated by a combination of the two simple elements described above or more conveniently described in terms of the two elements, the Voigt and the Maxwell model. A four element joint model can be generated by a Voigt joint in series with a Maxwell joint with different spring and damping constants in each part. Alternatively one could consider two Maxwell joints in parallel, again each one with its own spring and damping constants. Alternative four element joint models are obtained by having a spring element, a damper element and a Maxwell element all in parallel, or having two Voigt joints in series. Three element joints can be derived from the four element joints by letting one spring or damping constant approach infinity.

Typically these models add dynamics to the joint. For a three element elastic joint which is characterized by a spring in parallel with a Maxwell model (spring and damper in series), the transmitted force is given by

$$F = c \dot{x}_1 + kx \quad (217)$$

where

$$\dot{x}_1 = \frac{k}{c} (x - x_1) \quad (218)$$

Hence a large variety of models are possible to approximate a joint made with a viscoelastic material and which experiences no slipping. The models discussed can all be represented by ordinary linear differential equations.

A more general representation is suggested in Ref. 41 which can include nonlinear contributions. For example if a dead band exists

in the joint a proposed force model looks like

$$F = k_0 + k_1 \dot{x} + c_1 \ddot{x} + k_n x^n + c_n \dot{x}^n + k_{DB} + c_{DB} + F_f \text{sign } \dot{x} + g|x| \text{sign } (\dot{x}) \quad (219)$$

where

$$k_{DB} = \begin{cases} k_{DB} (x - x_{DB}) & x_{DB} < x \\ 0 & -x_{DB} \leq x \leq x_{DB} \\ k_{DB} (x + x_{DB}) & x \leq -x_{DB} \end{cases} \quad c_{DB} = \begin{cases} c_{DB} \dot{x} & x_{DB} < x \\ 0 & -x_{DB} \leq x \leq x_{DB} \\ c_{DB} \dot{x} & x \leq -x_{DB} \end{cases}$$

and g in the last term corresponds to the appropriate terms in eq. (215).

The generic form of the force equation (219) is suggested to be

$$F = k(x, \dot{x})x + c(x, \dot{x})\dot{x} + k q(t) \quad (220)$$

where

$$q(t) = \int_0^t Q(x, \dot{x}) dt, \quad (221)$$

and $Q(\cdot)$ represents some time history of the motion which contributes to the "memory" of the material.

One form of the memory term which is linear that has been suggested (see Ref. 41) is

$$\dot{q}(t) = -pq + \dot{x}(t). \quad (222)$$

Then

$$q(t) = \int_0^t e^{-p(t-\tau)} x(\tau) d\tau. \quad (223)$$

The above review represents the current thinking on models to represent the effects of joints on the dynamic systems. Most researchers consider the models which include local slipping the most

accurate. Hence coulomb friction and its associated hysteresis loops would be present in real systems. As indicated previously, these effects have been observed in the laboratory (Ref. 35). It would seem appropriate to consider a general model such as equation (220) and fit the coefficients to match results of laboratory experiments. As a last resort to obtain a model which would possibly admit analysis, the viscoelastic models described by ordinary differential equations might be the best procedure.

The inclusion of joint models in the state-space setting can be simple or difficult, depending on the choice of joint model. In any case numerical algorithms have not yet been developed for most of these models. The main difficulty with coulomb friction models is that the state-space system is a non-linear differential inclusion that requires new theoretical tools (see Ref. 19).

NUMERICAL RESULTS

In this section we report on a number of numerical experiments for the control problems discussed in the previous sections. The goal of this section is to demonstrate the basic features of the computational algorithms based on the state-space models. The numerical runs presented below are intended to illustrate the technique and to point out various difficulties associated with the different models.

We conducted six runs on the slewing beam-tip-body problem and one run on the plate control problem.

BEAM PROBLEMS

For the purposes of this report we selected a beam (aluminum) with the following characteristics:

$$L = 30 \text{ ft. (length of the beam)}$$

$$B = 1 \text{ ft. (width of the beam)}$$

$$h = .02083 \text{ ft. (thickness of the beam)}$$

$$I_A = 981 \text{ slug ft.}^2$$

$$\rho = 5.24 \text{ slug/ft.}^3$$

$$m_c = .327 \text{ slug}$$

$$I = Bh^3/12 = 7.53520 \times 10^{-7} \text{ ft.}^4$$

$$E = 1.44 \times 10^9 \text{ lb/ft.}^2$$

$$A = Bh = .02083 \text{ ft.}^2$$

$$K' = .84746$$

$$G = 5.76 \times 10^8 \text{ lb/ft.}^2$$

$$I_c = .3 \text{ slug ft.}^2$$

Note that

$$EI = 1,085.069 \text{ lb ft.}^2$$

and

$$K'AG = 10,169,519.98 \text{ lb.}$$

The control problem was solved for the Euler-Bernoulli beam using "strain sensors" located at

$$\bar{x}_1 = 0, \quad \bar{x}_2 = .3L$$

and "velocity sensors" located at

$$\hat{x}_1 = .5L, \quad \hat{x}_2 = .7L.$$

Thus, for the Euler-Bernoulli beam there are eight outputs and the weighting matrix is set to be the diagonal matrix

$$S_E = \text{dia} (100, 100, 102, 102, 102, 102, 100.2, 100.2) \quad (224)$$

For the Timoshenko beam we measured the mean values at $\bar{x}_1 = 0$, $\bar{x}_2 = .3L$ of $z_7(t) = [\psi_x(t, x)]$ and $z_8(t) = [u_x(t, x) - \psi(t, x)]$ and mean values at $\hat{x}_1 = .5L$, $\hat{x}_2 = .7L$ of $z_5(t) = [u_t(t, x) + x\omega(t)]$ and $z_6(t) = [\psi_t(t, x) + \omega(t)]$. Therefore, the weighting matrix is the diagonal matrix

$$S_T = \text{dia} (100, 100, 10, 10, 102, 102, 100.2, 100.2, 100, 100, 100, 100) \quad (225)$$

When actuator dynamics were included we also "sensed" the actuator position $x_1(t)$ and velocity $x_2(t)$. Weights of 1.0 were placed on these states so that for the Euler-Bernoulli beam with actuator dynamics the weighting matrix becomes

$$S_{ED} = \text{dia} (S_E, 1.0, 1.0), \quad (226)$$

and for the Timoshenko beam with actuator dynamics the weighting matrix becomes

$$S_{TD} = \text{dia} (S_T, 1.0, 1.0) . \quad (227)$$

The weight on the control is always taken to be $R = 1$.

We considered actuator dynamics with and without delays. For the model without delays the system parameters were set at (see equations (19) - (26))

$$\left. \begin{array}{llll} a_{11} = -100 & a_{12} = -1 & a_{21} = 0 & a_{22} = 0 \\ b_1 = 10 & c_1 = 10 & c_2 = 0 & r = 0 \end{array} \right\} \quad (228)$$

and for the delayed actuator we used the parameters

$$\left. \begin{array}{llll} a_{11} = -100 & a_{12} = -1 & a_{21} = 0 & a_{22} = -1.0 \\ b_1 = 10 & c_1 = 10 & c_2 = 0 & r = 0.1 \end{array} \right\} \quad (229)$$

Comparison of Open Loop Systems

We started by comparing the open-loop systems corresponding to the Euler-Bernoulli and Timoshenko beam models for various lengths of the beam. We used the scheme described by equations (143) - (154) for the Euler-Bernoulli beam and the scheme described by equations (161) - (172) for the Timoshenko beam. We denote by N the number of "elements" along the beam. More precisely, we sub-divide the interval $[0, L]$ into N equal subintervals and use cubic spline shape functions.

We added viscous damping to each model, so that all of the non-zero eigenvalues had real part equal to $(-.025)$. Both models have two zero eigenvalues corresponding to the rigid body modes. We based

calculations on $N = 4, 8, 16, 32$ and 64 "element" approximate models and compared the corresponding open-loop eigenvalues. We let

$$\lambda_j^N = \alpha_j^N + \omega_j^N i \quad (230)$$

denote the j th eigenvalue of the dynamic operator A^N .

In Table 1 we show the imaginary parts of the first eight eigenvalues for an Euler-Bernoulli beam of length thirty feet. Using N elements results in a system of order $2N + 4$. Since there are two zero eigenvalues, we also have $N + 1$ complex conjugate pairs. Comparing the first three columns of Table 1 to the last, it appears that using N elements gives a fairly accurate approximation to the first $N - 2$ eigenvalues. Table 2 shows the open-loop non-zero eigenfrequencies for the Timoshenko beam model.

Observe that the Euler-Bernoulli model gives more accurate estimates to the low frequency eigenvalues and needs fewer elements than the Timoshenko model in order to give accurate frequencies. As we shall see later, this may cause numerical difficulties in the control design if the Timoshenko model is used.

Recall that the Timoshenko model is more suitable for a short beam (see Ref. 3). We considered the open-loop eigenvalue problem for a 1 ft. beam to see if there was a significant difference between the two models. These results are presented in Table 3 and Table 4.

Tables 3 and 4 show that for the short 1 foot beam, the Timoshenko model produces more accurate frequencies than the Euler-Bernoulli model. Note that the relative "error" between the eighth frequency $\omega_8 \approx 40,244$ and the 16 element model prediction based on the Euler-

TABLE 1. Euler-Bernoulli Frequencies, L = 30 ft.

N	4	8	16	32	64
ω_1^N	0.48908	0.48908	0.48908	0.48908	0.48908
ω_2^N	2.1723	2.1700	2.1700	2.1700	2.1700
ω_3^N	6.1752	6.1077	6.1046	6.1044	6.1044
ω_4^N	12.431	12.077	12.049	12.047	12.047
ω_5^N	27.381	20.074	19.419	19.912	19.912
ω_6^N	-	30.129	29.543	29.520	29.519
ω_7^N	-	42.446	40.714	40.650	40.647
ω_8^N	-	57.314	53.392	53.238	53.231

TABLE 2. Timoshenko Frequencies, L = 30 ft.

N	4	8	16	32	64
ω_1^N	0.48961	0.48935	0.48914	0.48896	0.48884
ω_2^N	3.0544	2.4240	2.1752	2.1701	2.1701
ω_3^N	42.019	9.7023	6.249	6.1065	6.1045
ω_4^N	278.57	33.435	13.250	12.065	12.047
ω_5^N	1219.30	111.35	24.925	19.996	19.913
ω_6^N	-	321.49	43.393	29.806	29.522
ω_7^N	-	834.22	77.314	41.413	40.656
ω_8^N	-	-	144.56	55.019	53.252

TABLE 3. Euler-Bernoulli Frequencies, $L = 1$ ft.

N	4	8	16	32	64
ω_1^N	52.463	52.463	52.463	52.463	52.463
ω_2^N	215.44	215.44	215.44	215.44	215.44
ω_3^N	2,297.20	2,293.5	2,293.3	2,293.3	2,293.3
ω_4^N	6,326.20	6,218.3	6,213.8	6,213.6	6,213.5
ω_5^N	12,496.0	12,162.0	12,121.0	12,119.0	12,119.0
ω_6^N	-	20,232.0	20,001.0	19,991.0	19,991.0
ω_7^N	-	30,791.0	29,867.0	29,833.0	29,831.0
ω_8^N	-	44,158.0	41,746.0	41,644.0	41,639.0

TABLE 4. Timoshenko Frequencies, $L = 1$ ft.

N	4	8	16	32	64
ω_1^N	52.462	52.462	52.462	52.462	52.462
ω_2^N	215.31	215.31	215.31	215.31	215.31
ω_3^N	2,343.6	2,287.6	2,286.8	2,286.8	2,286.8
ω_4^N	7,782.1	6,197.4	6,173.1	6,172.8	6,172.8
ω_5^N	28,281.0	12,260.0	11,982.0	11,979.0	11,979.0
ω_6^N	-	21,440.0	19,649.0	19,637.0	19,637.0
ω_7^N	-	37,089	29,137.0	29,083.0	29,083.0
ω_8^N	-	-	40,436.0	40,245.0	40,244.0

Bernoulli model $\omega_8^{16} = 41,746$ is 3.7%. On the other hand, the Timoshenko 16 element model produces the estimate $\omega_8^{16} = 40,436$ so that here the relative error is less than .5%.

We turn now to computing suboptimal gain operators. We consider six beam models and one plate model. In each case the goal is to compute an estimate of the optimal feedback gain operator. We used the numerical schemes and state space formulations developed in the previous sections.

MODEL 1: EULER-BERNOULLI BEAM; NO ACTUATOR

• State-Space: $\mathbf{z} = \mathbf{y}$ defined by (41) - (42)

$\mathbf{A} = \mathbf{A}_E$ defined by (43) - (44)

$\mathbf{B} = \mathbf{B}_E$ defined by (45)

$\mathbf{C} = \mathbf{C}_E$ defined by (121)

Optimal Feedback Operator:

$$\begin{aligned} K_E z_E(t) = & K_1 \theta(t) + K_2 \omega(t) \\ & + K_3 [u_t(t, L) + L\omega(t)] \\ & + K_4 [u_{xt}(t, L) + \omega(t)] \\ & + \int_0^L K_5(x) [u_{xx}(t, x)] dx \\ & + \int_0^L K_6(x) [u_t(t, x) + x\omega(t)] dx \end{aligned} \quad (231)$$

We used the approximation scheme (143) - (154) to construct the finite dimensional system (150) - (151) and the corresponding approximate Riccati equation (134). Potter's method (see Ref. 20) was used

to solve (134) and construct the approximating gain operator K_E^N defined by (140). Again, K_E^N will have the form

$$\begin{aligned} K_E^N z_E(t) = & K_1^N \theta(t) + K_2^N \omega(t) \\ & + K_3^N [u_t(t, L) + L\omega(t)] \\ & + K_4^N [u_{xt}(t, L) + \omega(t)] \\ & + \int_0^L K_5^N(x) [u_{xx}(t, x)] dx \\ & + \int_0^L K_6^N(x) [u_t(t, x) + x\omega(t)] dx . \end{aligned} \quad (232)$$

The convergence of K^N to K is equivalent to the convergence of the four gains

$$K_1^N \rightarrow K_1 , \quad K_2^N \rightarrow K_2 , \quad K_3^N \rightarrow K_3 , \quad K_4^N \rightarrow K_4$$

in R and the two functional gains

$$K_5^N(x) \rightarrow K_5(x) , \quad K_6^N(x) \rightarrow K_6(x)$$

in $L_2(0, L)$.

Table 5 shows the convergence of K_i^N to K_i for $i = 1, 2, 3, 4$ and $N = 8, 12, 16, 32$. Note that K_1^N and K_2^N have "converged numerically" for $N = 16$ while K_3^N and K_4^N seem to converge more slowly.

TABLE 5. Sub-optimal Gains; MODEL 1

N	K_1^N	K_2^N	K_3^N	K_4^N
8	- 10.0000	- .47911	4.0716	- .24652
12	- 10.0000	- .47915	4.0352	- .19589
16	- 10.0000	- .47916	4.0276	- .18769
32	- 10.0000	- .47916	4.0155	- .18376

Figure 4 shows the convergence of the functional gain $K_5^N(\cdot)$. Observe that $K_5^{16}(\cdot)$ and $K_5^{32}(\cdot)$ are almost identical and hence we do not show $K_5^{64}(\cdot)$. Figure 5 shows the convergence of $K_6^N(\cdot)$. Again, there is no difference between $K_6^{64}(\cdot)$ and $K_6^{32}(\cdot)$ so we plot only the $N = 32$ functional gain. Table 6 shows the closed-loop eigenvalues for $N = 8, 16$, and 32 . Recall that the viscous damping model gives open-loop eigenvalues λ with $\text{Re}(\lambda) = - .025$.

TABLE 6. Closed-Loop Eigenvalues; MODEL 1

N = 8	N = 16	N = 32
- .046444 + .047666 i	- .046444 + .047666 i	- .046444 + .047666 i
- .19907 + .44751 i	- .19907 + .44751 i	- .19907 + .44751 i
- .04155 + 2.1694 i	- .041547 + 2.1693 i	- .041547 + 2.1693 i
- .026758 + 6.1076 i	- .026758 + 6.1045 i	- .026758 + 6.1043 i
- .025423 + 12.078 i	- .025419 + 12.049 i	- .025419 + 12.047 i
- .025136 + 20.074 i	- .025136 + 19.919 i	- .025135 + 19.912 i
- .025109 + 30.129 i	- .025106 + 29.543 i	- .025106 + 29.520 i
- .025035 + 42.446 i	- .025029 + 40.714 i	- .025029 + 40.650 i

This example shows how the computational scheme can produce excellent convergence for the basic problem with an Euler-Bernoulli beam model. We turn now to the Timoshenko model.

MODEL 2: TIMOSHENKO BEAM; NO ACTUATOR

• State-Space: $Z = \mathbb{D}$ defined by (53) - (54)

$A = A_T$ defined by (55) - (56)

$B = B_T$ defined by (57)

$C = C_T$ where

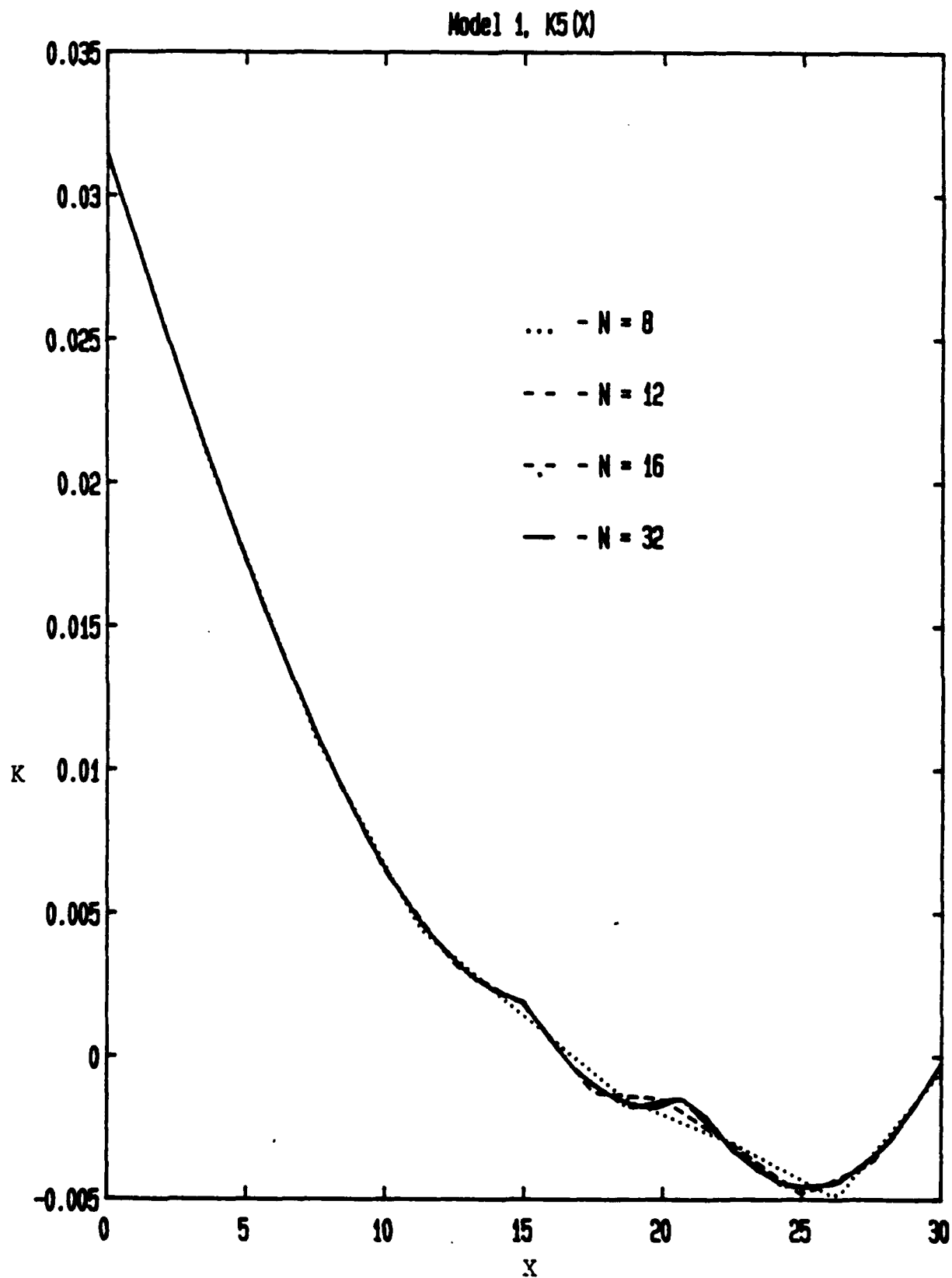


Figure 4. Functional Gain K_5 ; Model 1

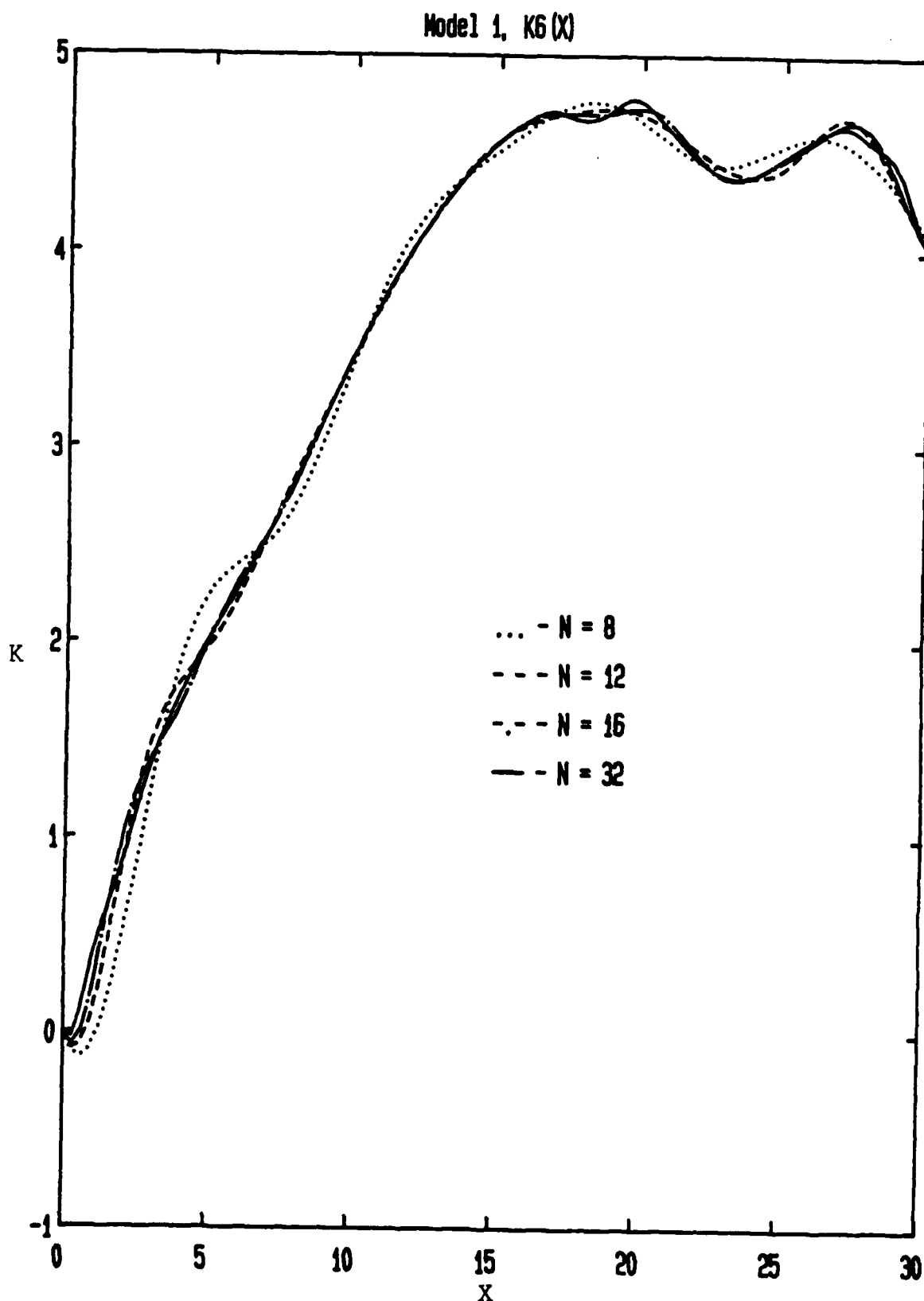


Figure 5. Functional Gain K_6 ; Model 1

$$C_T^z = \begin{bmatrix} z_1 \\ z_2 \\ z_3 \\ z_4 \\ \hline C_{Ts}^z \\ \hline C_{Tv}^z \end{bmatrix} \quad (233)$$

and

$$C_{Ts}^z = \begin{bmatrix} m^e(0)z_7 \\ m^e(.3L)z_7 \\ m^e(0)z_8 \\ m^e(.3L)z_8 \end{bmatrix}, \quad C_{Tv}^z = \begin{bmatrix} m^e(.5L)z_5 \\ m^e(.7L)z_5 \\ m^e(.5L)z_6 \\ m^e(.7L)z_6 \end{bmatrix}. \quad (234)$$

Optimal Feedback Operator:

$$\begin{aligned} K_T z_T(t) = & K_1 \theta(t) + K_2 \omega(t) \\ & + K_3 [u_t(t, L) + L\omega(t)] \\ & + K_4 [\psi_t(t, L) + \omega(t)] \\ & + \int_0^L K_5(x) [u_t(t, x) + L\omega(t)] dx \\ & + \int_0^L K_6(x) [\psi_t(t, x) + \omega(t)] dx \\ & + \int_0^L K_7(x) [\psi_x(t, x)] dx \\ & + \int_0^L K_8(x) [u_x(t, x) - \psi(t, x)] dx. \end{aligned} \quad (235)$$

We now use the approximation scheme defined by (161) - (172) to construct the finite dimensional model (171) - (172) and the corresponding Riccati equation (134). Again, Potter's method was used to compute the approximating gain operator K_T^N and as in the Euler-Bernoulli case K_T^N has the same form as K_T .

Table 7 shows the convergence of K_i^N to K_i for $i = 1, 2, 3, 4$. Observe that as in the Euler-Bernoulli beam K_1^N , K_2^N and K_3^N behave nicely. The convergence of K_4^N is not as rapid.

TABLE 7. Sub-optimal Gains; MODEL 2

N	K_1^N	K_2^N	K_3^N	K_4^N
8	- 9.9996	- .48306	4.2078	.55767
12	- 9.9996	- .48075	4.2090	.34931
16	- 9.9984	- .48025	4.1900	9.9691 E-3
32	-10.023	- .48373	4.1721	-8.7446 E-2

The convergence property of the functional gains for the Timoshenko model is not as well-behaved as in the Euler-Bernoulli model. At this time we do not have a full understanding of this problem. There may be several reasons for this slow (or non-) convergence, including numerical roundoff and the failure of the Timoshenko model to approximate "long thin" beams (see the lecture notes by Taylor, Ref. 42). Figures 6 through 9 show plots for the functional gains $K_5^N(\cdot)$, $K_6^N(\cdot)$, $K_7^N(\cdot)$ and $K_8^N(\cdot)$. Note that $K_1^N(\cdot)$ seem to remain close for $N = 8, 12$ and 16 and $i = 5, 6, 7$ and 8 . Only $K_8^N(\cdot)$ seems

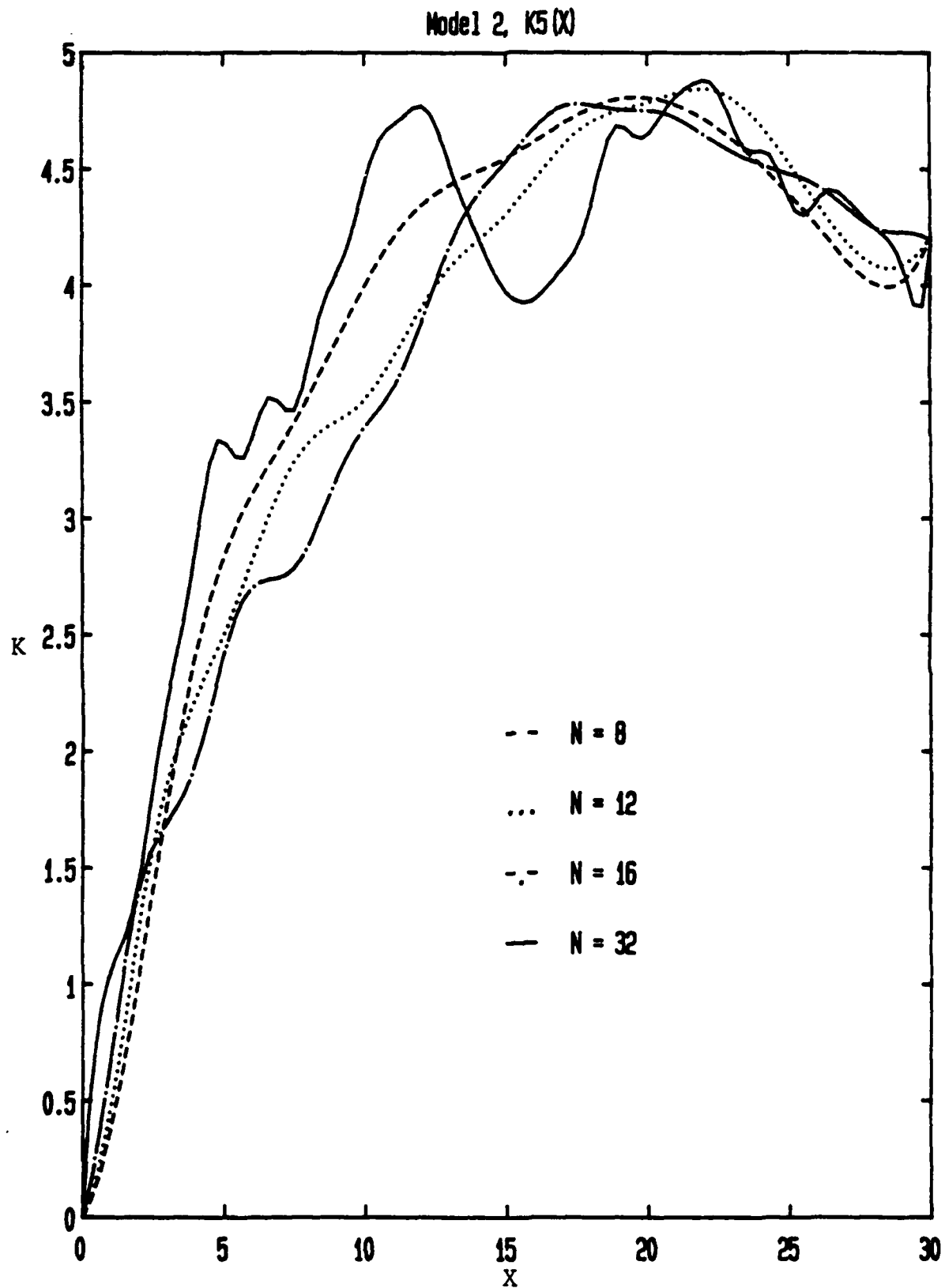


Figure 6. Functional Gain K_5 ; Model 2

AD-A207 520

CONTROL OF FLEXIBLE STRUCTURES(U) OPTIMIZATION INC
BLACKSBURG VA J A BURNS ET AL. APR 89 K511-3
AL-TR-89-001 F04611-86-C-0008

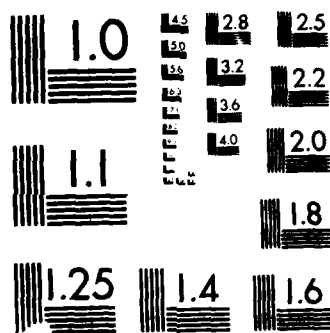
2/2

UNCLASSIFIED

F/G 13/13

NL

UNCL
CLASS
DTIC



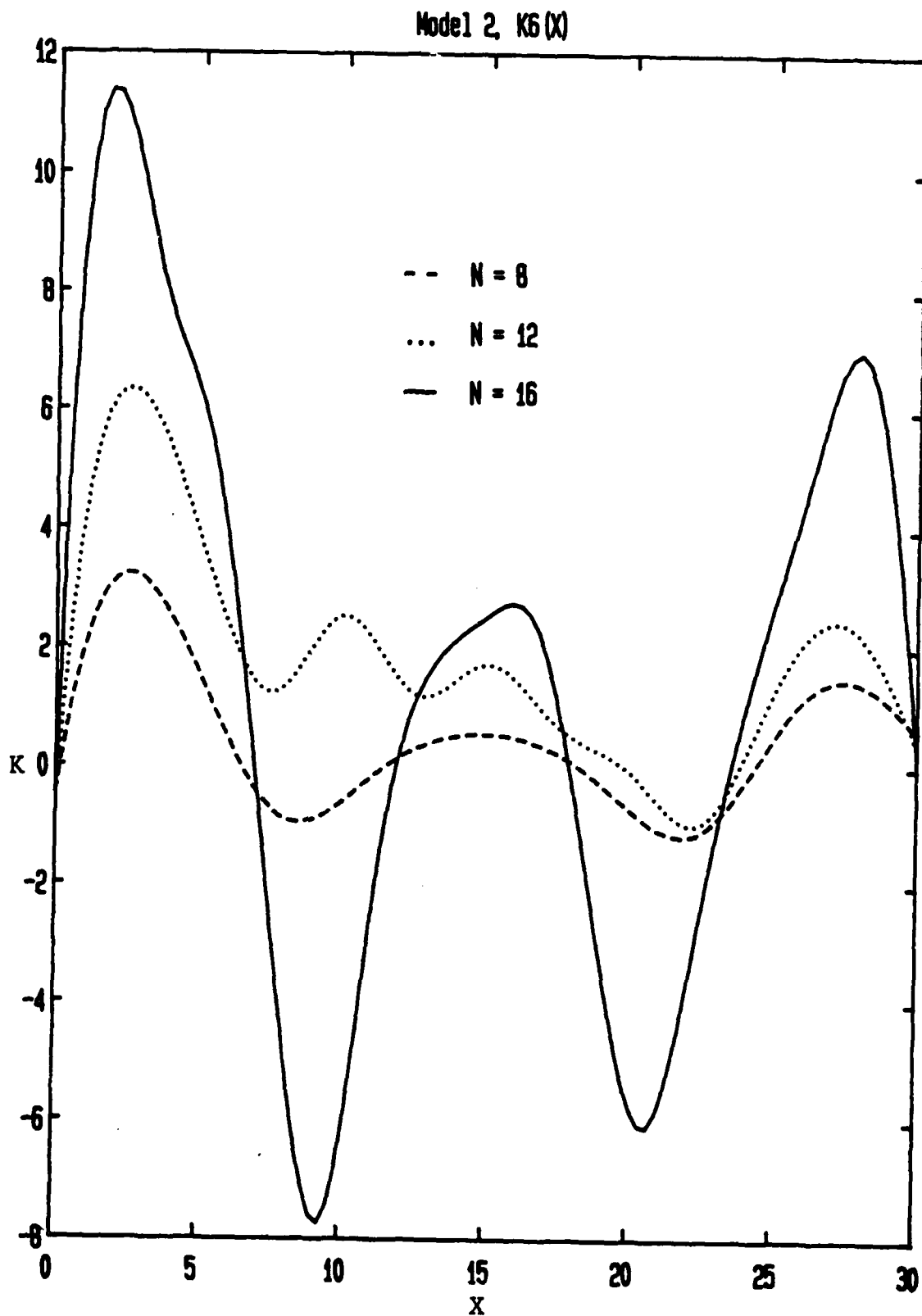


Figure 7. Functional Gain K_6 ; Model 2

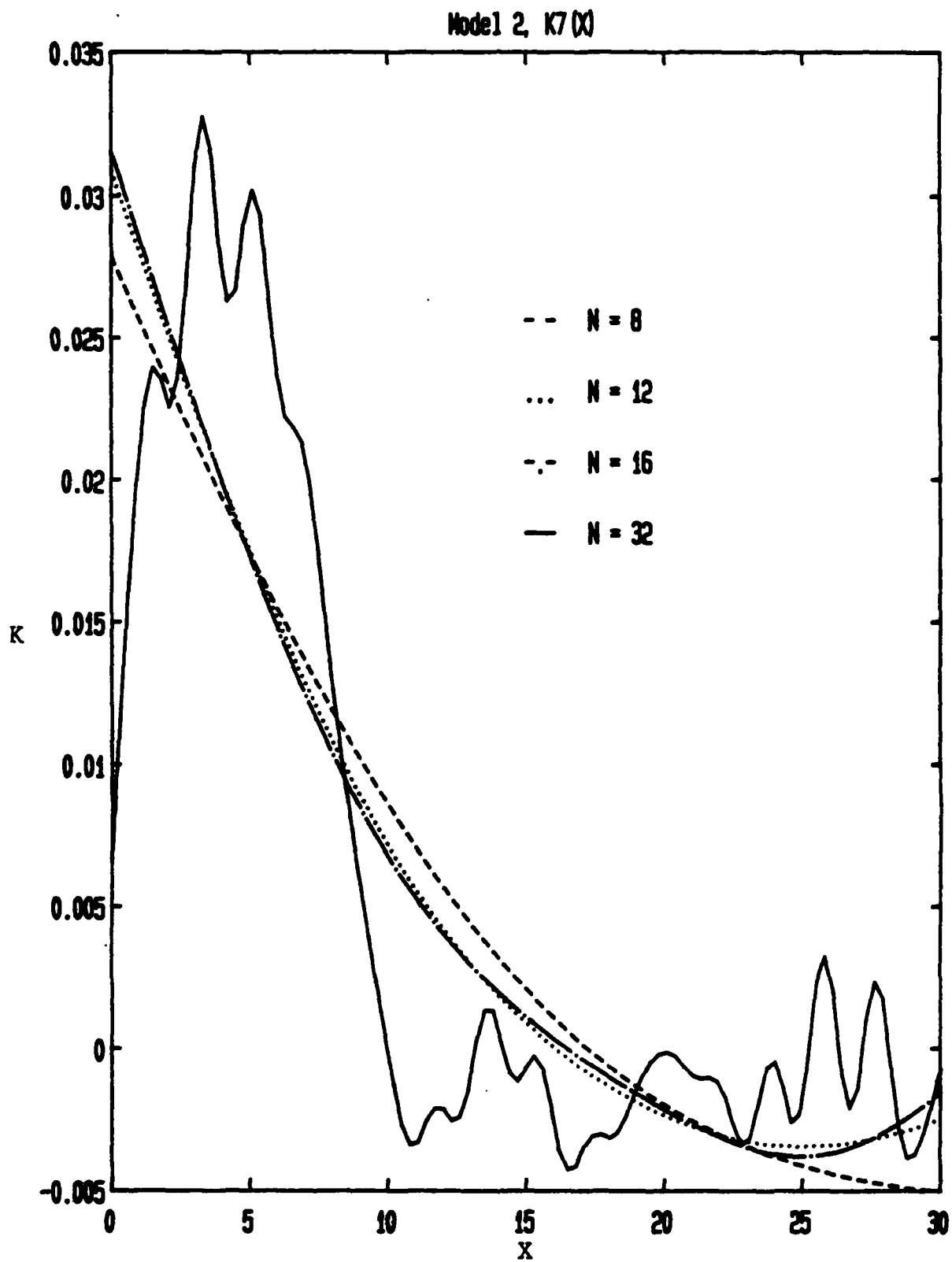


Figure 8. Functional Gain K_7 ; Model 2

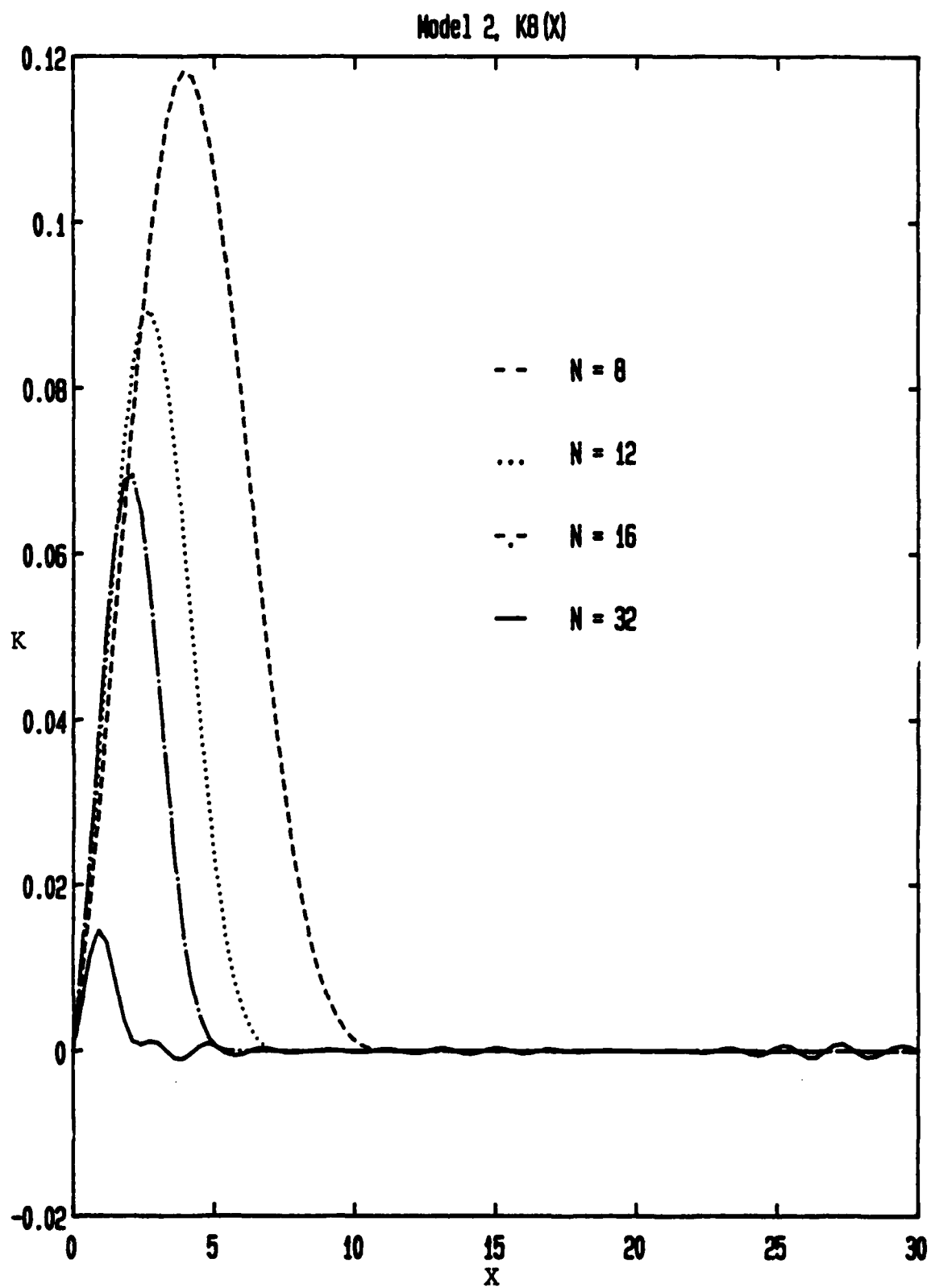


Figure 9. Functional Gain K_8 ; Model 2

to be converging in a monotone fashion for $N = 8, 12, 16$ and 32 . Although the functional gains do not seem to "rapidly converge", the closed-loop eigenvalues do appear to be correct in that the $N = 32$ sub-optimal gain produces reasonable closed-loop eigenvalues. This is illustrated in Table 8.

TABLE 8. Closed-Loop Eigenvalues; MODEL 2

$N = 8$	$N = 16$	$N = 32$
$-.046441 + .047660 i$	$-.046426 + .047675 i$	$-.046620 + .047618 i$
$-.19916 + .44774 i$	$-.19934 + .44741 i$	$-.19926 + .44733 i$
$-.042086 + 2.4236 i$	$-.041603 + 2.1746 i$	$-.042331 + 2.1694 i$
$-.027471 + 9.7022 i$	$-.026820 + 6.2488 i$	$-.027401 + 6.1064 i$
$-.025743 + 33.435 i$	$-.025451 + 13.250 i$	$-.025764 + 12.064 i$
$-.025414 + 111.35 i$	$-.025213 + 24.925 i$	$-.025232 + 19.996 i$
$-.025099 + 321.49 i$	$-.025110 + 43.393 i$	$-.025061 + 29.806 i$
$-.025069 + 834.22 i$	$-.025072 + 77.314 i$	$-.025067 + 41.413 i$

MODEL 3: EULER-BERNOULLI BEAM; ACTUATOR, NO DELAY

• State-Space: $\dot{z} = z_E^\circ$ defined by (63) - (64)

$A = A_0$ defined by (65) - (66)

$B = B_0$ defined by (67)

and

$$c_{E_0} z_E^\circ = c_{E_0} \begin{bmatrix} z_E \\ x_1 \\ x_2 \end{bmatrix} = \begin{bmatrix} c_E z_E \\ x_1 \\ x_2 \end{bmatrix} \quad (236)$$

. Optimal Feedback Operator:

$$\begin{aligned}
 K_{E0} z_E^o(t) &= K_E z_E(t) + K_7 x_1(t) + K_8 x_2(t) \\
 &= K_1 \theta(t) + K_2 \omega(t) \\
 &\quad + K_3 [u_t(t, L) + L\omega(t)] \\
 &\quad + K_4 [u_{xt}(t, L) + \omega(t)] \\
 &\quad + \int_0^L K_5(x) [u_{xx}(t, x)] dx \\
 &\quad + \int_0^L K_6(x) [u_t(t, x) + x\omega(t)] dx \\
 &\quad + K_7 x_1(t) + K_8 x_2(t) .
 \end{aligned} \tag{237}$$

Note that the only difference between MODEL 1 and MODEL 3 is the addition of the actuator states $x_1(t)$ and $x_2(t)$. Table 9 shows the convergence of the gains K_i^N for $i = 1, 2, 3, 4, 7$ and 8 . Observe that the convergence of each of the finite sub-optimal gains is much faster than for the case with no-actuator dynamics (compare to Table 5).

TABLE 9. Sub-optimal Gains; MODEL 3

N	K_1^N	K_2^N	K_3^N	K_4^N	K_7^N	K_8^N
8	-10.000	-.47902	4.1250	-1.4946 E-2	-.54392	-.95773
12	-10.000	-.47902	4.1241	-1.5977 E-2	-.54392	-.95773
16	-10.000	-.47902	4.1242	-1.6004 E-2	-.54392	-.95773
32	-10.000	-.47902	4.1241	-1.6061 E-2	-.54392	-.95773

The addition of actuator dynamics also increased the rate of convergence for the functional gains $K_5^N(\cdot)$ and $K_6^N(\cdot)$. This is shown in Figures 10 and 11. In Figure 11 only the graph of $K_6^{32}(\cdot)$ is shown. The graphs for $N = 8, 12, 16$ and 32 are not distinguishable on the scale shown. The addition of actuator dynamics changed the gains as expected. However, we did not expect to see the increase in convergence of the functional gains. We do not fully understand the reason why the addition of actuator dynamics would improve the numerical convergence of the optimal gains.

As expected, the addition of actuator dynamics does affect the location of the closed-loop eigenvalues. However, as shown in Table 10 the closed-loop eigenvalues of the Euler-Bernoulli beam with actuator dynamics are almost the same as the closed-loop eigenvalues for the Euler-Bernoulli beam without actuator dynamics (see Table 6). Observe that the second-order actuator introduces two open-loop eigenvalues at

$$\lambda_A = -.50 \pm 9.9875 i$$

Table 10 gives the closed-loop eigenvalues for the actuator mode and the next seven frequencies.

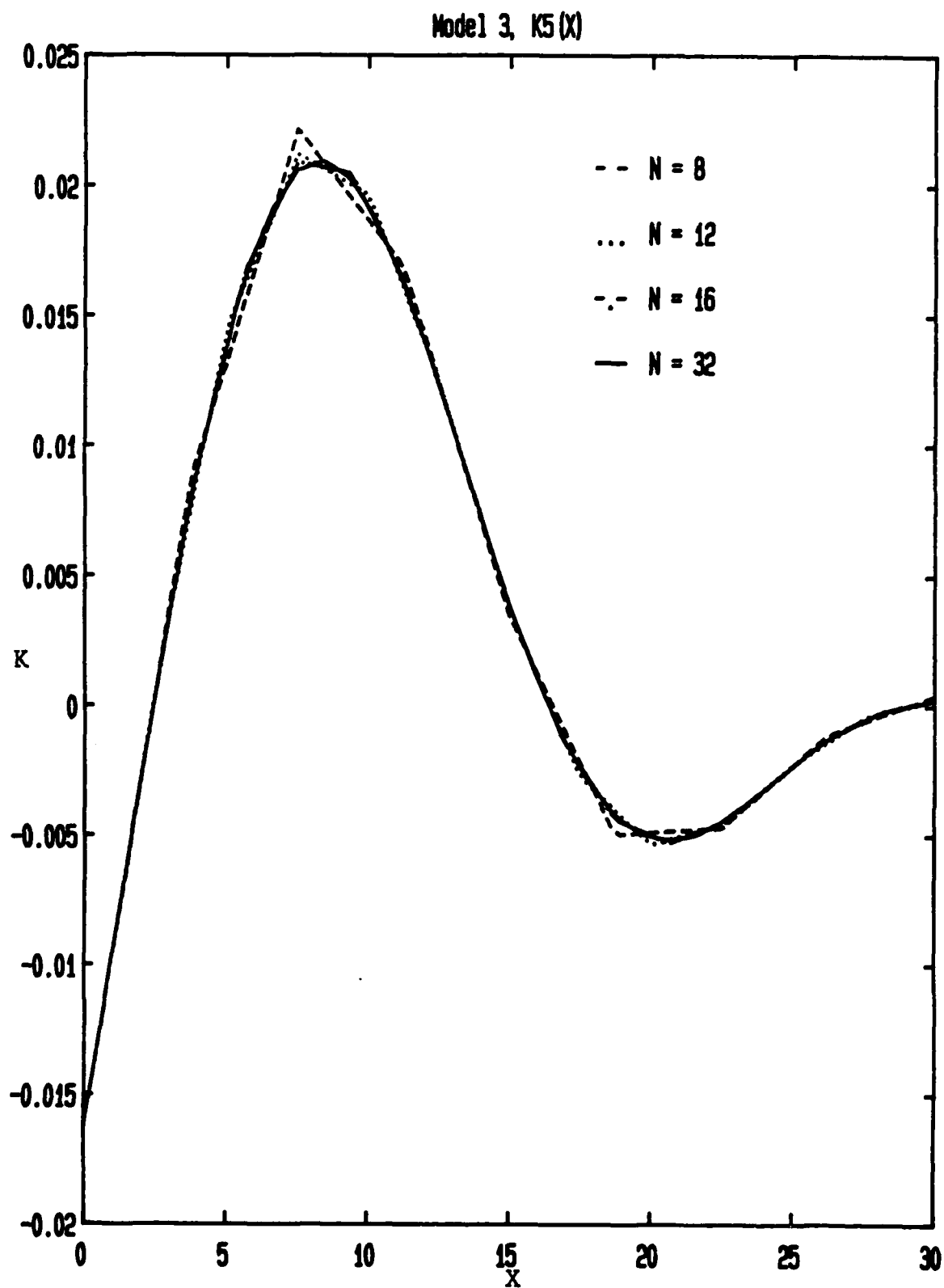


Figure 10. Functional Gain K_5 ; Model 3

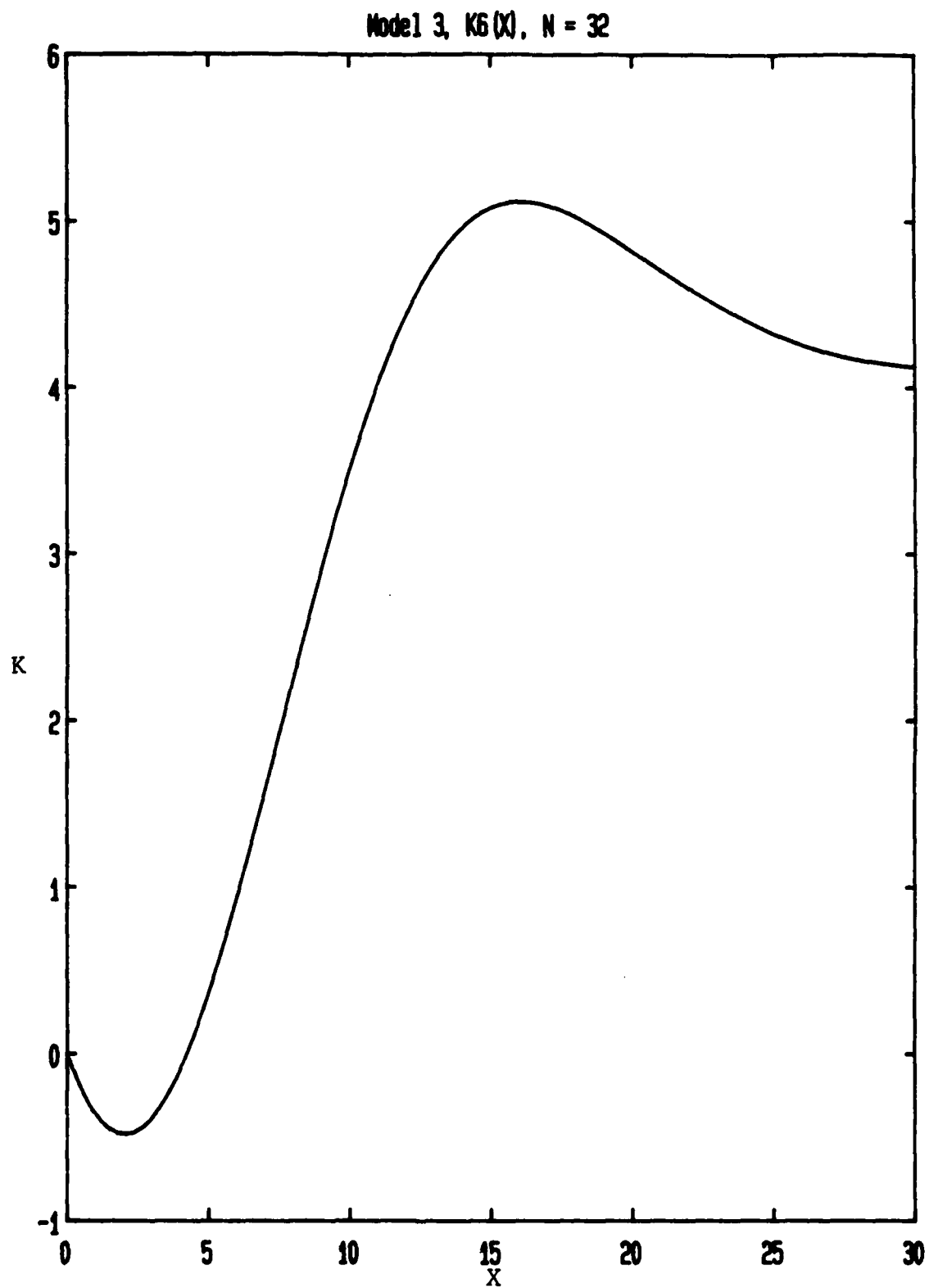


Figure 11. Functional Gain K_6 ; Model 3

TABLE 10. Closed-Loop Eigenvalues; MODEL 3

N = 8	N = 16	N = 32
-5.050 + 8.665 i	-5.050 + 8.665 i	-5.050 + 8.665 i
-.0463 + .0475 i	-.0463 + .0475 i	-.0463 + .0475 i
-.1982 + .4470 i	-.1982 + .4477 i	-.1982 + .4477 i
-.0420 + 2.169 i	-.0420 + 2.169 i	-.0420 + 2.169 i
-.0272 + 6.108 i	-.0272 + 6.104 i	-.0272 + 6.104 i
-.0253 + 12.077 i	-.0253 + 12.049 i	-.0253 + 12.047 i
-.0250 + 20.074 i	-.0250 + 19.919 i	-.0250 + 19.912 i
-.0250 + 30.129 i	-.0250 + 29.543 i	-.0250 + 29.520 i

MODEL 4: EULER-BERNOULLI BEAM; ACTUATOR DYNAMICS WITH DELAY

. State-Space: $\mathbf{z} = \mathbf{z}_E$ defined by (69) - (70)

$\mathbf{A} = \mathbf{A}$ defined by (71) - (72)

$\mathbf{B} = \mathbf{B}$ defined by (73)

$\mathbf{C} = \mathbf{C}_{E0}$ defined by (236)

. Optimal Feedback Operator

$$K_{ED} \mathbf{z}(t) = K_{E0} \mathbf{z}_E^o(t) + \int_{-r}^0 K_9(s) \phi_1(s) ds + \int_{-r}^0 K_{10}(s) \phi_2(s) ds$$

Since we have set $a_{21} = 0$, one can show that $K_9(s) \equiv 0$ (see Refs. 6 and 13). This choice is made merely to reduce some of the computational burden.

In this case the approximation scheme [see eqns. (175) - (183)] involves a spatial discretization parameter $[N]$, and a 'past-history' parameter $[M]$. Based on our earlier study of this model [see Ref. 1], we have chosen to present results only for the value $M = 8$. As before, Potter's method was used to compute a solution for the Riccati equation (134) and the approximating gain operator was constructed. The gain operator $K_{ED}^{N,M}$ has the form [see eqn. (126)]

$$\begin{aligned}
K_{ED}^{N,M} z_{ED}(t) = & K_1^{N,M} \theta(t) + K_2^{N,M} \omega(t) \\
& + K_3^{N,M} [u_t(t,L) + L\omega(t)] \\
& + K_4^{N,M} [u_{xt}(t,L) + \omega(t)] \\
& + \int_0^L K_5^{N,M}(x) [u_{xx}(t,x)] dx \\
& + \int_0^L K_6^{N,M}(x) [u_t(t,x) + x\omega(t)] dx \\
& + K_7^{N,M} x_1(t) + K_8^{N,M} x_2(t) \\
& + \int_{-r}^0 K_9^{N,M}(s) \phi_1(s) ds \\
& + \int_{-r}^0 K_{10}^{N,M}(s) \phi_2(s) ds
\end{aligned}$$

As noted above, with $a_{21} = 0$ in the 'delay' matrix A_2 it can be shown that $K_9^{N,M}(s) = 0$. The structural differences between this model and MODEL 3 is the functional gain $K_{10}(s)$ and the dependence on two discretization parameters $[N$ and $M]$.

Table 11 shows the convergence of the gains $K_i^{N,\delta}$ for $i = 1, 2, 3, 4, 7$ and 8 . As expected, the results are quite similar to the MODEL 3 case [c.f. Table 9].

TABLE 11. Sub-optimal Gains; MODEL 4

N	$K_1^{N,\delta}$	$K_2^{N,\delta}$	$K_3^{N,\delta}$	$K_4^{N,\delta}$	$K_7^{N,\delta}$	$K_8^{N,\delta}$
8	-10.000	-.47888	4.1044	-3.3480 E-2	-.56202	-.94504
12	-10.000	-.47888	4.1034	-3.4480 E-2	-.56201	-.94504
16	-10.000	-.47888	4.1035	-3.4500 E-2	-.56201	-.94504
32	-10.000	-.47888	4.1034	-3.4554 E-2	-.56201	-.94504

The graphs of the functional gains $K_5^{N,M}(x)$ and $K_6^{N,M}(x)$ are shown in Figures 12 and 13, respectively. These differ very little from the corresponding results in MODEL 3 (see Figures 10 and 11). Figure 14 displays the gain functional for the history term $K_{10}^{N,\delta}(s)$. The results for $N = 8, 12, 16$ and 32 are indistinguishable. Note that the history variables have been approximated using the "AVE" scheme with $M = 8$. Thus, the graph shown in Figure 14 is a piecewise constant approximation for $K_{10}(s)$ and the interval $[-.1, 0]$ has been partitioned into eight subintervals.

The closed-loop eigenvalues for the 'actuator mode' and the first seven 'structural modes' are virtually identical to those shown in Table 10. It should be noted that this model also includes some approximations for the "past history modes". For this case these have

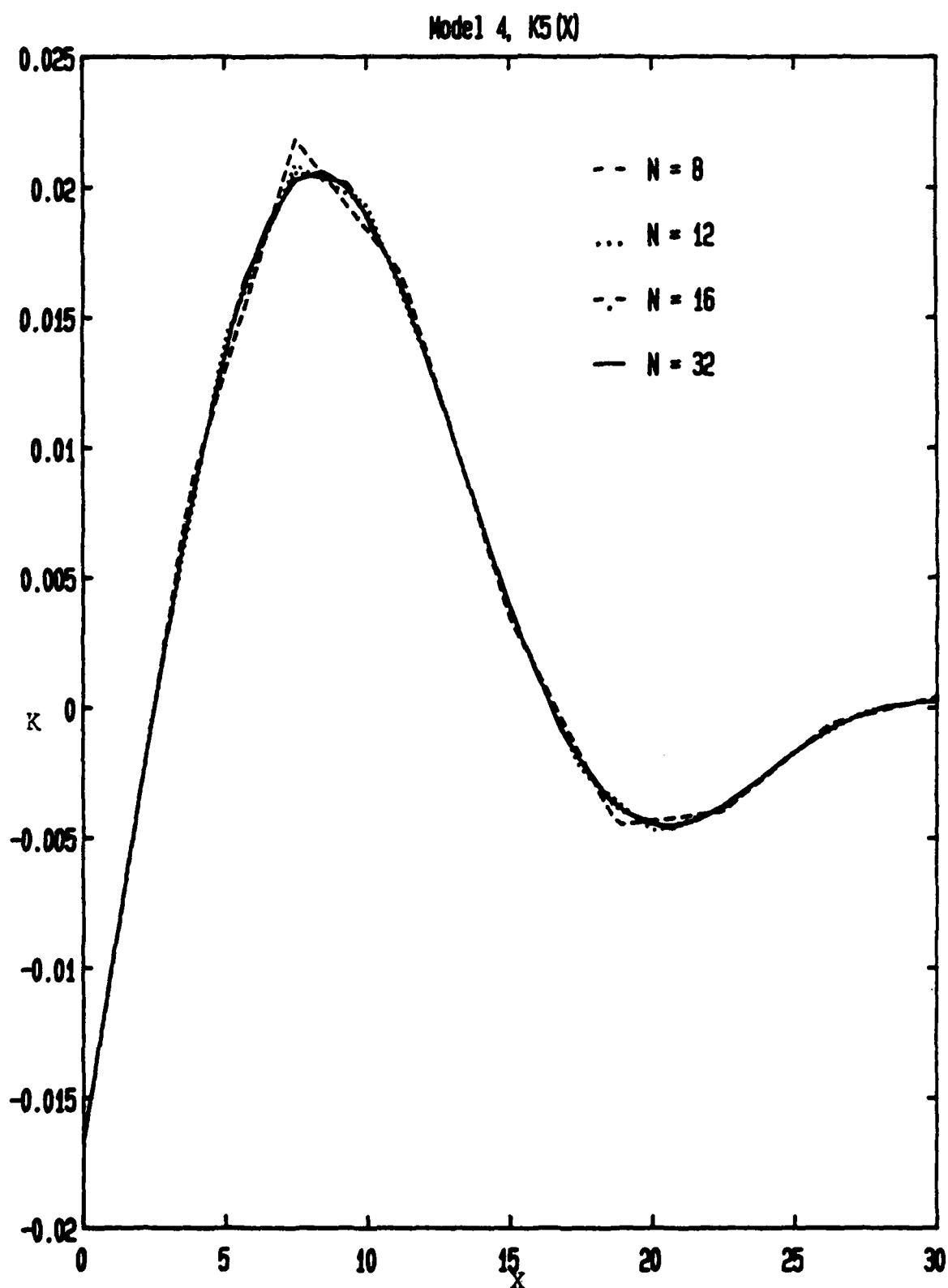


Figure 12. Functional Gain K_5 ; Model 4

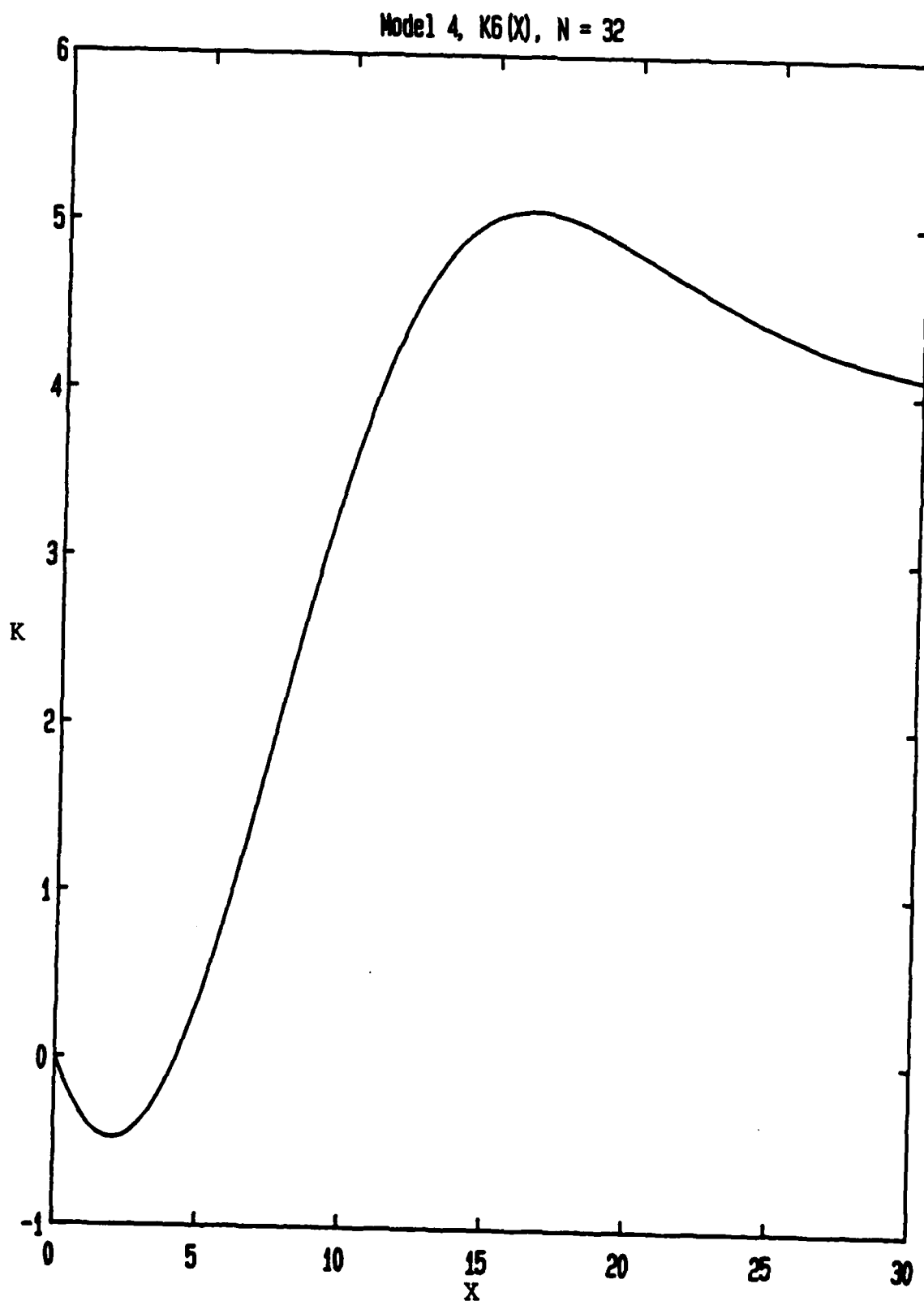


Figure 13. Functional Gain K_6 ; Model 4

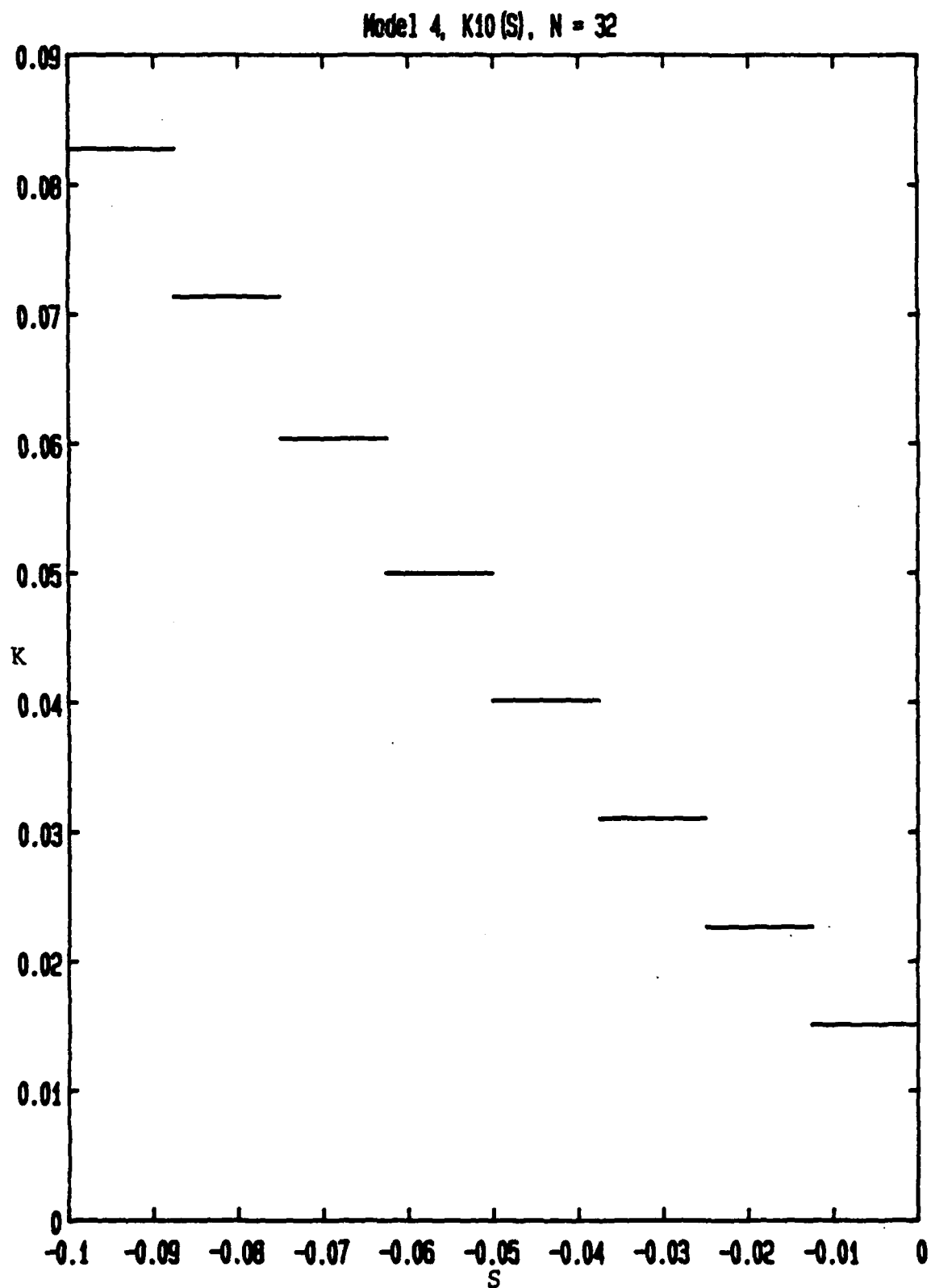


Figure 14. History Functional Gain ; Model 4

significantly higher damping than the other modes.

MODEL 5: TIMOSHENKO BEAM; ACTUATOR DYNAMICS WITH NO DELAY

• State-Space: $\bar{z} = \bar{z}$ defined by (76) - (77)

$A = A_0$ defined by (78) - (79)

$B = B_0$ defined by (80)

$C = C_0$,

where C_0 has the block structure

$$C_0 = \begin{bmatrix} C_T & 0 & 0 \\ 0 & 1 & 0 \\ 0 & 0 & 1 \end{bmatrix} \quad (238)$$

and C_T is given in (233) - (234).

• Optimal Feedback Operator

$$\begin{aligned} K_{T0} z_{T0}(t) = & K_1 \theta(t) + K_2 \omega(t) \\ & + K_3 [u_t(t, L) + L\omega(t)] \\ & + K_4 [\psi_t(t, L) + \omega(t)] \\ & + \int_0^L K_5(x) [u_t(t, x) + x\omega(t)] dx \\ & + \int_0^L K_6(x) [\psi_t(t, x) + \omega(t)] dx \\ & + \int_0^L K_7(x) [\psi_x(t, x)] dx \\ & + \int_0^L K_8(x) [u_x(t, x) - \psi(t, x)] dx \\ & + K_9 x_1(t) + K_{10} x_2(t) \end{aligned} \quad (239)$$

As in the previous cases we employ the approximation scheme to construct the finite-dimensional model (185) - (187). Potter's method is used to compute the approximate gain operator $K_{T_0}^N$ which has the same form as K_{T_0} [see eqn. (239)].

Table 12 shows the convergence of the gain values K_i^N for $i = 1, 2, 3, 4, 9$ and 10 .

TABLE 12. Sub-optimal Gains; MODEL 5

N	K_1^N	K_2^N	K_3^N	K_4^N	K_9^N	K_{10}^N
8	-10.000	-.47759	3.0496	-.49331	-.54523	-.95785
12	-9.998	-.47927	4.1594	.10191	-.54459	-.95779
16	-9.999	-.47982	4.1898	1.5195 E-2	-.54488	-.95782
32	-10.002	-.47992	4.2168	1.9758 E-2	-.54506	-.95783

The first four gains behave very much like their counterparts in the case without an actuator [see Table 7]. The actuator gains also compare well with the values for the corresponding Euler-Bernoulli case [c.f. gains K_7^N and K_8^N in Table 9].

The convergence results for the functional gains K_i^N , $i = 5, 6, 7, 8$ are shown in Figures 15 through 18, respectively. These gains appear better behaved than the case with no actuator [MODEL 2] but still not as good as the Euler-Bernoulli case [MODEL 3]. The closed-loop eigenvalues are shown in Table 13. The actuator mode is identical to the corresponding Euler-Bernoulli case [MODEL 3], while the structural

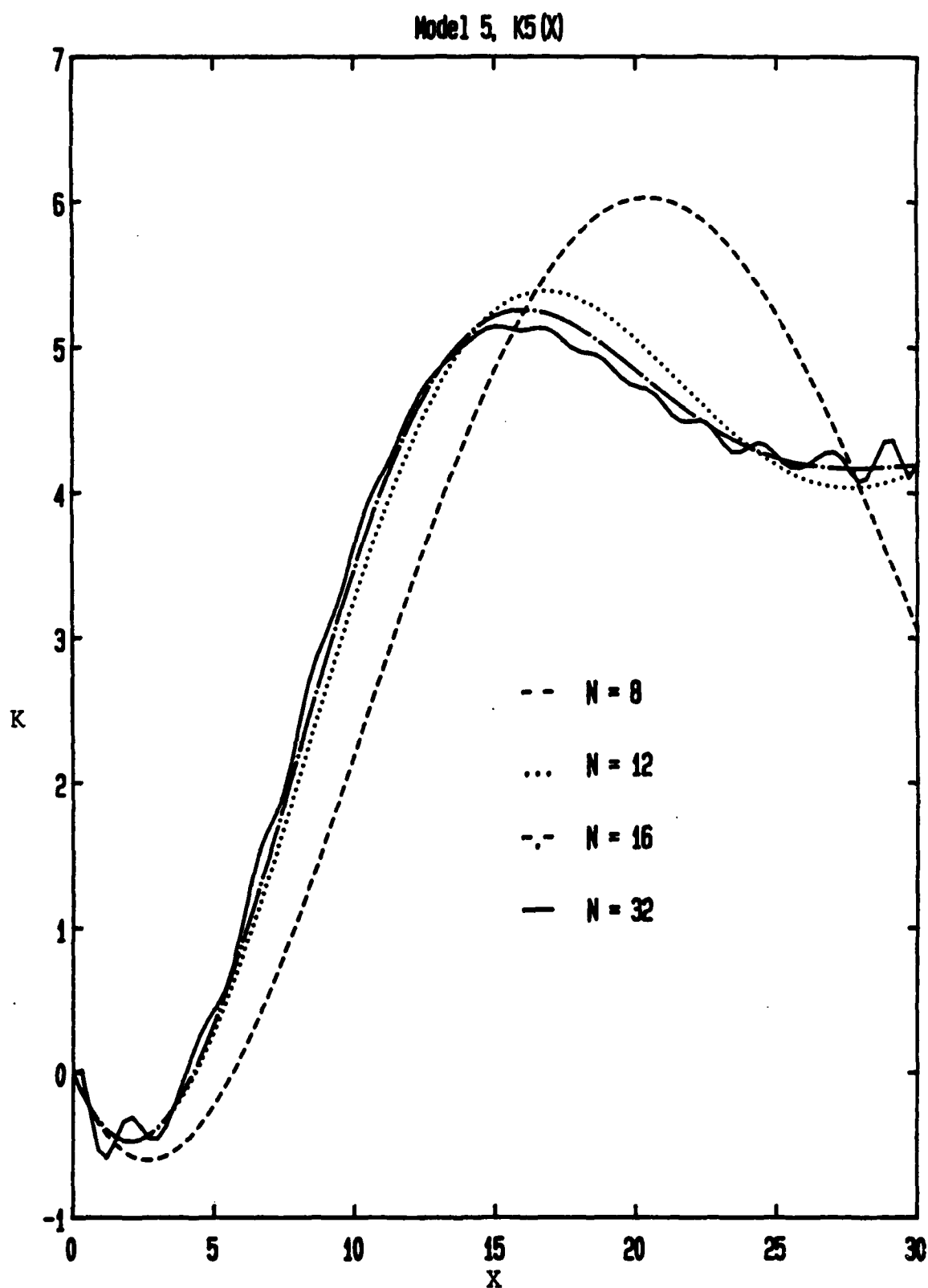


Figure 15. Functional Gain K_5 ; Model 5

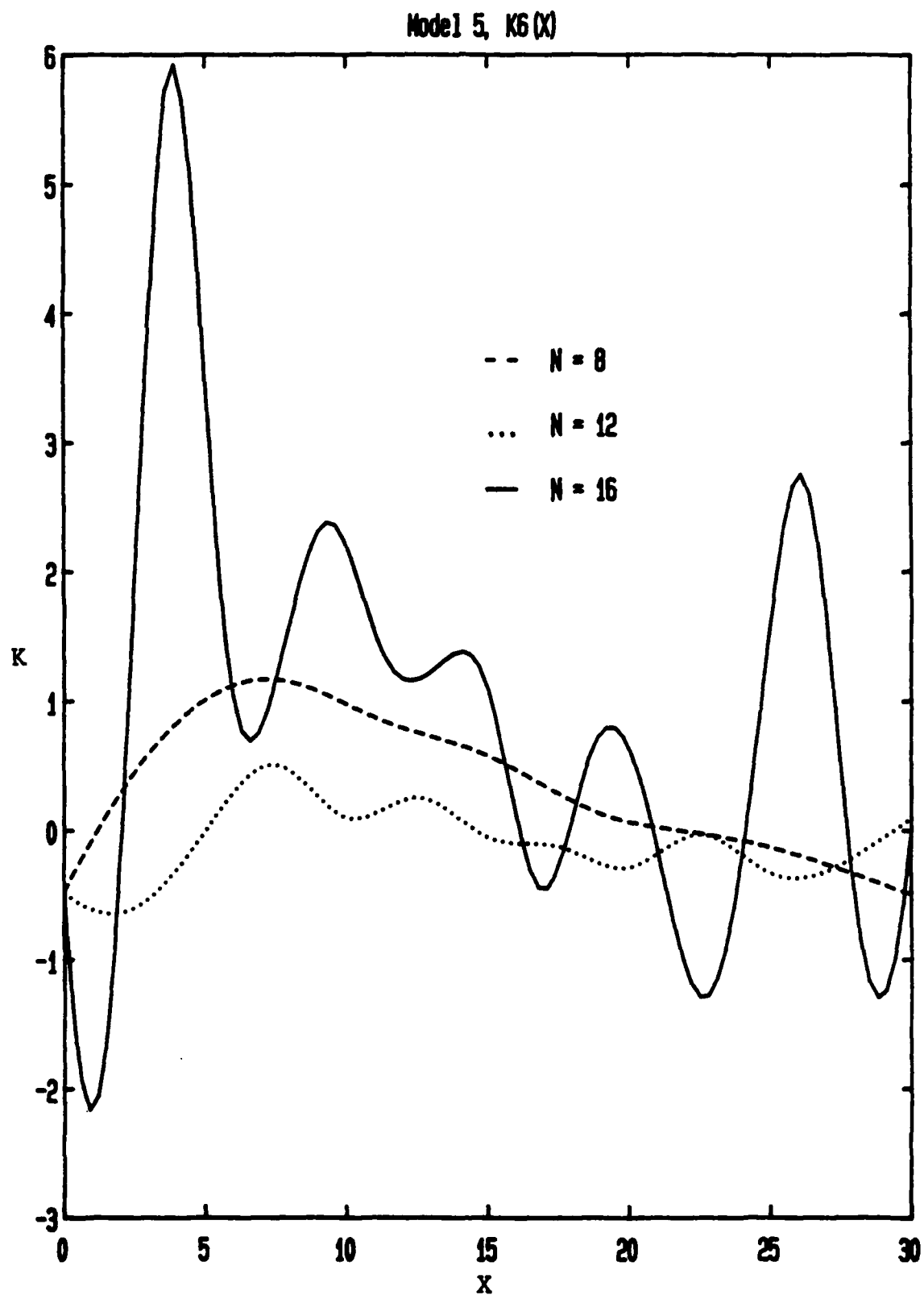


Figure 16. Functional Gain K_6 ; Model 5

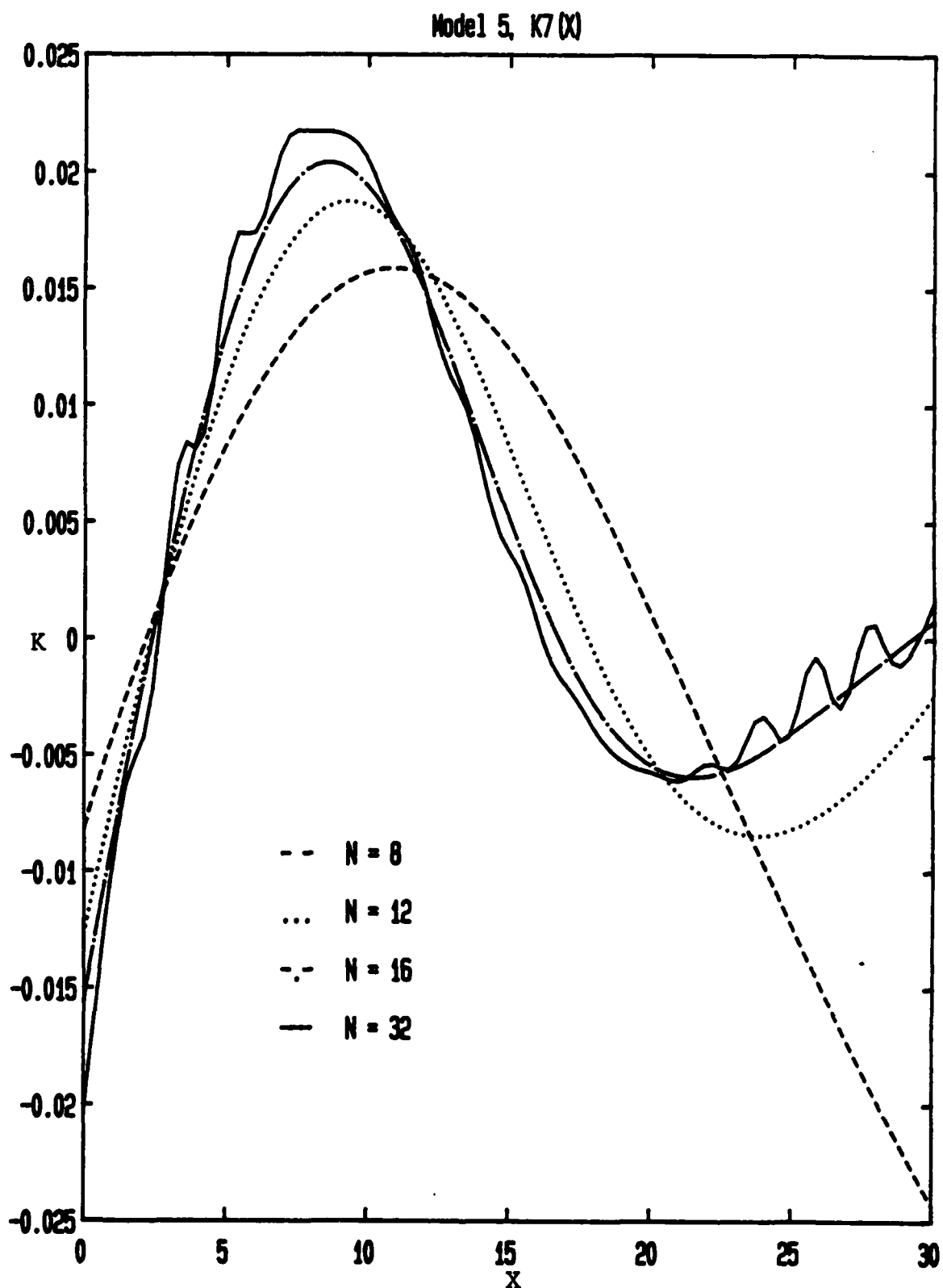


Figure 17. Functional Gain K_7 ; Model 5

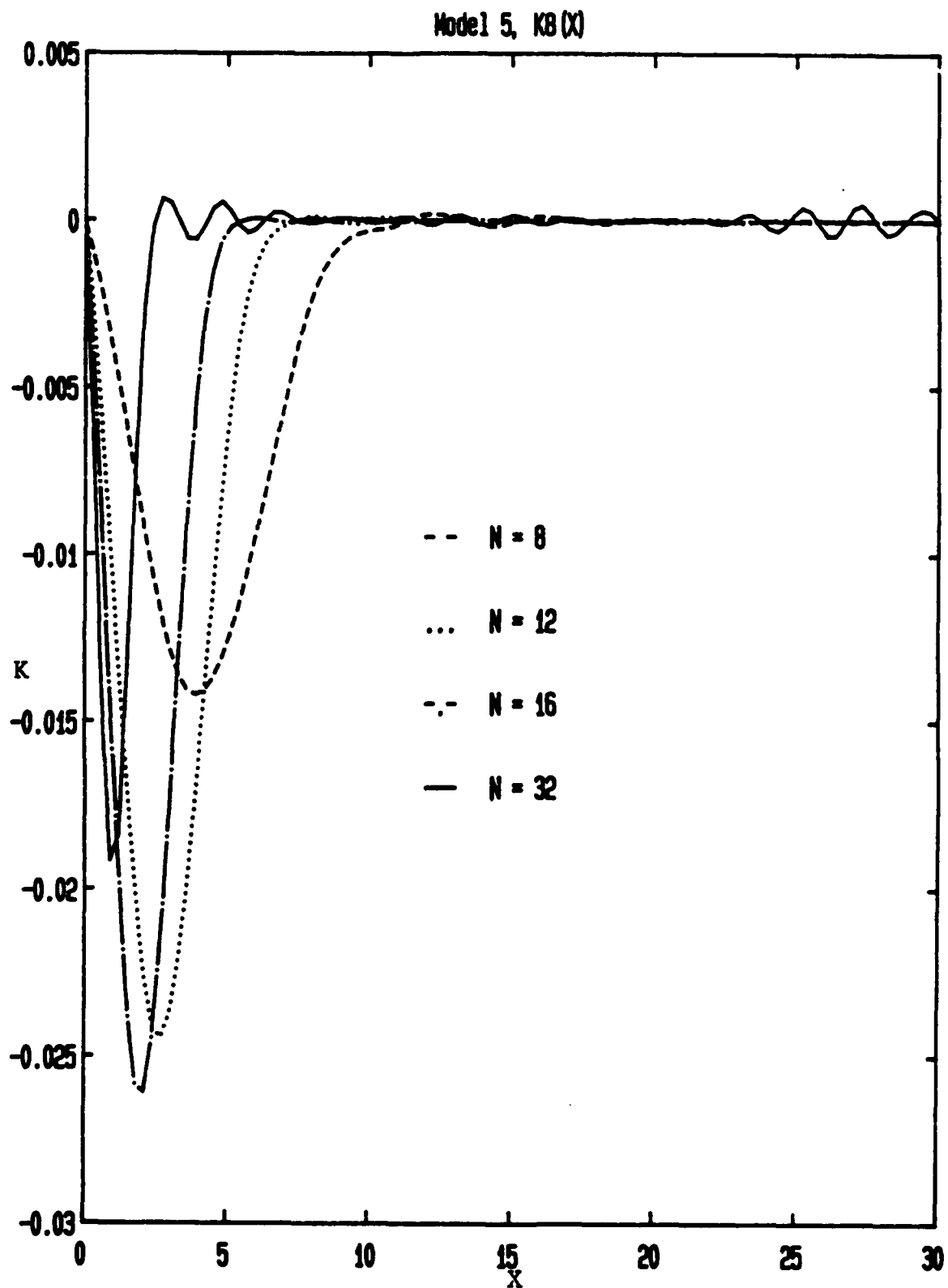


Figure 18. Functional Gain K_8 ; Model 5

TABLE 13. Closed-Loop Eigenvalues; MODEL 5

N = 8	N = 16	N = 32
-5.049 + 8.665 i	-5.050 + 8.665 i	-5.050 + 8.665 i
-.0463 + .0475 i	-.0463 + .0475 i	-.0464 + .0475 i
-.1982 + .4479 i	-.1985 + .4477 i	-.1984 + .4477 i
-.0427 + 2.4235 i	-.0421 + 2.1745 i	-.0420 + 2.1694 i
-.0276 + 9.7022 i	-.0273 + 6.2488 i	-.0275 + 6.1063 i
-.0250 + 33.435 i	-.0252 + 13.250 i	-.0253 + 12.065 i
-.0250 + 111.347 i	-.0250 + 24.925 i	-.0250 + 19.996 i
-.0250 + 321.485 i	-.0250 + 43.393 i	-.0250 + 29.806 i

modes are almost identical to the Timoshenko beam without actuator dynamics [MODEL 2].

MODEL 6: TIMOSHENKO BEAM; ACTUATOR DYNAMICS WITH DELAY

• State-Space: $\tilde{z} = \tilde{z}_T$ defined by (81) - (82)

$A = A$ defined by (83) - (84)

$B = B$ defined by (85)

$C = C_{TD}$,

where

$$C_{TD} = [C_0, 0, 0]$$

and C_0 is given by (238).

• Optimal Feedback Operator

$$K_{T0} z(t) = K_{T0} z_T^o(t) + \int_{-r}^0 K_{11}(s) \phi_1(s) ds + \int_{-r}^0 K_{12}(s) \phi_2(s) ds ,$$

where K_{T0} is defined by (239).

As in MODEL 4 we have a two-stage approximation scheme involving both a spatial discretization parameter $[N]$, and a past-history parameter $[M]$. Again we present numerical results for the case $M = 8$. We employ the approximation scheme described by equations (185) - (187) and use Potter's method to solve the appropriate Riccati eqn. (134). The gain operator has the form

$$\begin{aligned}
 K_{TD}^{N,M} z(t) = & K_1^{N,M} \theta(t) + K_2^{N,M} \omega(t) \\
 & + K_3^{N,M} [u_t(t,L) + L\omega(t)] \\
 & + K_4^{N,M} [\psi_t(t,L) + \omega(t)] \\
 & + \int_0^L K_5^{N,M}(x) [u_t(t,x) + x\omega(t)] dx \\
 & + \int_0^L K_6^{N,M}(x) [\psi_t(t,x) + \omega(t)] dx \\
 & + \int_0^L K_7^{N,M}(x) [\psi_x(t,x)] dx \\
 & + \int_0^L K_8^{N,M}(x) [u_x(t,x) - \psi(t,x)] dx \\
 & + K_9^{N,M} x_1(t) + K_{10}^{N,M} x_2(t) \\
 & + \int_{-r}^0 K_{11}^{N,M}(s) x_1(t-s) ds \\
 & + \int_{-r}^0 K_{12}^{N,M}(s) x_2(t-s) ds
 \end{aligned} \tag{240}$$

As was noted for the case of the Euler-Bernoulli beam with delayed actuator [MODEL 4], the special choice $a_{21} = 0$ in the delayed actuator

model implies that the gain functional associated with the delayed term $x_1(t-r)$ is identically zero. Thus, to approximate the gain operator we must compute the six gain values $K_i^{N,M}$ for $i = 1, 2, 3, 4, 9$ and 10 , and the five functional gains $K_i^{N,M}$, $i = 5, 6, 7, 8$ and 12 .

Table 14 shows convergence of the gain values (recall $M = 8$) for $N = 8, 12, 16$ and 32 . The trends in this problem are very similar to the case without the delay [c.f. Table 12].

TABLE 14. Sub-optimal Gains; MODEL 6

N	$K_1^{N,8}$	$K_2^{N,8}$	$K_3^{N,8}$	$K_4^{N,8}$	$K_9^{N,8}$	$K_{10}^{N,8}$
8	-10.000	-.47771	3.1485	-.42911	-.56338	-.94517
12	-10.001	-.47926	4.1686	.10434	-.56277	-.94511
16	-10.000	-.47968	4.1756	-3.028 E-4	-.56300	-.94513
32	-10.003	-.48239	4.2755	8.047 E-2	-.56669	-.94547

The spatially distributed gains are shown in Figures 19 through 22. These exhibit the same behavior we have seen in the previous Timoshenko beam models [MODELS 2 and 5]. The history gain $K_{12}^{N,8}$ is shown in Fig. 23 and is virtually identical to the corresponding gain functional for the Euler-Bernoulli model with delayed actuator [see $K_{10}^N(s)$ in Fig. 14].

While the spatial gains do not behave very well for this Timoshenko model the closed-loop eigenvalues seem to be converging nicely, especially for the lower frequencies.

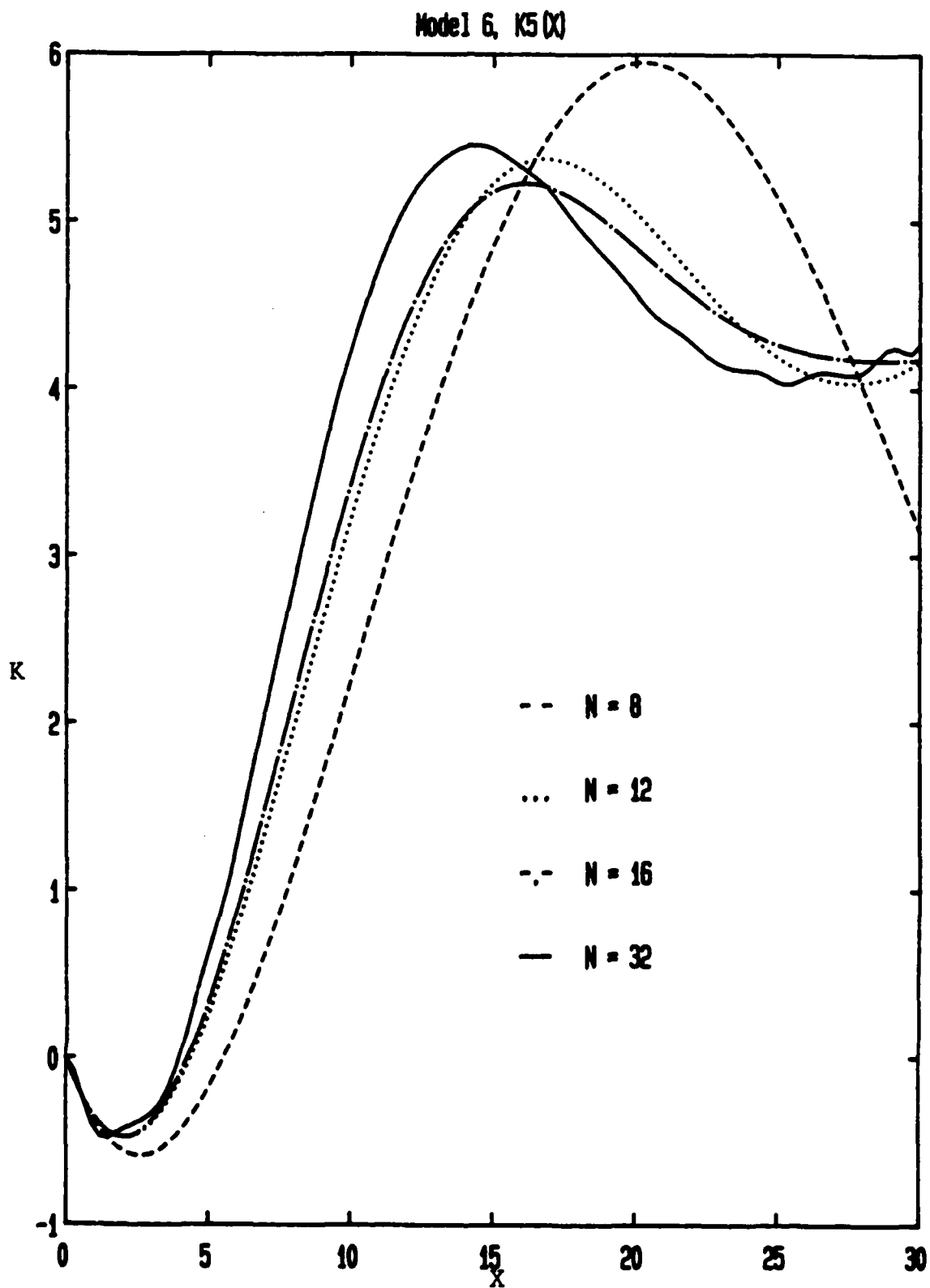


Figure 19. Functional Gain K_5 ; Model 6

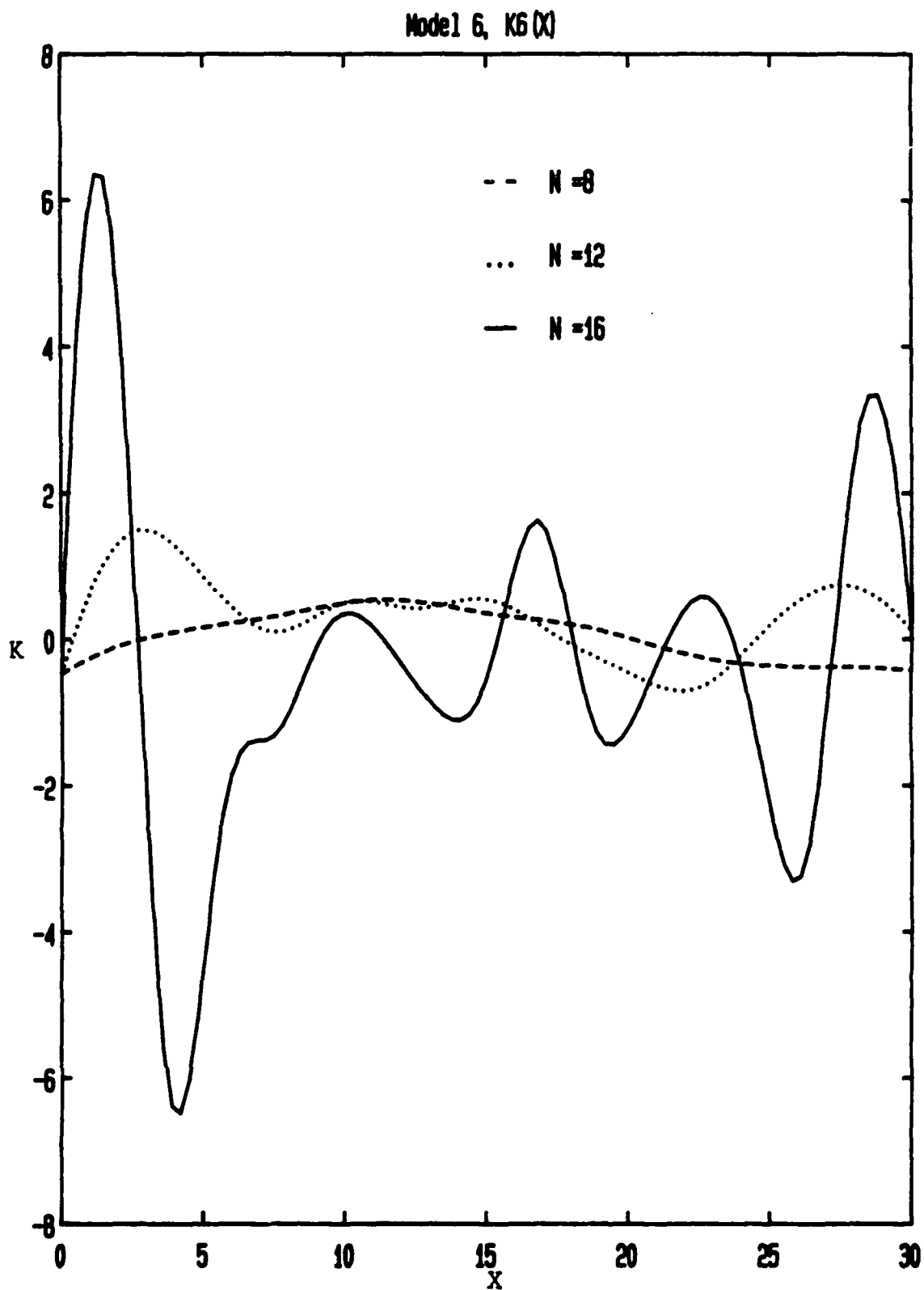


Figure 20. Functional Gain K_6 ; Model 6

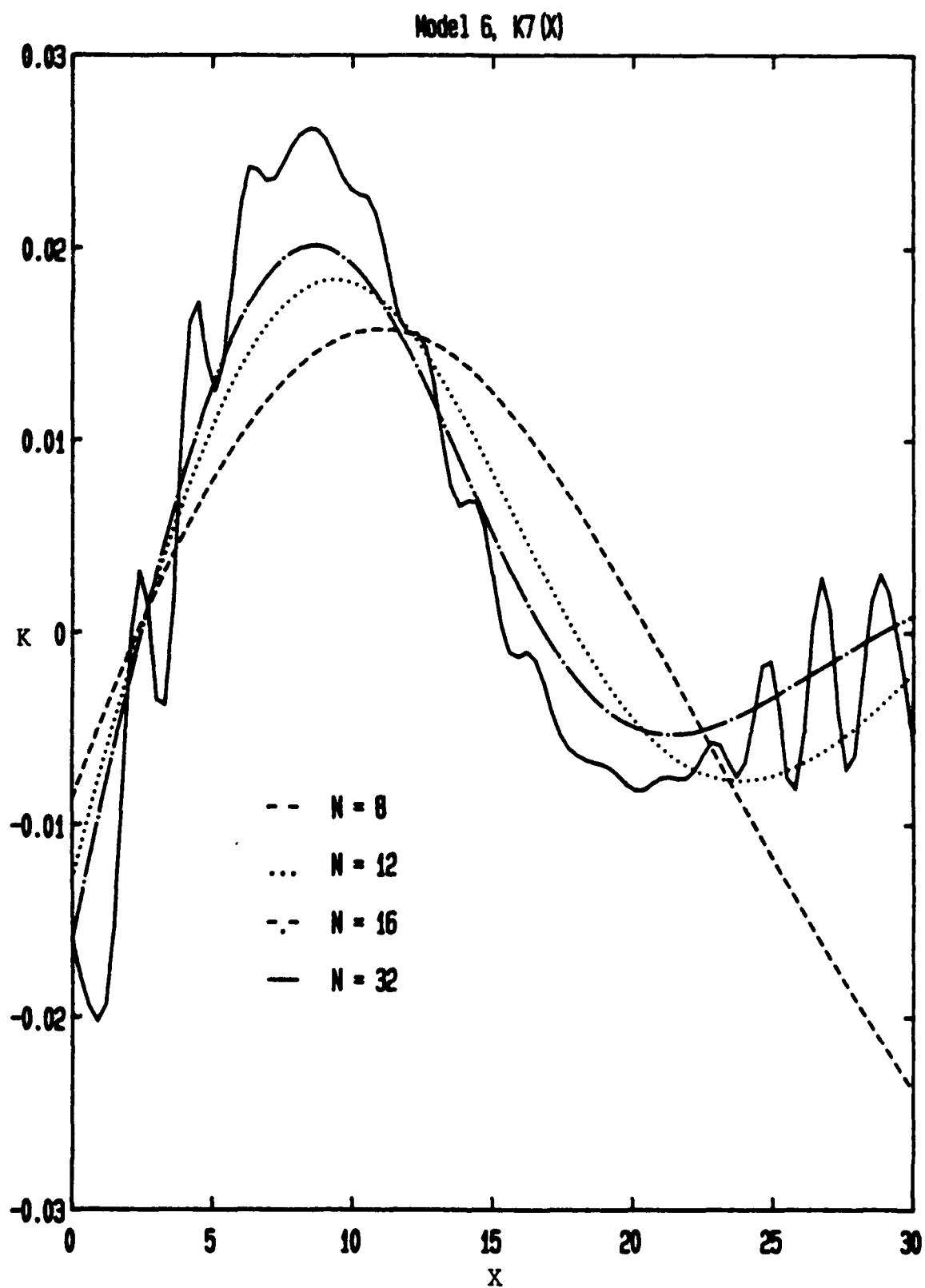


Figure 21. Functional Gain K_7 ; Model 6

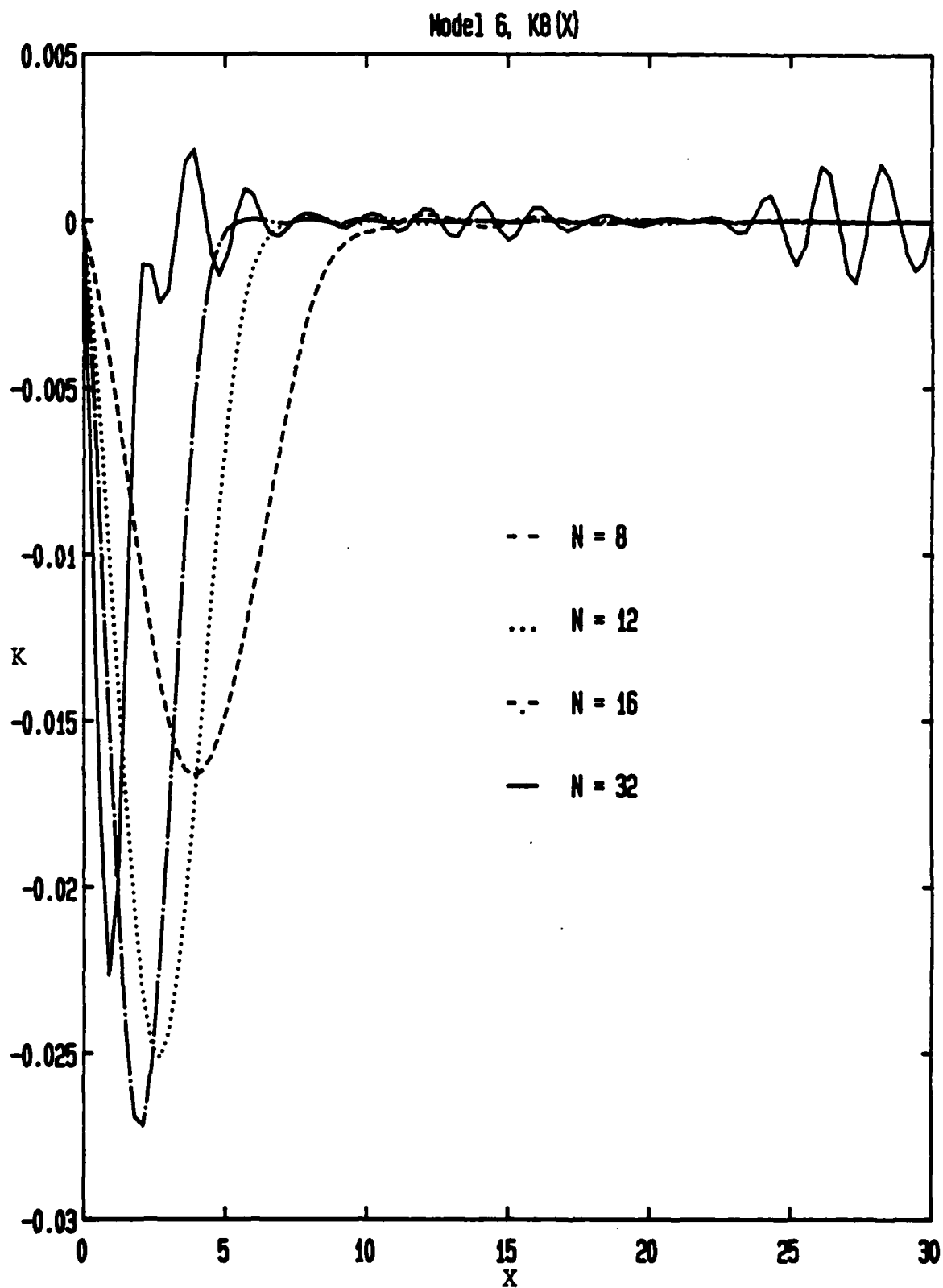


Figure 22. Functional Gain K_8 ; Model 6

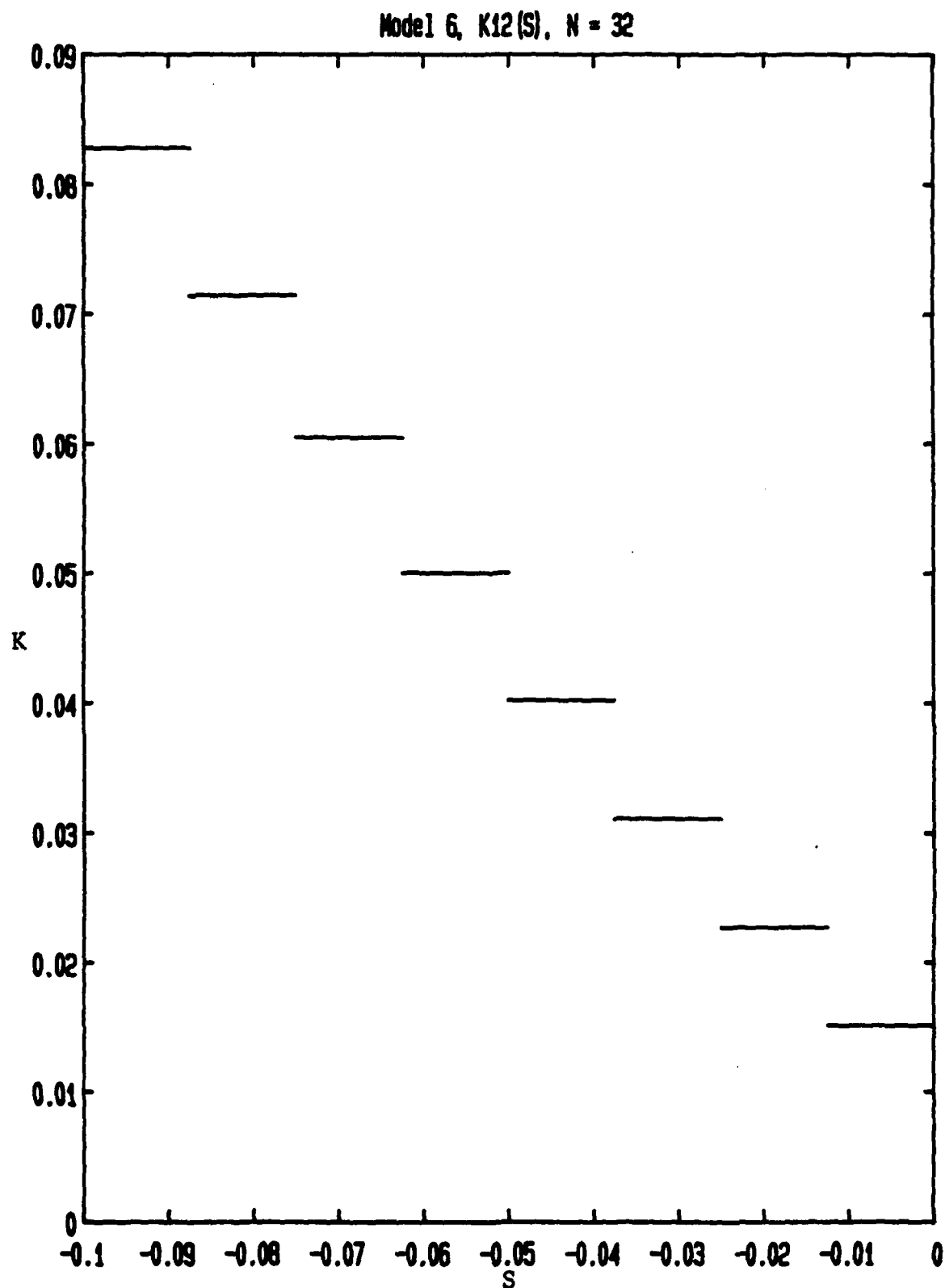


Figure 23. History Functional Gain ; Model 6

TABLE 15. Closed-Loop Eigenvalues; MODEL 6

N = 8	N = 16	N = 32
-5.526 + 9.064 i	-5.526 + 9.064 i	-5.526 + 9.064 i
-.0463 + .0475 i	-.0463 + .0475 i	-.0463 + .0476 i
-.1982 + .4480 i	-.1985 + .4477 i	-.1984 + .4476 i
-.0425 + 2.4235 i	-.0419 + 2.1745 i	-.0427 + 2.1695 i
-.0275 + 9.7022 i	-.0272 + 6.2488 i	-.0280 + 6.1064 i
-.0250 + 33.435 i	-.0252 + 13.250 i	-.0253 + 12.065 i
-.0250 + 111.347 i	-.0250 + 24.925 i	-.0250 + 19.996 i
-.0250 + 321.485 i	-.0205 + 43.393 i	-.0250 + 29.806 i

Note from Table 15 that the actuator mode has somewhat higher damping and frequency than for the Timoshenko model without delay [MODEL 5]; they are also higher than either of the relevant Euler-Bernoulli models [MODEL 3 and 4]. The structural eigenvalues are virtually identical to the previous Timoshenko modes [see Tables 8 and 13].

MODEL 7: ISOTROPIC PLATE

The model, as described previously, can be written as the second-order partial differential equation

$$\bar{m} u_{tt}(t,x,y) = D \Delta^2 u(t,x,y) + u(t) \phi(x,y) . \quad (241)$$

Here \bar{m} is the plate mass, per unit area, so that $\bar{m} = \rho \cdot h$ where ρ is the mass density of the plate material and h is the plate thickness. The stiffness parameter D is given by

$$D = \left[\frac{E h^3}{12 (1 - \nu^2)} \right]$$

where E is Young's modulus for the plate material and ν is Poisson's ratio. The symbol Δ denotes the Laplacian operator. The function ϕ describes the (fixed) distribution of the applied control force and $u(t)$ is the control. The plate has length a in the x direction and b in the y direction. Internal damping is modelled in the Kelvin-Voigt form. Thus, the right-hand side of (241) is modified by the addition of a term

$$e[\Delta^2]_t$$

For simplicity the parameters taken for the numerical calculations are $D = \bar{m} = a = b = 1$. The force distribution function is

$$\phi(x,y) = 1 - [4(x - 1/2)(y - 1/2)]^2, \quad (242)$$

and the damping parameter e is 10^{-4} .

Following the procedures outlined in Section IV the appropriate state-space model is

State-Space: $\dot{Z} = \dot{Z}_p$ defined by (92) - (93)

$A = A_p$ defined by (94) - (95)

$B = B_p$ defined by (96).

Before discussing numerical results for the control problem we first demonstrate the model with no input (open-loop). The approximation scheme is given by equations (196) - (200). In all numerical results we use equal numbers of divisions along the x and y plate axes (i.e., $N_x = N_y = N$). The dimension of the approximating subspace is $2(N - 1)^2$. With the parameters taken at unit value the frequency of undamped motions of the clamped plate can be shown to be given by

[see Ref. 5, p. 495].

$$\omega = \pi^2 [m^2 + n^2] \quad (243)$$

$m, n = 1, 2, \dots$

TABLE 16. Open-Loop Frequencies; MODEL 7

m	n	N = 4	N = 8	"exact"
1	1	19.7428	19.7394	19.7392
1	2	49.5106	49.3556	49.3480
2	2	79.2358	78.9707	78.9568
1	3	101.2630	98.7953	98.6960
2	3	130.7811	128.4034	128.3049
3	3	181.9428	177.8226	177.6529

Table 16 shows a comparison of the exact and computed frequencies for $N = 4$ and 8. It should be noted that due to the geometric symmetry the "off-diagonal" modes ($m \neq n$) come in pairs. Only one such mode is shown in Table 16, thus with $N = 4$ we have actually estimated nine modes.

The final information needed to define the control problem is specification of the cost function. The standard quadratic functional in the form (104) is used with control weight R taken as unity, output map C given by

$$C \begin{bmatrix} u(t, x, y) \\ u_t(t, x, y) \end{bmatrix} = \begin{bmatrix} m^e(.2, .2) [\Delta u(t, x, y)] \\ m^e(.7, .7) [u_t(t, x, y)] \end{bmatrix} \quad (244)$$

and diagonal weights $S = \text{diag} [1., 1.]$.

The first controlled output is thus the "strain" (measured by the Laplacian of the displacement) at $x = y = .2$, while the second output is the velocity at the point $x = y = .7$. The feedback operator for this model is from (179)

$$K_p z_p(t) = \int_{\Omega} K_1(x,y) \Delta u(t,x,y) dx dy \\ + \int_{\Omega} K_2(x,y) u_t(t,x,y) dx dy$$

Following the same procedures as for the previous models, we employ the approximation scheme (196) - (202) to construct an approximate gain functionals $K_1^N(x,y)$ and $K_2^N(x,y)$. Just as in the open-loop frequency calculation we have used the same discretization parameter for the two spatial variables (i.e. $N_x = N_y = N$). Recall that the approximating system has dimension $2(N - 1)^2$.

We employ Potter's method to construct a solution of the Riccati equation and then compute the functional gains.

Figures 24-26 present the graphs of $K_1^N(x,y)$ for $N = 4, 8$ and 12 . Since these functionals depend on two independent variables each N value is a separate plot. To provide some comparison we show values along the line $x = y$ for $K_1^N(x,y)$, $N = 4, 8$ and 12 in Fig. 27.

Figures 28-30 present the results for the second functional gain $K_2^N(x,y)$, $N = 4, 8$ and 12 . Again the section at $x = y$ is compared for all three N values in Fig. 31.

The closed-loop eigenvalues are shown in Table 17. These all appear to be "converging", except for the damping in the low frequency mode which suddenly jumps at $N = 12$.

Model 7, $K_1(X, Y)$, $N = 4$

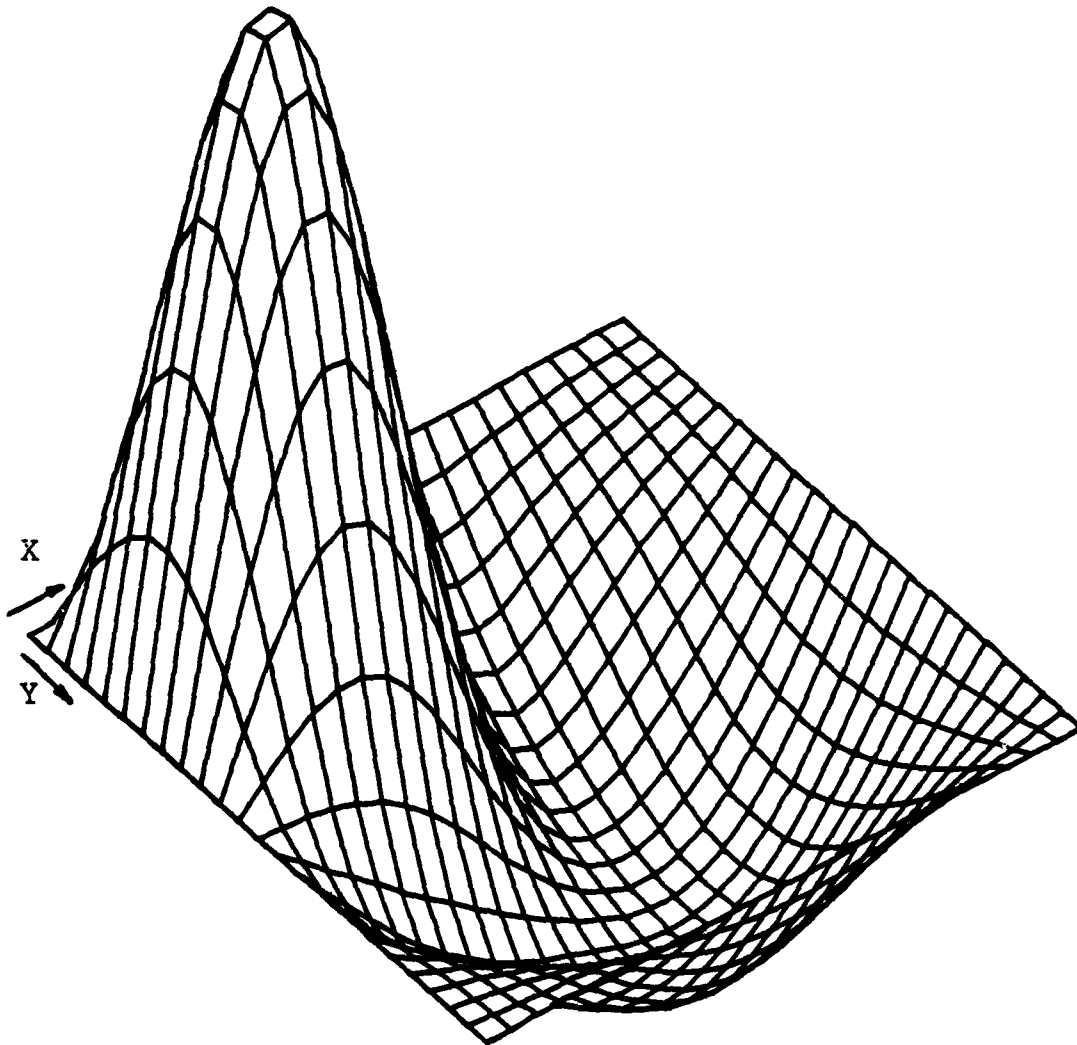


Figure 24. Functional Gain K_1 , $N = 4$; Model 7

Model 7, $K_1(X, Y)$, $N = 8$

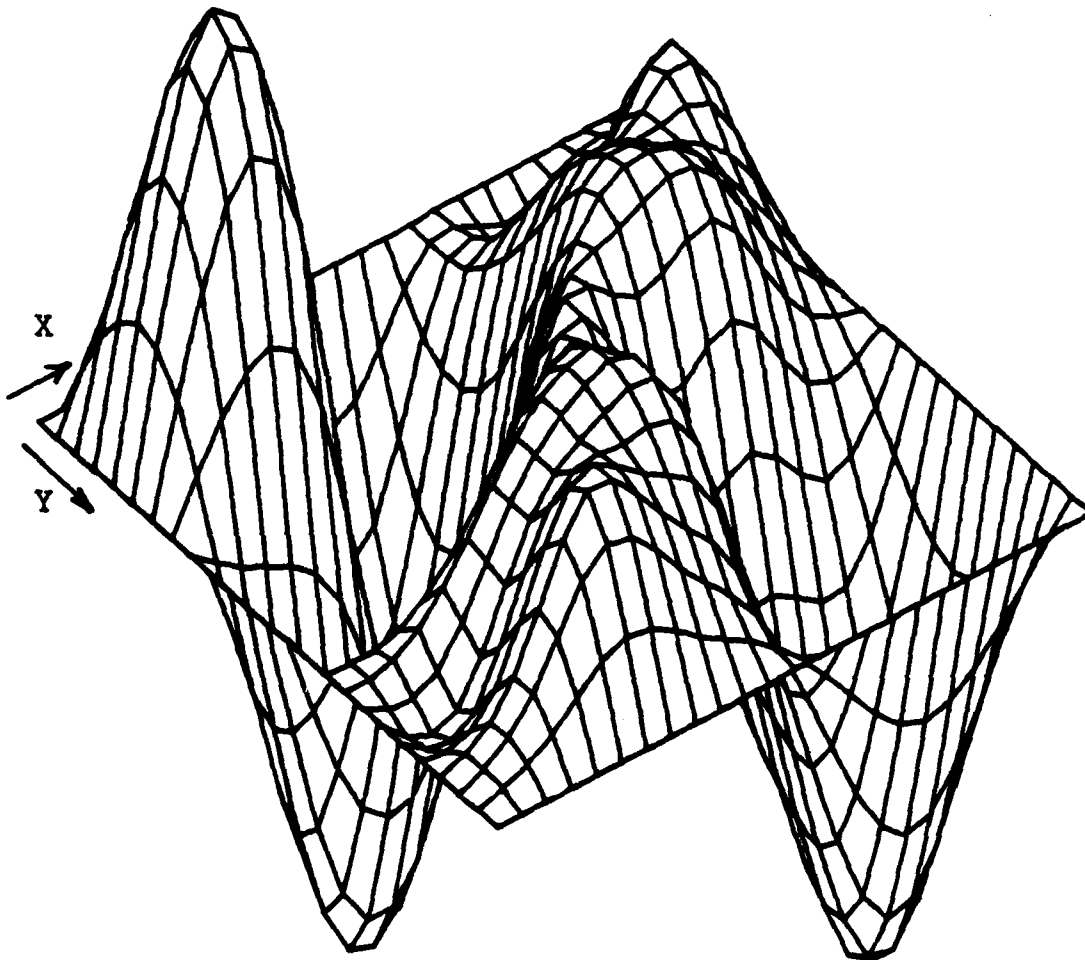


Figure 25. Functional Gain K_1 , $N = 8$; Model 7

Model 7, $K_1(X, Y)$, $N = 12$

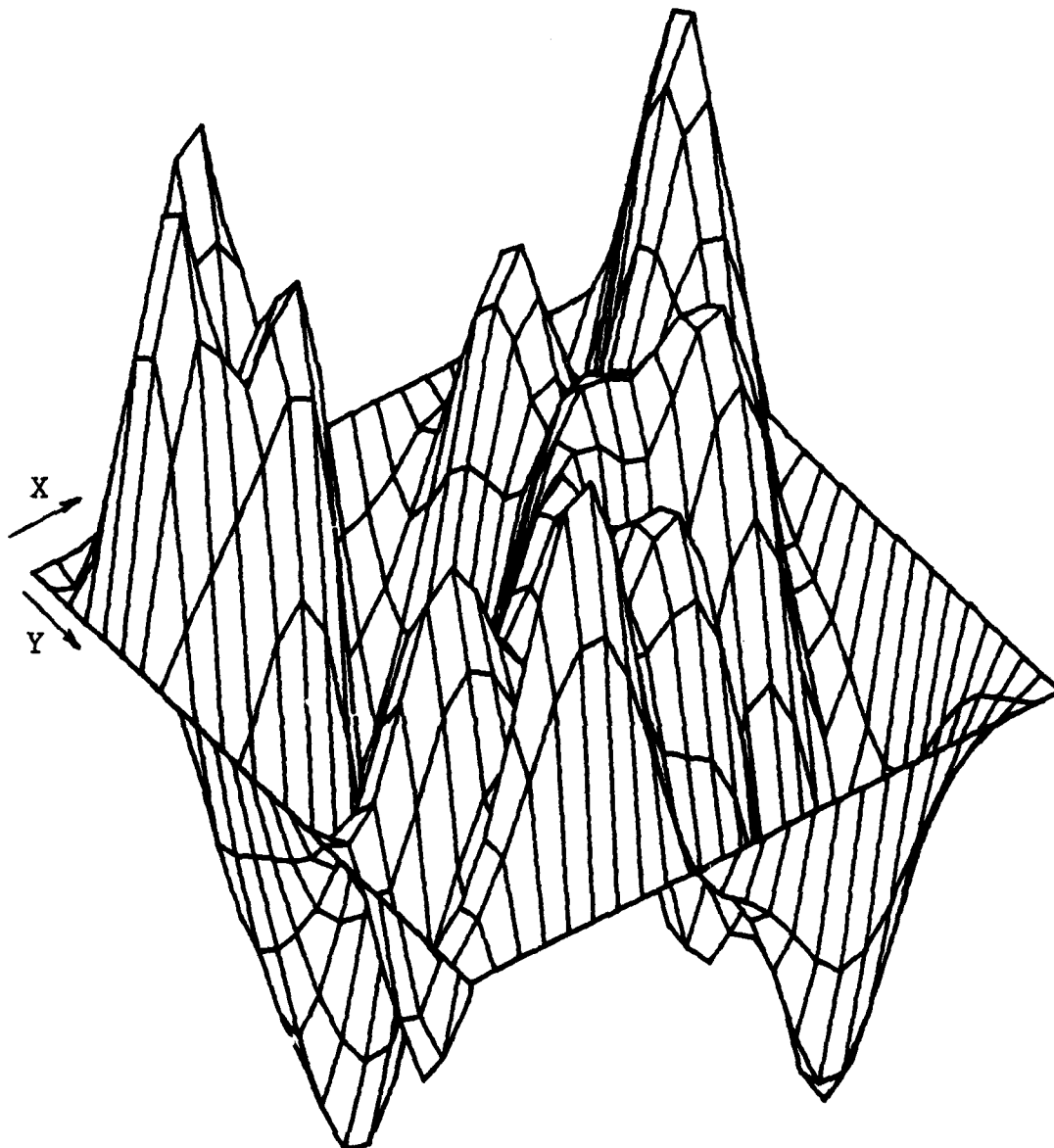


Figure 26. Functional Gain K_1 , $N = 12$; Model 7

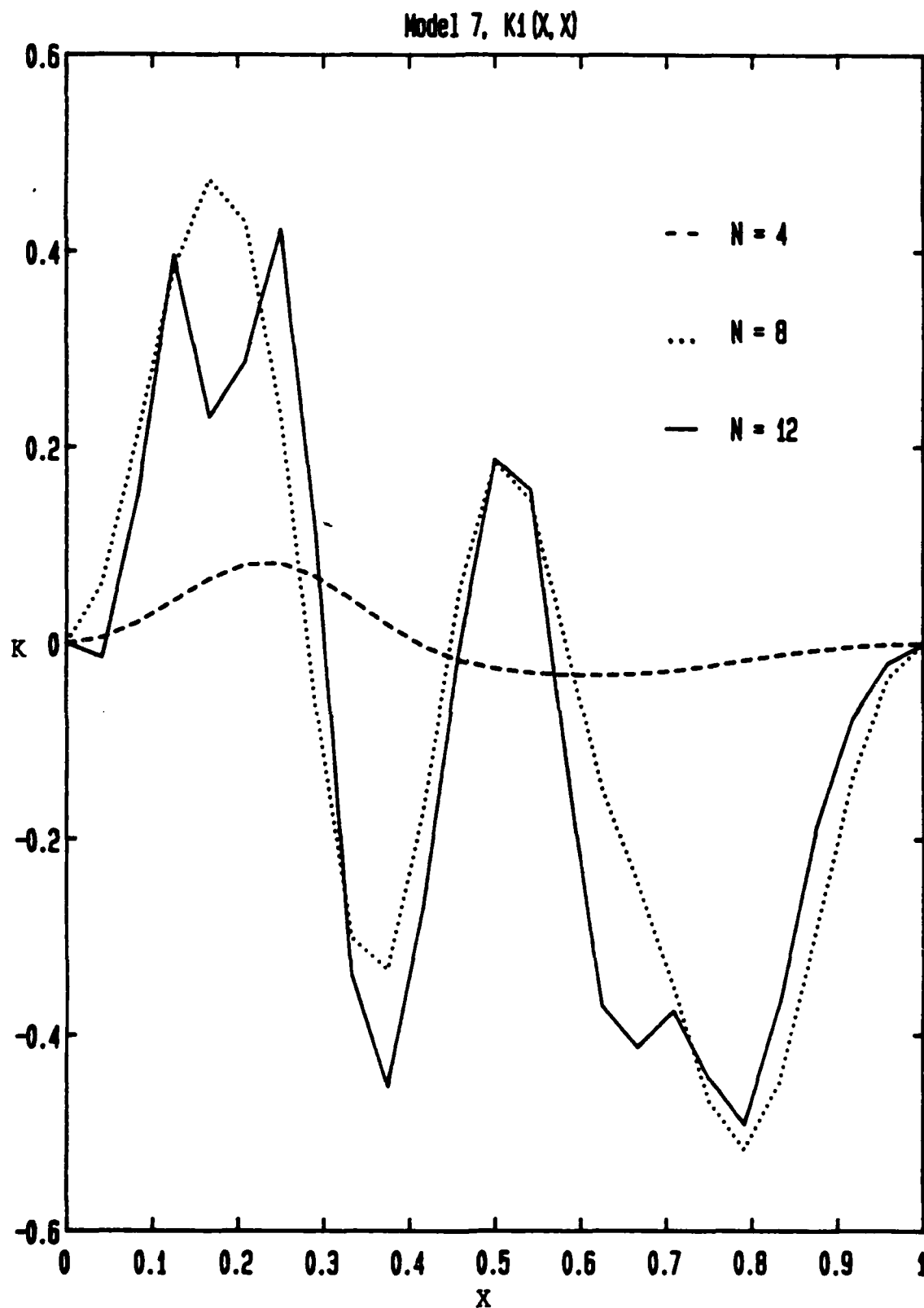


Figure 27. Functional Gain K_1 , Cross section $Y=X$; Model 7

Model 7, $K_2(X, Y)$, $N = 4$

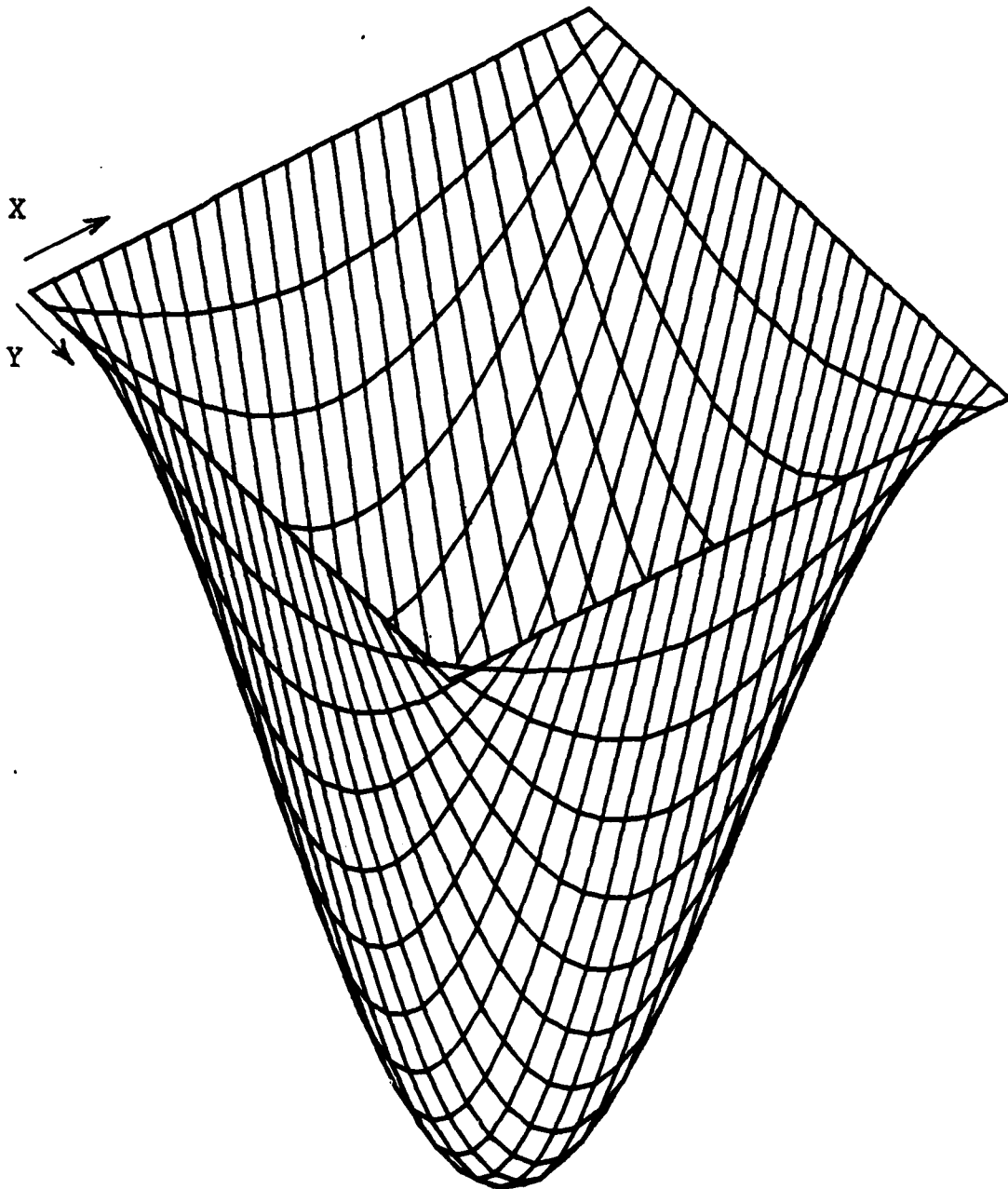


Figure 28. Functional Gain K_2 , $N = 4$; Model 7

Model 7, $K_2(X, Y)$, $N = 8$

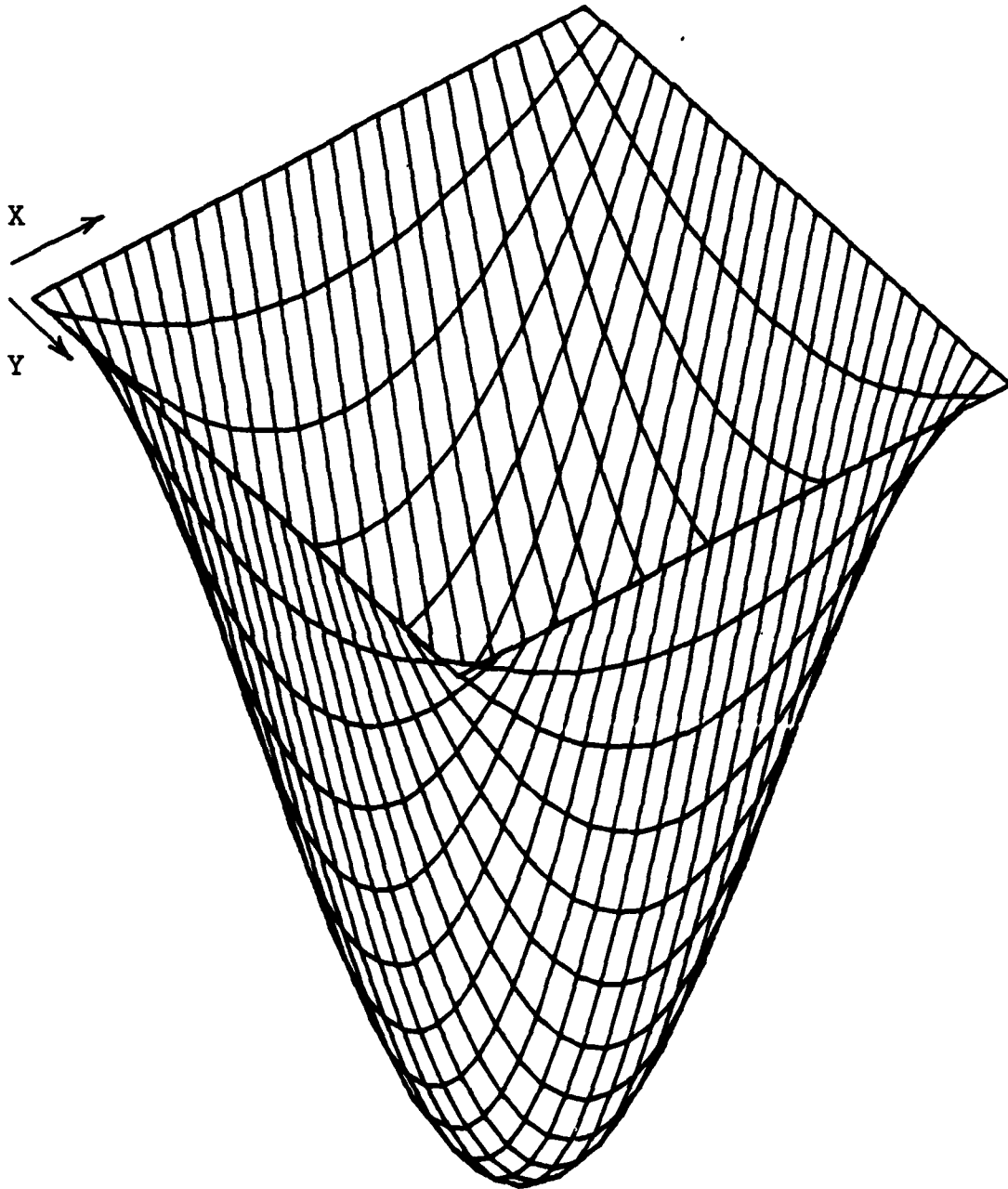


Figure 29. Functional Gain K_2 , $N = 8$; Model 7

Model 7, $K_2(X, Y)$, $N = 12$

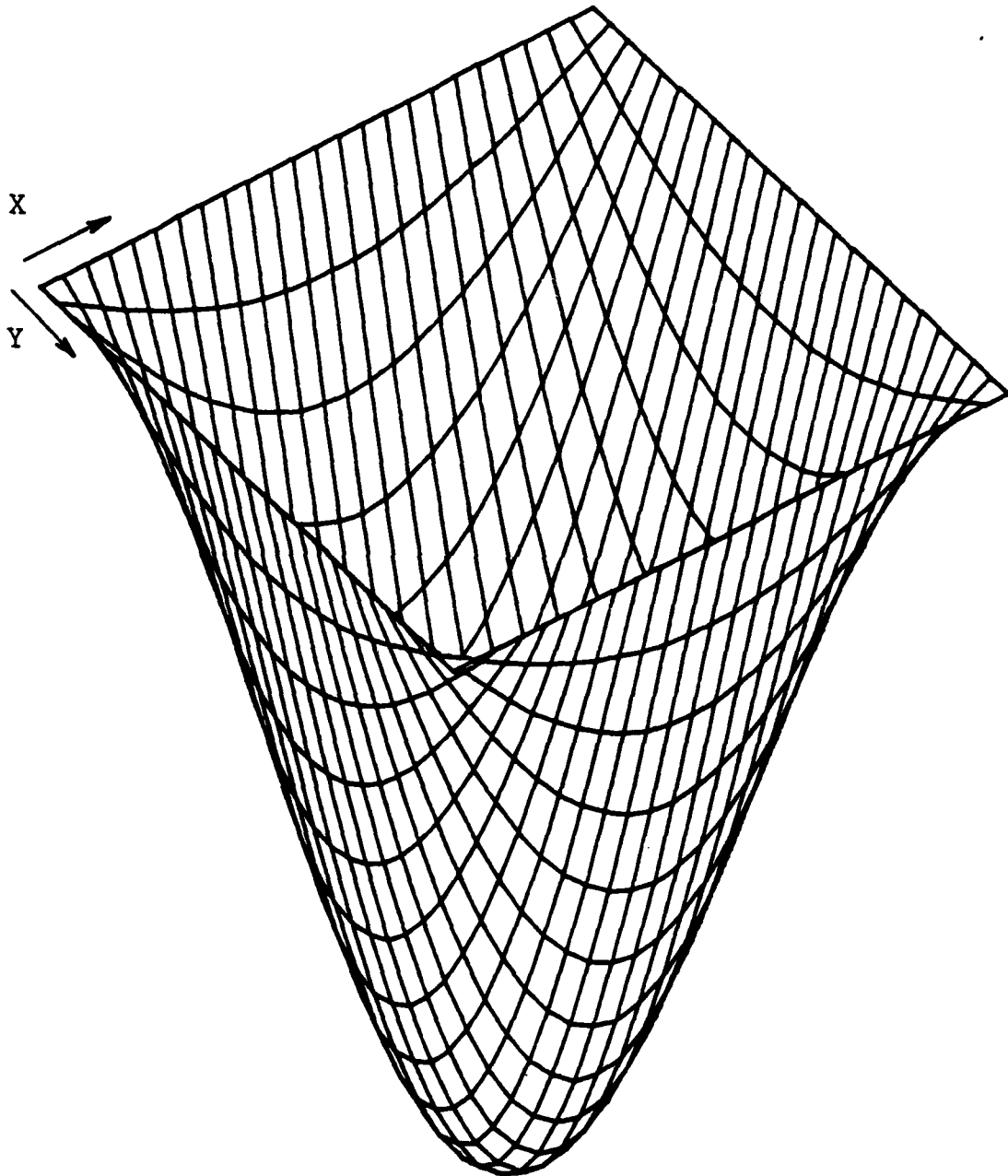


Figure 30. Functional Gain K_2 , $N = 12$; Model 7

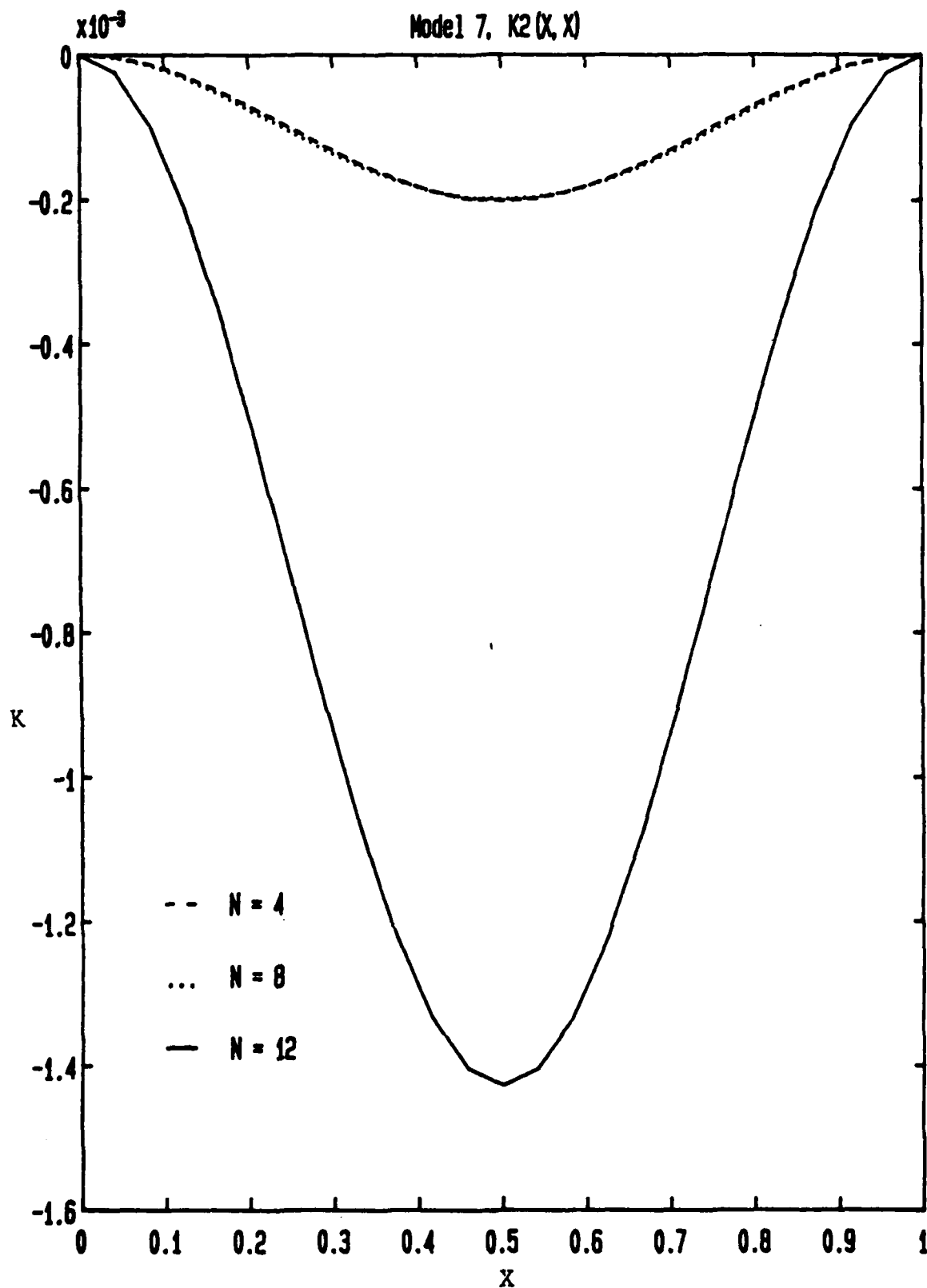


Figure 31. Functional Gain K_2 Cross Section $Y=X$; Model 7

TABLE 17. Closed-Loop Eigenvalues; MODEL 7

N = 4	N = 8	N = 12
$-.274 + 19.746 i$	$-.269 + 19.743 i$	$-1.767 + 19.664 i$
$-.123 + 49.511 i$	$-.122 + 49.356 i$	$-.122 + 49.349 i$
$-.314 + 79.236 i$	$-.311 + 78.971 i$	$-.312 + 78.959 i$
$-.513 + 101.263 i$	$-.488 + 98.795 i$	$-.487 + 98.712 i$
$-.855 + 130.781 i$	$-.824 + 128.403 i$	$-.823 + 128.320 i$
$-1.655 + 181.943 i$	$-1.581 + 177.823 i$	$-1.579 + 177.678 i$

SOFTWARE ISSUES

As part of preparing the numerical studies reported earlier it was necessary to develop the related research software. Since the MODELS studied are interrelated [i.e. Euler-Bernoulli and Timoshenko beam models; actuator models with and without delays] some effort was devoted to organizing the software in an efficient way. The objective of this section is to report on this structure in the set of software procedures. We also assess what additions and enhancements would be needed to provide a reasonable environment for studying linear quadratic regulator synthesis in a class of models including combinations of the beam and plate models studied here.

Starting from the quadratic regulator synthesis procedure, the fundamental step is the solution of a rather large matrix Riccati equation. As noted previously, the procedure used is an implementation of Potter's method (see Ref. 20). The main calculations required in this method include finding the eigenvalues and eigenvectors of a Hamiltonian matrix and solving a linear system. Our implementation employed standard IMSL (Version 10) routines for these calculations.

In order to use the same procedure for all the dynamical systems it was helpful to think of the Potter procedure as an 'operator' which "transforms" data files. This idea of a 'filter' or pipeline has been engendered by growing popularity of the UNIX operating system. It is very useful for the simplicity it produces when a variety of procedures are involved.

Specifically in the Potter procedure we envision a data set consisting of the system matrices A, B and C in the now familiar description

$$\begin{aligned}\dot{x}(t) &= A x(t) + B u(t) \\ y(t) &= C x(t)\end{aligned}\tag{245}$$

The code reads in the matrices, including the integer variables describing the size of each matrix. After the calculation is complete the code writes a file consisting of the optimal gain values K. Other information, including closed-loop eigenvalues, is also written.

Once the gain matrix is known for a certain approximation it is still necessary to construct the components of the gain operator (i.e. the gain values and the functional gains, see eqns. (123), for example).

To understand this calculation it is helpful to recall that our finite-dimensional models in the form [245] are coordinate representations of infinite-dimensional systems. That is, the 'state' of the system is given by

$$z^N(t) = \sum x_i(t) e_i^N, \tag{246}$$

where the e_i^N are the basis vectors chosen for a particular representation [see eqns. (145) - (148), for example].

The matrix gains computed by the Potter procedure give the optimal control as

$$u^{N*}(t) = K^N x(t), \tag{247}$$

where the matrix K has one row for each control component (a scalar for our examples). In terms of the state-space one has

$$u^{N*}(t) = K^N z^N(t) \quad (248)$$

and the task is to 'compute' the operator K^N . In our Hilbert space setting a bounded linear functional can be represented as an inner product so that the control can be expressed as

$$u^{N*}(t) = \langle K^N, z^N(t) \rangle_{Z^N} \quad (249)$$

where $K^N \in Z^N$.

Combining the representations given by equations (247) and (249) one has

$$K^N x = \langle K^N, \sum x_i e_i^N \rangle_{Z^N} \quad (250)$$

Since (250) must hold for all x and since K^N can be represented in terms of the basis $\{e_i^N\}$ as

$$K^N = \sum \beta_i e_i^N \quad (251)$$

equation (250) leads to

$$G^N \beta = [K^N]^T \quad (252)$$

where G^N is the Gram matrix

$$G^N(i,j) = \langle e_i^N, e_j^N \rangle_{Z^N} \quad (253)$$

Once the β coordinates have been determined one uses the basis elements to compute the 'operator' K^N . For the results presented in the previous section, these calculations were done on a PC using the MATLAB software. This provided a convenient mechanism for generating the

plots for the various functional gains.

As noted in the Numerical Procedures section the beam models with actuator dynamics can be 'naturally' constructed from the original models and the necessary 'data' describing the actuator. Thus, in its final form our "beam" software set has a single procedure that reads data files describing the appropriate beam model. This data is combined with the actuator description to produce a system in the form (245). This data is written to a file so that it can be read by the Potter procedure.

The software set contains two codes for producing the beam models. Each procedure reads the same 'data' file to describe the beam properties. Since the Timoshenko model requires several parameters not utilized by the simpler Euler-Bernoulli model this practice may seem strange. It was adapted so that we could be sure that the two models were given consistent data. This greatly facilitated the comparison reported in the beginning of the Numerical Results Section. The two beam procedures, called Euler and Timo, produce data files containing the A, B and C descriptions needed by Potter (or by the procedure to add actuator dynamics). The plate procedure also produces a file of this type.

Except for the final gain 'operator' calculations, all of the codes used in the study were written in FORTRAN-77. The A, B, C 'system' files produced by the beam and plate procedures can be quite large. Since these are most often not read by the analyst, it was decided to write them as unformatted files. For debugging purposes it was convenient to include a simple procedure to generate a human

readable file from this data.

The seven FORTRAN procedures developed for the numerical experiments are:

EULER: Assembles (A,B,C) system description for Euler-Bernoulli beam model

TIMO: Assembles (A,B,C) system description for Timoshenko beam model

ACT: Assembles (A,B,C) system description for beam model with actuator dynamics

PLATE: Assembles (A,B,C) system description for isotropic plate model

POTTER: Reads (A,B,C) description, computes matrix Riccati solution and feedback gain matrix

GAIN: Reads gain matrix and Gram matrix, computes coordinate representation of gain operator

RSYS: Reads unformatted (A,B,C) system description and writes out formatted version of the same

As a final consideration we briefly discuss the possibility of generating a research code for use in studying LQR optimal feedback controllers for a class of systems consisting of beam elements and rigid bodies coupled with joints and actuators. For definiteness we consider only two-dimensional planar models.

Among the first issues to decide is which 'elementary' structures are to be allowed and then precisely how are they to be characterized. For discussion purposes we propose to include

Euler-Bernoulli beams

Timoshenko beams

Rigid bodies

Force/torque actuators

Since we are suggesting a linear dynamical model, it is clear that some features of the motions are not included.

Before beginning a discussion of some of the technical issues at stake, it is important that we make clear that we are not contemplating a computer code that generates a finite-dimensional (A^N, B^N, C^N) approximating model for such a class of systems. The experience reported in Ref. (2) should make clear that such simulation models can be treacherous when used in control problems. Rather we have in mind a computer aided procedure for assembling an infinite-dimensional, state-space model from the "elementary" models for the constituent pieces of the system.

The use of signal-flow graphs or block diagrams to construct models including feed forward and feedback elements are a weak paradigm for the process we have in mind. The parallel is weak because in the present situation one has to realize that not all interconnections of the elementary systems are permissible. This is because the interconnections amount to imposing certain boundary conditions on the adjoining elements. It should be clear from the state space modelling discussed in that section that these boundary conditions play a crucial role in the formulation. In our approach, the boundary conditions have an effect on the state space \mathcal{Z} [see the plate model,

eqs. (87) and (92)] and, more commonly, on the generator A through its domain [see the Euler-Bernoulli model, eqn. (44)].

One aspect of the problem is a system theoretic issue: given a collection of dynamical systems $[\Sigma_i]$, consisting of operators A_i , B_i and C_i and appropriate spaces Z_i , etc., under what conditions does an interconnection produce a dynamical system? What is the composite state-space? Loosely, one expects that a combination of two systems Σ_1 and Σ_2 would result in a product space $Z = Z_1 \times Z_2$. The boundary conditions, however would tend to make the correct space smaller, that is the space is some proper subset of Z . We are proposing that one could provide an automated procedure for constructing the composite system Z .

One key aspect of such a procedure is a convenient graphics environment for the user interface. A combination of icons and 'pop-open' windows would provide cues for the required data. A number of currently available system modeling packages provide such interfaces.

A second requirement is an underlying geometry manager that would assemble the necessary mappings from the local geometry of the individual elementary systems to the 'world' coordinates of the complete system. The final need is the procedure that constructs the composite state-space model. Since not all system connections are permissible, this module would need special care to present the user with suitable prompts and diagnostics should an inadmissible connection be requested.

In summary we note that the software we have in mind does not simply construct a finite dimensional approximation for the system

(that is a simulation model). Rather it is our strong belief that for control problems one should retain the true (infinite-dimensional) system model as long as possible. Numerical approximations are to be introduced only at the last step, just prior to computation.

CLOSING REMARKS

We have constructed state space models and computational algorithms for control of seven structural vibration problems. Convergence of feedback operators is dependent upon the numerical schemes satisfying (131) - (132) and (133) - (137). As indicated above all of these conditions can be rigorously established for MODELS 1, 3 and 4. Conditions (131) - (136) can be proven to hold for all of the model problems considered in this report. However, condition (137) is more difficult to handle. In fact, numerical evidence seems to indicate that (137) may not hold for the standard finite element approximation of the Timoshenko beam models (see Figures 7, 16 and 20) and for the finite element approximation of the plate (see Figures 24, 25, 26 and 31). This is an unsolved problem. If one can show that (137) does not hold for these schemes, then this would raise several practical problems involving the use of finite element models in control design. This is an area of research that needs further study.

The results in this paper show that practical software tools for control design can be constructed for problems that include actuator dynamics and time delays as part of the complete model. This integrated approach has many advantages and a few limitations. However, there are several practical and theoretical questions that must be answered before a "computer aided package" could be developed into a useful design tool. These questions are particularly important

when dealing with Timoshenko beams and plates. More fundamental research, numerical experimentation and laboratory experiments are needed.

REFERENCES

1. Burns, J. A., et al., Modeling and Control of Flexible Structures, AFRPL-TR-85-030, Contract F04611-84-C-0032, Blacksburg, VA, May 1985.
2. Burns, J. A., Cliff, E. M., Kelley, H. J. and Lutze, F. H., "Optimal control of a slewing beam with delayed actuator dynamics," Optimization Inc. Report K511-2, Blacksburg, VA, Oct. 1987.
3. Timoshenko, S., Young, D. H. and Weaver, W., Vibration Problems in Engineering, John Wiley & Sons, New York, 1974.
4. Lagnese, J. E. and Lions, J. L., "Modelling, Analysis and Control of Thin Plates," Preprint, unpublished report, Department of Mathematics, Georgetown Univ., Washington, DC, 1988.
5. Szilard, Rudolph, Theory and Analysis of Plates, Classical and Numerical Methods, Prentice Hall, Englewood Cliffs, NJ, 1974.
6. Banks, H. T., Burns, J. A. and Cliff, E. M., A Comparison of Numerical Methods for Identification and Optimization Problems Involving Control Systems with Delay, Brown Univ. LCDS Tech. Rep. 79-7, Providence, RI, 1979.
7. Banks, H. T., Burns, J. A. and Cliff, E. M., "Parameter estimation and identification for systems with delays," SIAM J. Control Opt., Vol. 19 [1981], pp. 791-828.
8. Banks, H. T., Rosen, I. C. and Ito, K., "A spline based technique for computing Riccati operators and feedback controls in regulator problems for delay equations," SIAM J. Sci. Stat. Comput., Vol. 5 [1984], pp. 830-855.
9. Burns, J. A. and Cliff, E. M., "Optimal control of a distributed system," Proc. Workshop on Optimal Control, Oberwolfach, FRG, June 1986, Springer-Verlag, [1987], pp. 304-318.
10. Burns, J. A., Cliff, E. M. and Powers, R. K., "Computational methods for the control of distributed parameter systems," 24th IEEE Conference on Decision and Control, December 1985, pp. 1994-1998.
11. Cliff, E. M. and Burns, J. A., "Reduced approximations in parameter identification of hereditary systems," Proc. IFIP Conference on Modeling and Optimization, Springer-Verlag, 1981, pp. 241-249.
12. Gibson, J. S., "The Riccati integral equations for optimal control problems in Hilbert spaces," SIAM J. Control and Opt., Vol. 17 [1979], pp. 537-565.

13. Gibson, J. S., "Linear quadratic optimal control of hereditary differential systems: Infinite dimensional Riccati equations and numerical approximations," SIAM J. Control and Opt., Vol. 21 [1983], pp. 95-139.
14. Gibson, J. S. and Adamian, A., "Approximation theory for LQG optimal control of flexible structures," Technical Report, Mechanical Aerospace and Nuclear Engineering Dept., UCLA, Los Angeles, CA, 1986.
15. Gibson, J. S. and Naved, M., "Approximate solution of Riccati algebraic equations in optimal control and estimation of hyperbolic systems," Int'l. Symposium on Mathematical Theory of Networks and Systems, August 1981, Santa Monica, CA.
16. Adams, R. A., Sobolev Spaces, Academic Press, New York, NY, 1975.
17. Hille, E. and Phillips, R. S., Functional Analysis and Semi-groups, AMS Colloq. Pub. Vol. 31, 1957.
18. Pazy, A., Semigroups of Linear Operators and Applications to Partial Differential Equations, Springer-Verlag, New York, NY, 1983.
19. Walker, J. A., Dynamical Systems and Evolution Equations, Plenum Press, New York, NY, 1980.
20. Kwakernaak, H. and Sivan, R., Linear Optimal Control Systems, Wiley-Interscience, New York, NY, 1972.
21. Burns, J. A. and Fabiano, R., "Feedback control of a hyperbolic partial-functional differential equation with viscoelastic damping," Control Theory and Advanced Technology, to appear.
22. Rudin, W., Functional Analysis, McGraw-Hill, New York, NY, 1973.
23. Trotter, H. F., "Approximations of semi-groups of operators," Pacific J. Math., Vol. 8 [1958], pp. 887-919.
24. Banks, H. T. and Kunisch, K., "The linear regulator problem for parabolic systems," SIAM J. Contr. Opt., Vol. 22, No. 5, September 1984, pp. 684-698.
25. Prenter, P. M., Splines and Variational Methods, John Wiley & Sons, 1975, New York, NY.
26. Schultz, M. H., Spline Analysis, Prentice-Hall, Englewood Cliffs, NJ, 1973.

27. Beards, C. F. and Woowet, A., "The control of frame vibration by friction damping in joints," Journal of Vibration, Acoustics, Stress and Reliability in Design, Vol. 106, Jan. 1985, pp. 26-32.
28. Richardson, R. S. H. and Nolle, H., "Energy dissipation in rotary structural joints," Journal of Sound and Vibration, Vol. 54, No. 4, 1977, pp. 577-588.
29. Ponovko, Y. G., Goltzev, D. I. and Strakov, G. N., "Vaproši dinamiki i prochousti v, riga," (Institute of Machine Design, Academy of Science, Latvian SSR). Elementary problems of structural hysteresis, 1958.
30. Metherell, A. F. and Diller, S. V., "Instantaneous energy dissipation rate in a lap joint - uniform clamping pressure," Journal of Applied Mechanics, Vol. 35, 1968, pp. 123-128.
31. Alspaugh, D. W., "Analysis of coulomb friction vibration dampers," Journal of Sound and Vibration, Vol. 57, No. 1, 1978, pp. 65-78.
32. Tomlinson, G. R. and Hibbert, J. H., "Identification of the dynamic characteristics of a structure with coulomb friction," Journal of Sound and Vibration, Vol. 64, No. 2, 1979, pp. 233-242.
33. Jezequel, L., "Structural damping by slip in joints," Journal of Vibration, Acoustics, Stress and Reliability in Design, Transactions of the ASME, Vol. 105, October, 1983, pp. 497-504.
34. Dowell, E. H., "Damping in beams and plates due to slipping of the support boundaries," Journal of Sound and Vibration, Vol. 105, 1986, pp. 243-253.
35. Hertz, T. J. and Crawley, E. F., "Damping in space structure joints," AIAA Dynamic Specialists Conference, Palm Springs, CA. AIAA paper 84-1039-CP, May 1984.
36. Mentel, T. J., "Viscoelastic boundary damping of beams and plates," ASME Journal of Applied Mechanics, March, 1964, pp. 61-71.
37. Goodman, L. E., "A review of progress in analysis of interfacial slip damping," ASME Colloquium Structural Damping, 1960, pp. 35-48.
38. Earles, W. E. and Philpot, M. G., "Energy dissipation of plane surfaces in contact," Journal of Mechanical Engineering Science, Vol. 9, No. 2, 1967.
39. Den Hartog, J. P., "Forced vibrations with combined coulomb and viscous friction," Transactions ASME, Vol. 53, p. 107.

40. Crandell, S. H., "The role of damping in vibration theory," Journal of Sound and Vibration, Vol. 11, No. 1, 1970, pp. 3-18.
41. Crawley, E. F. and O'Donnel, K. J., Identification of Nonlinear System Parameters in Joints Using the Force State Mapping Technique, Space Systems Laboratory, MIT Report SSL 16-85, July 1985, also AIAA Paper 86-1013-CP, 27th SDM Conference, May 1986.
42. Taylor, R. L., Structural Analysis and Modeling; Lecture Notes, Pajaro Dunes Workshop on Control of Space Structures, July 1985.

END
FILMED

6-89

DTIC